European
Oral Research

EOR

ISTANBUL
UNIVERSITY
PRESS

INDEXING AND ABSTRACTING

SCOPUS
Emerging Sources Citation Index (ESCI)
PUBMED Central
TÜBİTAK ULAKBİM TR-Index
Proquest
EBSCO Dentistry & Oral Sciences Source
Directory of Open Access Journals (DOAJ)
Open Aire
Chemical Abstracts
SOBIAD

Authors bear responsibility for the content of their published articles.

The publication languages of the journal is English.

This is a scholarly, international, peer-reviewed and open-access journal published triannually in January, May and September.

Publication Type: Periodical

Contents

Original Research Articles

European
Oral Research

Contents

Invited Review Article

Clinical and demographic profile of oral lichen planus in Sri Lanka: a retrospective study

Purpose

Several relatively large series from developed countries have extensively described the demographic and clinical characteristics of oral lichen planus (OLP). However, such descriptions from developing countries are rare. This study aimed to investigate the differences in these aspects within a cohort of Sri Lankan patients affected by OLP.

Materials and Methods

Cases diagnosed with OLP between 1999 and 2019 were retrieved. Demographic data, clinical presentation, main complaints, age, sex, lesion sites, and histological information, were collected from the database. Cases with lichenoid reactions and incomplete data were excluded. Instances with multiple biopsies were treated as single cases. Frequencies were compared using chi-square statistics.

Results

The database identified a total of 3734 cases. The male-to-female ratio was 1:1.6, indicating an overall female predominance. The youngest patient reported was 1 year and 2 months old, presenting with brownish pigmentations on the right side of the buccal mucosa. The highest number of cases were observed in the 41-50-year age group, followed by the 51-60-year age group. The most common clinical type was the reticular type, followed by atrophic and erosive types. 200 patients presented with blackish pigmentations in the oral mucosa, experiencing a burning sensation without evidence of the typical reticular background. The plaque type was more common on the dorsal surface of the tongue, showing a statistically significant association (p<0.05). Ninety cases exhibited dysplastic changes ranging from mild to moderate degrees, accounting for 2.4% of the total sample.

Conclusion

While the malignancy rate is not significantly high enough to reduce morbidity and mortality from cancer arising on OLP lesions, regular follow-up and examinations are recommended for early diagnosis of malignant transformation.

Keywords: Oral lichen planus, reticular, dysplasia, prevalence, pigmented lesion

B.S.M. Samadarani Siriwardenaa[1] [ID],

Kalani Hettiarachchi[2] [ID],

Ruwan D Jayasinghe[2] [ID]

Introduction

Oral lichen planus (OLP) is a chronic mucocutaneous disease with an immune-mediated pathogenesis. The etiopathogenesis of OLP remains incompletely understood. This disease is multifactorial, triggered by various agents, including dental materials, drugs, viruses like hepatitis C, liver dysfunction, and psychological stress (1). Primarily affecting the oral mucosa, OLP can also involve other mucosal sites, such as the vulvar, vaginal mucosae, skin, particularly the flexor surfaces of hands and legs, scalp leading to alopecia, and nails. The prevalence of OLP may vary from 0.5% to 2.2%. In the general population, the average rate is 0.89%, and among clinical patients, it is 0.98% (2,3). Typically manifesting a female predilection, OLP is commonly observed in the 4th to 6th decade of life.

The oral mucosal lesions in OLP are usually bilateral but not necessarily symmetrical, commonly found in sites such as the buccal mucosa, tongue, and gingiva, often leading to desquamative gingivitis. With multiple clinical presentations, some are asymptomatic, while others cause a significant burning sensation and pain. Although around 17 different clinical types have been described in the skin, only 6 types are identified in the oral mucosa such as papular, reticular, erosive, plaque-like, atrophic, and bullous (4).

The most common is the reticular type, often asymptomatic and characterized by a white line on the buccal mucosa, known as "Wickham striae." The papular type is rare, mostly asymptomatic, with small white raised areas and occasional whitish fine striae. Plaque-type OLP can resemble oral leukoplakia, appearing as thick white patches on the buccal mucosa and dorsum of the tongue. Erosive, atrophic, and bullous types appear reddish and are symptomatic. Erosive OLP presents as inflamed, ulcerated areas, often mixed with a reticular pattern, causing severe pain. Atrophic OLP exhibits diffuse reddish lesions and may coexist with other subtypes, notably the reticular type. Bullous OLP begins with blisters that rupture, resulting in painful ulcerations (1). Different clinical forms might coexist or merge in the same patient (2). The clinical features, especially in the asymptomatic "classic" reticular form, may be adequate for diagnosis. However, as several conditions with similar clinical appearances exist, histopathological confirmation through biopsy, although the clinical evidence is evident, can be essential (2).

Considered a potentially malignant disorder with a very low transformation potential, OLP patients who smoke, consume alcohol, are seropositive for HCV, or present reddish types, carry a higher risk of malignant transformation (4-6). Multiple mucosal lesions clinically and histopathologically resembling OLP are termed "oral lichenoid" lesions (OLL). The main differentiating factor between OLP and OLL is the identification of the etiological agent in OLL. Lichenoid lesions can stem from dental materials, drugs, or other systemic diseases. Contact of oral mucosa with dental materials used for restorations, particularly amalgam, can cause oral lichenoid contact lesions (OLCL) due to contact allergic mucositis (delayed immune-mediated hypersensitivity). Oral lichenoid drug reactions (OLDR) are associated with specific medications such as angiotensin-converting enzyme inhibitors, nonsteroidal anti-inflammatory agents, and oral hypoglycemic agents. Lichenoid lesions are also seen in graft-versus-host disease (OLL-GVHD) (2). Several relatively large series from developed countries have extensively described the demographic and clinical characteristics of oral lichen planus (OLP). However, such descriptions from developing countries are rare. This study aimed to investigate the differences in these aspects within a cohort of Sri Lankan patients affected by OLP.

Materials and Methods

Ethical approval

The study protocol received approval from the Sri Lanka Peradeniya University Ethics Committee (project no: ERC/FDS/UOP/2016/06).

Database search criteria

Cases diagnosed as OLP were retrieved from the Oral Pathology database spanning 1999-2019 at the Department of Oral Pathology, Faculty of Dental Sciences, University of Peradeniya, Sri Lanka. Demographic data, including clinical presentation, main complaints, age, sex, lesion sites, and histological information, were collected. Cases with lichenoid reactions and inadequate data were excluded, while instances with multiple biopsies were consolidated into single cases.

Data classification

The gathered data were entered into a Microsoft Excel worksheet and categorized based on age to identify frequency distribution, as well as site of occurrence (right buccal mucosa, left buccal mucosa, bilateral buccal mucosae, palate, tongue - ventral, dorsal, lateral - lips, and gingiva). Additionally, data were categorized according to clinical types, such as reticular, atrophic, erosive, bullous, and pigmented. Patients presenting with the aforementioned clinical types and a pigmented background were included. OLP, as defined by the WHO, falls under the category of an oral potentially malignant disorder (OPMD). Hence, histological reports were assessed to identify cases exhibiting dysplastic changes.

Statistical analysis

Chi-square tests were employed to determine associations. Different combinations of each variable were analyzed to identify statistically significant relationships. A confidence interval of 95% was set, with the significance level considered at p<0.05.

Results

Inclusion criteria and demographics

A total of 3734 cases met the inclusion criteria, comprising 1441 males and 2293 females, resulting in a male-to-female ratio of 1:1.6, demonstrating an overall female predominance. Within the study population, nearly 90% were of Sinhalese ethnicity, while Tamils and Muslims each represented 5%, reflecting the country's ethnic distribution (Table 1). The overall average age was 45.98 years. However, there were marked age-specific variations across each category (Table 1). Gender distribution also showed variability across different age groups (Figure 1a and Figure 1b).

Clinical presentation and types

The chief complaint among the majority of cases was a burning sensation. Clinically, OLP manifested as reticular, atrophic, erosive, and bullous types. The youngest reported patient was a 1-year and 2-month-old baby with brownish pigmentations on the right-side buccal mucosa. The highest number of cases appeared in the 41-50 age group, followed by the 51-60 age group. When categorizing the total sample by clinical type, the worst presentation was considered. For instance, if a lesion displayed erosions/ulcers against a back-

Table 1. *Number of OLP cases distribution within different age groups.*

Age group	Number of cases	M	F	Average number of cases per decade
1-10	51	20	31	5
11-20	173	74	99	17.3
21-30	439	199	240	43.9
31-40	699	266	433	69.9
41-50	861	311	550	86.1
51-60	798	271	527	79.8
61-70	524	209	315	52.4
71-80	163	80	83	16.3
81-90	26	11	15	2.6
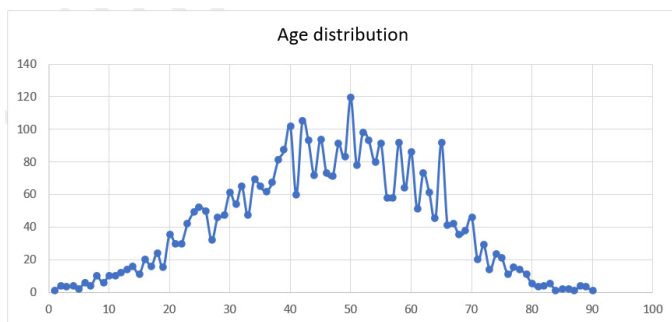
Figure 1a. *Age distribution among the total sample.*
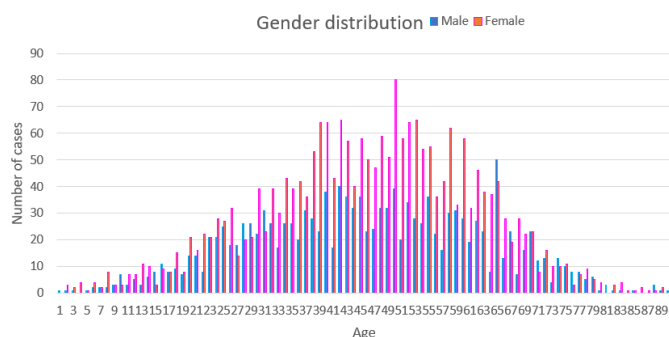
Figure 1b. *Gender distribution within the test group.*

Figure 2a. *Clinical presentation of OLP of the study sample.*
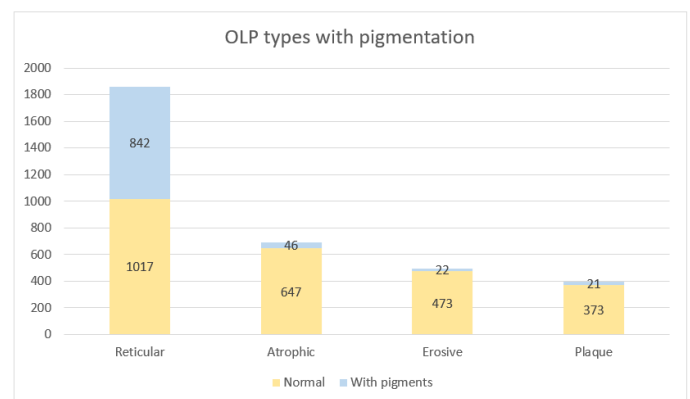
Figure 2b. *OLP cases that showed blackish pigmentation*
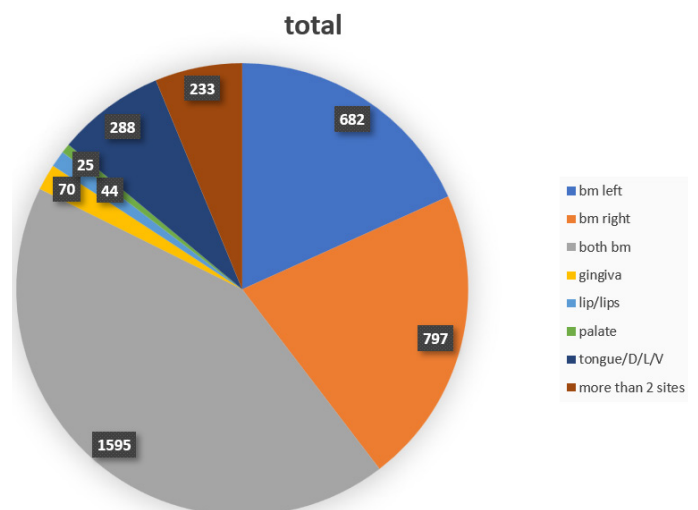
Figure 3. *Site distribution of the OLP cases.*

ground of reticular areas, it was classified as an erosive type. The most common type observed was the reticular type, followed by atrophic and erosive types. Notably, 200 patients presented with blackish pigmentations in the oral mucosa and a burning sensation, devoid of the typical reticular background (Figure 2a). It's intriguing to note the association of various clinical presentations with pigmentation (Figure 2b).

Distribution and association

Bilateral buccal mucosae harbored 42.7% of OLP cases (1595 cases), while the least common site was the palate (Figure 3). Moreover, the plaque type predominantly occurred on the dorsal surface of the tongue (Fig 4). A statistically significant association (p<0.001) was observed between the distribution of OLP types and the site of the tongue (Table 2). Figure 5a to Figure 5d illustrated typical clinical appearances of different OLP types.

Reticular OLP

The most common clinical type observed was the reticular type, constituting 49.8% of the total sample. Among these cases, 842 exhibited reticular lesions against a background of blackish/brownish pigmentation. The primary site affected by reticular lesions was the buccal mucosa, with the majority presenting bilateral lesions (54.2%). The right side of the buccal mucosa was more frequently affected, followed by the left side and the tongue, with 303, 342, and 62 cases respectively. A similar trend was observed when analyzing cases with pigmentation and those without as separate categories.
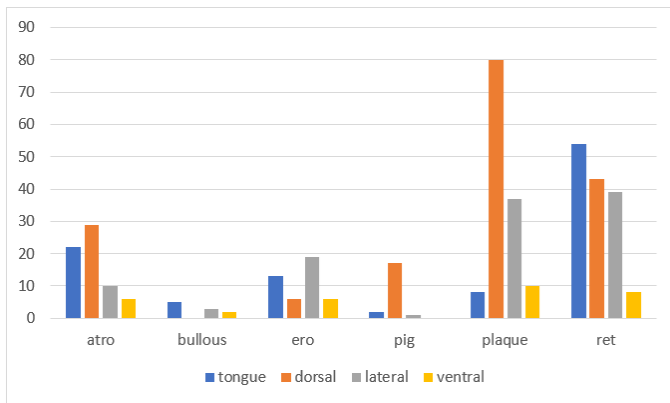
Figure 4. *Distribution of differenet types of OLP that occurred in the tongue.*
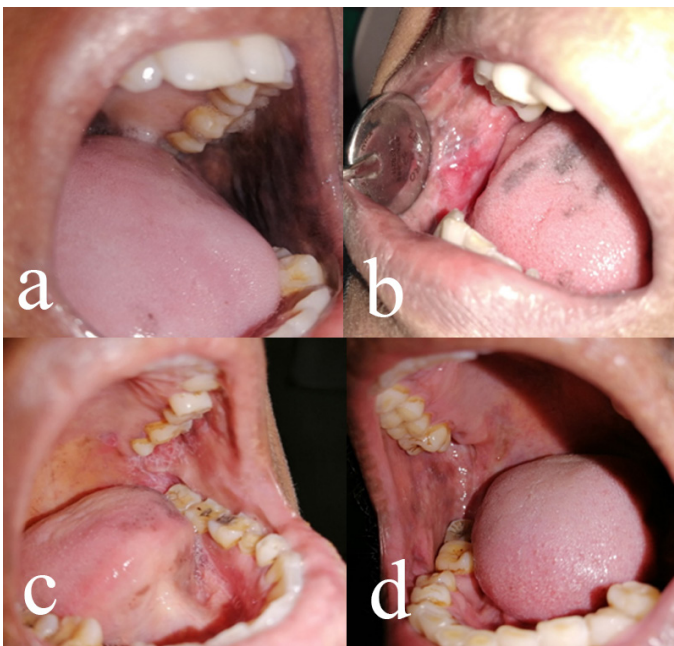
Figure 5. *Types of OLP, (a) pigmented, (b) erosive with pigmentation, (c) typical reticular OLP, (d) athrophic OLP with pigmentation.*

Table 2. *The heat map presentation of the OLP distribution in the tongue. The chi-square statistic : 80.5769. p-value < 0.001.*

	atrophic	bullous	erosive	pigmented	plaque	reticular
tongue	22	5	13	2	8	54
dorsal	29	0	6	17	80	43
lateral	10	3	19	1	37	39
ventral	6	2	6	0	10	8

Atrophic OLP

Lesions characterized by erythematous areas within a background of white radiating striae at the periphery, accompanied by a burning sensation, are classified as the atrophic type. In this study, the atrophic type constituted 18.6% (693 cases), commonly affecting bilateral mucosa as the most prevalent presentation (43.7%). Among the total atrophic cases, 6.6% displayed a pigmented background (46 cases). Specifically, 152 cases were observed on the right-side buccal mucosa, and 130 on the left side. Additionally, 12.4% of cases were reported on the tongue, predominantly on the dorsal surface (24 out of 54).

Erosive OLP

Atrophic, erosive, or ulcerative types are situated within the same spectrum. In this study, ulcerative lesions were categorized as the erosive type, with most displaying a reticular background, some of which exhibited pigmentation (4.4%). Among the total sample, 13.3% were classified as the erosive type, frequently affecting, akin to the other mentioned types, bilateral buccal mucosae (158 cases), followed by the right and left buccal mucosae. A few cases were presented with a pigmented background (4.4%).

Pigmentation associated with OLP

An important observation in this study was the presence of pigmentation in OLP, distinct from the typical reticular white striated background. Out of the total sample, 200 cases (5.4%) purely exhibited patchy blackish pigmentation, predominantly affecting the buccal mucosa. Intriguingly, 85% of the 20 cases related to the tongue were located on its dorsal surface. Additionally, affected sites included the gingiva, lips, and palate. While literature suggests that pigmentation might be due to aging or multiple episodes of OLP, this series noted pigmented lesions without the typical OLP background in both the youngest child and the oldest individual.

Bullous OLP

Clinically, bullous OLP presents with ulcers covered by a fibrin coat, surrounded by an erythematous zone with radiating white striae. Distinguishing between erosive and bullous types is crucial. In this study, 2.5% of cases were of the bullous type, most of which were histologically confirmed to have epithelial separation from the underlying corium. No associated pigmented areas were reported in this OLP subset. The most common site was the buccal mucosa (bilateral - 21.5%, right - 17.2%, left - 11.8%), followed by the gingiva (19.4%).

Plaque OLP

In the total sample, 10.5% (394 cases) presented as well-demarcated homogenous white plaques, often with a reticular pattern. The tongue was the most common site, with 118 cases. 5.3% of these cases were associated with pigmentation. Notably, 65.5% of tongue lesions (74 cases) resembled leukoplakia lesions, primarily on the dorsal surface, followed by the lateral border of the tongue (32 cases). Only 34 cases were bilateral lesions.

Intra oral sites

A significant majority (82.3%) of cases occurred on the buccal mucosa, either bilaterally or on a single side (Figure 3). Bi-

lateral presentation accounted for 42.7% of the total sample. Involvement of the buccal mucosa with other sites was observed in 233 cases (6.2%). The distribution of different types of OLP on the tongue is detailed in Table 3 as a heat map and Figure 4, showing highly significant results (p<0.001).

OLP as and OPMD

Notably, 132 cases were reported with associated dysplastic changes or candida superinfection. Within this group, OLP cases with a background of oral submucous fibrosis (OSF) were also noted. Ages ranged from 24 to 82 years, with a mean age of 52 years. OSF, recognized as an OPMD, was reported in 6 cases, and all clinical types except the reticular type were observed. Candidal superinfection partly exacerbated the burning sensation, evident in 42 cases. Of these, 90 cases exhibited dysplastic changes ranging from mild to moderate degree (2.4% of the total sample). Mild dysplasia was predominant, observed in 47 cases of the reticular type, 19 cases of the atrophic type, 11 cases of the erosive type, and 10 cases of the plaque type. Moderate dysplasia was reported in 2 cases of the plaque type and 1 case of the reticular type. There was a male predominance in cases showing dysplastic changes, contrary to conventional OLP, with 42 cases in females and 48 in males.

Discussion

In several relatively large series from developed countries, the clinical characteristics and demography of OLP have been well-described. However, such series from developing countries are rare and a possible reason for this may be the lower prevalence of OLP in Asian countries than in other countries (3). Therefore, this retrospective study was carried out with the aim to highlight the differences in these aspects in a cohort of Sri Lankan group of patients affected with OLP.

A study by Lauritano *et al.* (7) reports that OLP is a disease of elderly with a slight female predilection in 5th and 6th decades of life (2-7). The present study also confirms these results with many of patients belonging to the age group of 41-50 years (mean age 45.98 years) followed by 51-60 years. However, a study from India has reported a prevalence in 3rd decade of life with a mean age of 36.9 years (8) which is comparatively lower than mean ages reported from several other studies (9-11). The OLP prevalence in the elder population may be due to long-standing oral habits, lack of attention to oral hygiene, the age-related changes, decreased immunity, associated metabolic changes during aging, medication use, nutritional deficiencies, or denture wear (2-12). The occurrence of OLP in the paediatric population is extremely rare, with a prevalence of < 2-3% and the youngest patient reported in this study, was one year and two months old (13). The general acceptance is that the prevalence of OLP is higher in females than in males which is also evident in this present study as well. Fluctuating levels of oestrogen and progesterone in females could be the possible reasons especially during menstruation or menopause. However, Munde *et al.*(8), reported a male preponderance with a male to female ratio of 1.61:1.

As previously mentioned, even though the involvement of multiple oral sites is common in OLP, the lesions will typically and most commonly present in the bilateral, buccal mucosa in a symmetrical manner, followed by the gingiva and the tongue (8). In the Sri Lankan context, the involvement of bilateral buccal mucosae was observed 42.7% of OLP cases, while the palate was noted to be the least commonly affected site.

Many authors have described various clinical variants in the literature (14-16), however, the most common type found in this study was the reticular type, which was in par with the literature (3,10,11). Dark brownish pigments which are associated with OLP is frequently noted. A report by Cawson and Odell (17) indicated that the degenerative changes in basal keratinocytes frequently led to pigmentary incontinence. The melanin in pigment is ingested by macrophages in the superficial corium, resulting in a brownish-pigmented area in the mucosa, which can persist long after the OLP has resolved (17). However, various hypothesis has been reported in the literature regarding the hyperpigmentation associated with the OLP. A study proposed that the mechanism of hyperpigmentation is related to the GABA imbalance that occurs during stress and anxiety. They further indicated that 96.97% of patients having anxiety disorders showed OLP associated with hyperpigmentation. The imbalance of these patients might be passed through the cranial nerve, which stimulates the production of melanocytes, leading in large amount of melanin deposition in OLP (18). While Chitturi *et al.* (19) suggested that hyperpigmentation could be due to the results of inflammation in recurrence of flare-up and healing, which was mostly found in the chronic reticular form of OLP. In this present study almost, all types were associated with pigmentation and about 5.4% of cases were pigmented without reticular white striated background. Therefore, more studies are required to study further regarding the pigmentation associated with the OLP. It has been also suggested that the cytokines released by the band of lymphocytes stimulate the melanocytes (20). The exact mechanism of hyperpigmentation in OLP remains unclear, and needs further studies, to evaluate by means of immunohistochemistry or molecular biological techniques, in the occurrence of hyperpigmentation in OLP. Unfortunately, a main limitation of this study is that we could not exactly determine the mechanism of hyperpigmentation in our cases due to unavailability of details from the history.

In routine practice, evidence of dysplasia in a given lesion shows the cancer risk in OPMDs. However, the general acceptance of epithelial dysplasia as an accompanying histologic feature in OLP is subject to great controversy. Presence of dysplasia is considered by many pathologists as a criterion to exclude OLP when routinely reporting on OLP. The spreading of this practice among oral pathologists, has led to underestimate the malignant potential of OLP. In this present case 2.4 % of the patients demonstrated epithelial dysplasia. Therefore, OLP should be followed-up for a longer time, and should be investigated by a biopsy aiming to assess any dysplastic changes in the epithelium (21). Two cases of malignant transformation within Sri Lankan patients were also reported in the Sri Lankan literature (22).

Conclusion

Up-to-date OLP is considered as a potentially malignant disorder by the WHO. Malignancy rate is very low with lower morbidity and mortality that are arising from OLP. However, regular follow-up is recommended for early diagnosis of malignant transformation. Further, we recommend further studies in order to resolve the controversies in the hyperpigmentation and presence of dysplasia in relation to OLP.

Türkçe özet: Sri Lanka'da oral liken planusun klinik ve demografik profili: retrospektif bir çalışma. Amaç: Gelişmiş ülkelerdeki nispeten geniş birkaç seride oral liken planusun (OLP) demografik ve klinik özelliklerini kapsamlı bir şekilde tanımlanmıştır. Ancak gelişmekte olan ülkelerde yapılmış bu tür çalışmalar oldukça enderdir. Bu çalışma, OLP'den etkilenen Sri Lankalı hastalardan oluşan bir kohortun özelliklerini incelemeyi amaçlamıştır. Gereç ve Yöntem: 1999-2019 yılları arasında OLP tanısı alan olgulara ulaşıldı. Veritabanından demografik veriler, klinik görünüm, ana şikayetler, yaş, cinsiyet, lezyon bölgeleri ve histolojik bilgiler toplandı. Likenoid reaksiyonları olan ve eksik verileri olan vakalar hariç tutuldu. Çoklu biyopsi vakaları tek vaka olarak değerlendirildi. Sıklıklar ki-kare istatistikleri kullanılarak karşılaştırıldı. Bulgular: Veritabanında toplam 3734 vaka tespit edildi. Erkek-kadın oranı 1:1.6 olduğundan genel olarak kadın hastalarda daha sık rastlanan bir durum olarak belirlendi. Bildirilen en genç hasta 1 yıl 2 aylıktı ve yanak mukozasının sağ tarafında kahverengimsi pigmentasyonları bulunmaktaydı. En fazla vaka 41-50 yaş grubunda görüldü, bunu 51-60 yaş grubu takip etti. En sık görülen klinik tip retiküler tip olup bunu atrofik ve eroziv tipler izlemekteydi. 200 hasta oral mukozada siyahımsı pigmentasyonlarla başvurdu ve tipik retiküler arka plan belirtisi olmaksızın yanma hissi yaşadığını belirtti. Plak tipinin dilin dorsal yüzeyinde daha yaygın olduğu ve istatistiksel olarak anlamlı bir ilişki gösterdiği görüldü (p<0,05). Doksan vakada hafiften orta dereceye kadar değişen displastik değişiklikler görüldü ve bu toplam hastaların %2,4'ünü oluşturdu. Sonuç: Malignite oranı, OLP lezyonlarından köken alan kanserden kaynaklanan morbidite ve mortaliteyi azaltacak kadar anlamlı düzeyde yüksek olmasa da, malign dönüşümün erken tanısı için düzenli takip ve muayeneler önerilmelidir. Anahtar kelimeler: Oral liken planus, retiküler, displazi, prevalans, pigmente lezyon

References

1. Andrea E, Reyes E, Kamal E. Oral Lichen Planus: A review of clinical features, etiologies, and treatments, Dentistry Review 2022; 22: 100007 [CrossRef]
2. Al-Hashimi I, Schifter M, Lockhart PB, Wray D, Brennan M, Migliorati CA, et al. Oral lichen planus and oral lichenoid lesions: diagnostic and therapeutic considerations. Oral Surg Oral Med Oral Pathol Oral Radiol Endod 2007; 103 Suppl: S25.e1-12. [CrossRef]
3. Li C, Tang X, Zheng X, Ge S, Wen H, Lin X, et al. Global Prevalence and Incidence Estimates of Oral Lichen Planus: A Systematic Review and Meta-analysis. JAMA Dermatol 2020; 156:172–81. [CrossRef]
4. Pritam KM, Jayanti GH, Mandakini SM, Jyoti DB. Clinical profile of 108 cases of oral lichen planus. J Oral Sci 2016; 58: 43-7. [CrossRef]
5. Fumihiko T, Jinkyo S, Atsushi U, Yu O, Toshimitsu O, Yumi M, et al. Malignant transformation of oral lichen planus: a retrospective study of 565 Japanese patients. BMC Oral Health 2021; 21 :298. [CrossRef]
6. Idrees M, Kujan O, Shearston K, Farah CS. Oral lichen planus has a very low malignant transformation rate: A systematic review and meta-analysis using strict diagnostic and inclusion criteria. J Oral Pathol Med 2021; 50: 287-98. [CrossRef]
7. Lauritano D, Arrica M, Lucchese A, Valente M, Pannone G, Lajolo C, et al. Oral lichen planus clinical characteristics in Italian patients: a retrospective analysis. Head Face Med 2016; 26: 18 [CrossRef]
8. Munde AD, Karle RR, Wankhede PK, Shaikh SS, Kulkurni M. Demographic and clinical profile of oral lichen planus: A retrospective study. Contemp Clin Dent 2013; 4: 181-5. [CrossRef]
9. Bermejo-Fenoll A, Sánchez-Siles M, López-Jornet P, Camacho-Alonso F, Salazar-Sánchez N. A retrospective clinicopathological study of 550 patients with oral lichen planus in south-eastern Spain. J Oral Pathol Med 2010; 39: 491–6 [CrossRef]
10. Xue JL, Fan MW, Wang SZ, Chen XM, Li Y, Wang L. A clinical study of 674 patients with oral lichen planus in China. J Oral Pathol Med 2005; 34: 467–72. [CrossRef]
11. Gönül M, Gül U, Kaya I, Koçak O, Cakmak SK, Kılıç A, et al. Smoking, alcohol consumption and denture use in patients with oral mucosal lesions.J Dermatol Case Rep 2011; 5: 64-8. [CrossRef]
12. Ingafou M, Leao JC, Porter SR, Scully C. Oral lichen planus: A retrospective study of 690 British patients. Oral Dis 2006; 12: 463–8. [CrossRef]
13. Shikha, Gupta S, Mahajan A, Ambika, Garg R, Ghosh S. Childhood oral lichen planus: a case series with review of literature. Eur Arch Paediatr Dent 2022; 23: 341–53. [CrossRef]
14. Andreasen JO. Oral lichen planus. 1. A clinical evaluation of 115 cases. Oral Surg Oral Med Oral Pathol 1968; 25: 31-42. [CrossRef]
15. Gandolfo S, Richiardi L, Carrozzo M, Broccoletti R, Carbone M, Pagano M, et al. Risk of oral squamous cell carcinoma in 402 patients with oral lichen planus: A follow-up study in an Italian population. Oral Oncol. 2004;40:77–83. [CrossRef]
16. Carbone M, Arduino PG, Carrozzo M, Gandolfo S, Argiolas MR, Bertolusso G, et al. Course of oral lichen planus: A retrospective study of 808 northern Italian patients. Oral Dis 2009; 15: 235–43. [CrossRef]
17. Cawson RA and Odel EW. Essentials of Oral Pathology and Oral Medicine. 9th ed. Churchill Livingstone. Edinburgh. 2017
18. Anjum R, Singh J, Kudva S. A Clinicohistopathologic Study and Probable Mechanism of Pigmentation in Oral Lichen Planus. World J Dent 2012; 3: 330-4. [CrossRef]
19. Chitturi RT, Sindhuja P, Parameswar RA, Nirmal RM, Reddy BV, Dineshshankar J, et al. A clinical study on oral lichen planus with special emphasis on hyperpigmentation. J Pharm Bioallied Sci 2015; 7: S495-8. [CrossRef]
20. Mergoni G, Ergun S, Vescovi P, Mete Ö, Tanyeri H, Meleti M. Oral postinflammatory pigmentation: an analysis of 7 cases. Med Oral Patol Oral Cir Bucal 2011; 16: e11-4. [CrossRef]
21. González-Moles MÁ, Warnakulasuriya S, González-Ruiz I, Ayén Á, González-Ruiz L, Ruiz-Ávila I, et al. Dysplasia in oral lichen planus: relevance, controversies and challenges. A position paper. Med Oral Patol Oral Cir Bucal 2021; 26: e541-8. [CrossRef]
22. Medawela RMS, Ratnayake DRDL, Jayasooriya PR, Siriwardena BSMS, Tilakaratne WM, Jayasinghe RD. Malignant transformation of Oral Lichen Planus: The first two cases reported in Sri Lanka and literature review. SLDJ 2017; 47: 29-37.

External cold and vibration with BUZZY versus topical anesthetic gel for pain and anxiety associated with infiltrative anesthesia in pediatric dentistry: a double-blinded, split-mouth, randomized, controlled trial

Purpose
A way to reduce the pain of injection is applying of external cold or vibrations with BUZZY, along with spinal cord gate control systems. We aimed to evaluate the effectiveness of this method in reducing children's pain and anxiety during infiltrative anesthesia.

Materials and Methods
This was a double-blinded, randomized, split-mouth, controlled, trial. Thirty 6 to 12-year-old children with decayed first permanent molar tooth on both sides of their maxilla were enrolled. Each side of the children's mouths was randomly allocated to either BUZZY or topical anesthetic gel prior to infiltrative anesthesia. Pain and anxiety during infiltrative anesthesia were measured with the Baker-Wong (BWS), FLACC (Face, Leg, Activity, Cry, Consolability), and heart rate (HR) scales.

Results
A generalized estimating equation (GEE) adjusted for age and baseline HR, indicated, significantly-lower intra-procedural HRs associated with BUZZY (aOR [95%CI]: 0.02 [0.00, 0.91], p=0.04). GEEs adjusted for age revealed the BWS (aOR [95%CI]: 0.59 [0.30, 1.14], p=0.12) and FLACC (aOR [95%CI]: 0.82 [0.62, 1.09], p=0.17) scores to be comparable between the study arms.

Conclusion
Our study failed to demonstrate the superiority of BUZZY over anesthetic gels regarding WBS and FLACC measures of pain and anxiety, but demonstrated a decrease in HR associated with BUZZY.

Keywords: Pediatric dentistry, dental anxiety, behavioral control, pain, vibration

Introduction

Pain management, particularly in pediatric populations, is a challenging aspect of a wide range of practices. Appropriate management of pain in pediatric patients is crucial for providing appropriate and timely interventions; this is subject to an appropriate understanding of the mechanisms underlying pain itself. The gate control theory, proposed by Melzack and Wall in 1965 (1), provides a theoretical framework according to which, the perception of pain is not solely determined by nociceptive input, but other inputs such as the ones from vibration and temperature receptors as well as psychological, social, and environmental factors resemble controlling a gate through which the pain inputs pass and by which could be modified. This theory offers valuable insights into how pain can be effectively managed, especially in children. Furthermore, appropriate identification and assessment of the degree pain are necessary for its proper management;

Reyhaneh Faghihian[1] (iD),
Mohammad Moin Tofighi[2] (iD),
Sanaz Ziaei[1] (iD),
Sayed Lotfollah Afzali[3] (iD)

ORCID IDs of the authors: R.F. 0000-0002-5115-6940; M.M.T. 0000-0001-9957-8627; S.Z. 0000-0003-3345-0676; S.L.A. 0000-0002-4444-5760

[1]Dental Research Center, Department of Pediatric Dentistry, Dental Research Institute, Isfahan University of Medical Sciences, Isfahan, Iran

[2]Student Research Center, School of Dentistry, Isfahan University of Medical Sciences, Isfahan, Iran

[3]Department of Surgery, School of Medicine, Shahrekord University of Medical Sciences, Shahrekord, Iran

Corresponding Author: Sanaz Ziaei

E-mail: sanazziaei90@yahoo.com

in pediatric practice this could be performed via subjective measures such as the Wong-Baker Scale (WBS), and objective ones such as physiological measures e.g., the heart rate and behavioral measures such as the face, legs, activity, cry, consolability (FLACC) scale. Each of these standardized measures provides a unique insight on patients' perception of pain, and are used in current research and practices.

Non-pharmacological interventions exist aimed at alleviating pain based on the gate control theory. For instance, previous studies have shown, pain thresholds increase when skin temperature is reduced to 4°C (2, 3). Furthermore, besides the gate control theory, which states non-painful stimuli reduce the transmission of pain signals, this phenomenon could be explained by reduced sensitivity of terminal neurons, reduced edema, and slowing of signal transmission through nerves, due to vasoconstriction(4). A similar effect is observed for vibration; according to the gate control theory, activation of mechanoreceptors by external vibration, leads to blocking of the pain signals in the spinal cord, and/or their diversion to the spino-thalamic fibers (5-9).

The mentioned phenomena have been used, as bases of non-pharmacological management of injection-associated pain and/or anxiety, particularly in pediatric practices. For instance, Mohiuddin *et al*. (2) demonstrated that pre-cooling of the injection site with ice is more effective than topical anesthetic gel in reducing the pain perception in child (8–12 years) candidates of infiltration anesthesia and Albouni *et al*. (10) showed in a more recent study that a vibrating injection system reduces pain perception in child (6–9 years) candidates of intraoral injection. Consistently, simultaneous cooling and vibration has been shown to be effective as well, as indicated by Bilsin *et al*. (11) and a recent study by Nagpal *et al*. (12) demonstrated this effectiveness further increases by addition of a sound distraction. Yet, contrary evidence also exists, e.g., Smolarek *et al*. (13) conclude from their recent study on 5–8-year-old candidates of dental procedures that the vibrational technique is not associated with a reduced pain perception compared to the conventional method.

Among devices currently available that utilize "cold and vibration" for means of reduction of injection-associated pain/anxiety in pediatrics, VibraJect (VJ), DentalVibe (DV) and BUZZY could be cited (9). Among all, BUZZY (Pain Care Labs, USA) applies external vibration and cold simultaneously on the injection site. The device has a bee-like plastic body to transfer vibration, with a "wing" part accommodating 18 grams of ice, to apply cold (Figure 1). Furthermore, BUZZY has an attractive appearance to distract the child's attention during injection, and only a handful of contraindications exist regarding its use (8). Regarding the real-world effectiveness of BUZZY in reducing injection-associated pain/anxiety of children, results of previous studies have been contrary; the effectiveness seems to vary based on site of injection, and its type (14, 15). Particularly in pediatric dentistry, Faghihian *et al*. (16) concluded that inadequate data is available on the effectiveness of BUZZY in controlling injection pain, in their systematic review and meta-analysis study. Therefore, we aimed to contribute to the knowledge in this regard, with level-I evidence from a randomized trial. The null hypothesis is that there is no difference between the two anesthesia techniques.

Figure 1. BUZZY device and its use in pediatric dentistry. (Images from: dentaquick.com).

Materials and Methods

Study design, outcomes, and measurements

Herein reported in accordance with the CONSORT statement, is a double-blinded, randomized, split-mouth, active comparator-controlled, trial, with a 1:1 allocation ratio, conducted from 20 August 2021, until 20 December 2021, on children aged 6-12 years admitted to the clinics of the Isfahan Dental School, Isfahan, Iran. Participants were enrolled, whereby they met the following inclusion criteria: age from 6 to 12 years; adequate cooperation, with positive (+) or completely positive (++) Frankl classification; having first permanent molar tooth decayed on both sides of maxilla, requiring class I cavity preparation; being otherwise healthy, with no history of prior toothache and dental treatment; and no active use of painkillers and/or sedatives at the time of enrollment.

Participants were excluded after randomization, if any pathology and/or inflammation was discovered later in the face and/or the injection site; and/or if they were absent for the study procedures.

The primary outcome was pain during local anesthesia infiltration, measured by the following: the WBS, which is a subjective scale of pain; and the FLACC scale, which is an objective scale.

The WBS comprises 6 painted faces, each demonstrating a level of pain. Immediately after the injection, the child participant was asked to point to a face which demonstrates his/her subjective feeling of pain. The child's pain is then scored from 0 to 10, with 0 being the least, and 10 being the most severe pain.

In the FLACC scale, the pain, as demonstrated through involuntary movements and behaviors of the child during the painful procedure, is scored in accordance with a respective table. Score 0 suggests no pain, 1–3 shows mild pain, 4–6 indicates moderate pain, and 7–10 shows severe pain. The FLACC scores were assessed by a professional, based on video recordings of the procedures, whereby the sound was turned off for measuring of face, legs, and activity scores, and the sound was turned on for measuring of cry, and consolability scores.

Furthermore, the child's anxiety comprised a secondary outcome, measured by child's heart rate 5 minutes before, during, and 5 minutes after the painful procedure, monitored using a pulse oximeter device (Beurer PO80, Berlin Germany), in contact with the index finger of the children's left hand.

Sampling, randomization, and blinding

The sample size of 30 for each group was measured in order to detect significant difference for a type I error of 0.05 and power 0.8. Aiming to compensate for loss during follow-up, the sample size was increased by 36 percent, therefore a sample size of 41 was planned.

The recruitment of participants was from the clinics of the Isfahan Dental School, and in a simple random fashion. Randomization was in a split-mouth fashion with a 1:1 allocation ratio, with each side of each participant's mouth allocated to one of the study arms based on the results of an online coin flipper. Participants underwent their dental procedures in two sessions separated by a two-week interval, each session on one of the mouth sides.

The researchers, and the participants were all blinded to the results of random allocation. Random allocations and execution of procedures were done by a third person not involved in the study. Furthermore, the camera used for recording of treatment sessions was placed out of the child's vision, and recorded all procedures from the same angle. In order to further ensure blindness of the participants and the researchers, the BUZZY device (Pain Care Labs, USA) was placed on the child's face in all procedures, but it was turned off in the procedures of the comparator arm.

Intervention and comparator

The intervention arm underwent placement of BUZZY on the respective side of the face, with cold temperature, and vibration turned on, from two minutes before, until after infiltration of 1.8 ml lidocaine + 1:80,000 epinephrin. The comparator arm underwent placement of BUZZY on the respective side of the face, with ambient temperature, and vibration turned off, from two minutes before, until after infiltration of 1.8 ml lidocaine + 1:80,000 epinephrine, along with administration of a topical anesthetic gel (Benzocaine 20%, Prime Dental Gel) 30 seconds before the infiltration.

Statistical analysis

Data was analyzed in a per-protocol fashion, as outcome measurement was not possible for participants who were lost to follow up. Normality and/or lognormality of distributions were tested using the Kolmogorov–Smirnov method. Accordingly, continuous variables with normal distribution of measures were reported with mean and standard deviation (SD), and continuous variables without normal distribution were reported with median and range, and nominal variables were reported with count and percentage. Appropriate (non)parametric tests were used for comparisons involving study variables. Generalized estimating equations (GEE), adjusted for age were used to evaluate the adjusted effect of the BUZZY in comparison to active comparator; results were reported as adjusted odds ratio (aOR) along a 95% confidence interval (CI). Statistical analyses were carried out using SPSS IBM 25 software (IBM SPPS, Armonk, NY, USA) and p-value equal or below 0.05 was considered as the criterion of rejection of the null hypothesis.

Ethics, trial registration, and data availability

This study was approved by the research ethics committee (REC) of Isfahan University of Medical Sciences (approval ID: IR.MUI.RESEARCH.REC.1400.115), and was registered prospectively in the Iranian Registry of Clinical Trials (registration ID: IRCT20111219008458N3, 03/08/2021). The datasets originating from the current study are available upon request of qualified investigators, subject to approval of the REC of Isfahan University of Medical Sciences.

Results

As seen from the CONSORT flow diagram (Figure 2), a total of 44 children were assessed for eligibility, among whom, 41 underwent randomization. Of whom, 30 completed the study; they had a mean age (SD) of 8.9 (1.9) years, and 16 (53.3%) were girls. The baseline characteristics of the children and the measured outcomes in each group can be interpreted from Table 1. Moreover, no harms and/or unintended adverse effects were observed in either group. Furthermore, compared to active control, i.e., topical anesthetic
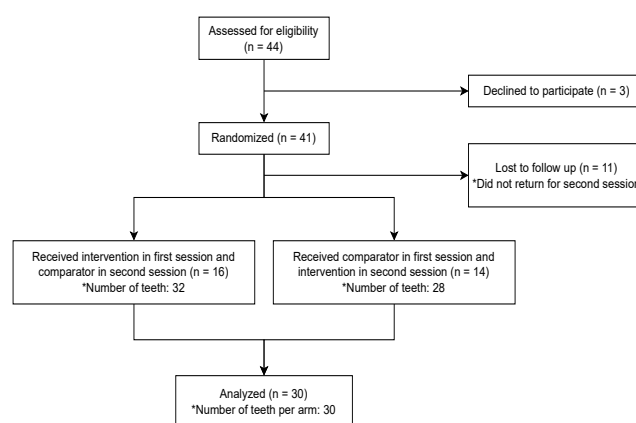
Figure 2. *CONSORT flow diagram.*

Table 1. *General demographics and outcomes.*

	Participants (n = 30)		
Mean age (SD)	8.9 (1.9)		
Female sex (n, %)	16 (53.3%)		
Study arm	BUZZY (n=30)	Topical Anesthetic Gel (n=30)	P-value
Mean heart rate (SD)			
• Before injection	104.0 (12.2)	100.8 (11.1)	0.06*
• During injection	107.7 (9.6)	109.9 (12.0)	0.33*
Median FLACC score (Range)	1 (0–3)	1 (0–4)	0.19**
Median Wong-Baker score (Range)	0 (0–8)	2 (0–10)	0.17**

Abbreviations: SD, standard deviation; FLACC, Face, Leg, Activity, Cry, Consolability scale.
* From paired samples T-test.
** From related-samples Wilcoxon signed rank test.

gel, a GEE adjusted for age and baseline heart rate, showed that usage of BUZZY is associated with significantly lower heart rates during the infiltration procedure (aOR [95%CI]: 0.02 [0.00, 0.91], P=0.04), yet, GEEs adjusted for age, showed that usage of BUZZY is associated with an insignificantly-decreased WBS (aOR [95%CI]: 0.59 [0.30, 1.14], P=0.12) and FLACC scores (aOR [95%CI]: 0.82 [0.62, 1.09], P=0.17) during the infiltration procedure.

Discussion

Our study failed to demonstrate the superiority of BUZZY over anesthetic gels regarding WBS and FLACC measures of pain and anxiety, but demonstrated a decrease associated with BUZZY, in the intra-procedural heart rate of child candidates of infiltrative anesthesia of teeth. These results, subject to replication by others, have implications for future practices in the field.

Feeling of pain is affected by different factors e.g., fear, anxiety, previous experiences, personality of the individual, confidence in the dentist; thus, it is difficult to measure (17, 18). Limited verbal communication further complicates the measurement of pain in pediatric practices. To counter this issue, and have an accurate measurement of the severity of pain, we used three different scales to measure the severity of pain, namely, a self-reported (WBS), a behavioral (FLACC scale), and a physiological (heart rate) scale. Regarding the usage of the FLACC scale, it should be noted that this scale is more frequently used, and therefore, optimized for children aged 6 months to 5 years; nevertheless, prior studies that were similar to the present study utilized this scale on children aged 5 to 12 years (10-13, 16, 19). Therefore, in order to maintain consistency and comparability with previous literature, we decided to use the FLACC scale as well.

Furthermore, we used a split-mouth design for the study; unlike parallel designs, this design could account for interpersonal differences that might exist in perception of pain between individuals. In other words, it could not be established whether two parallel group of people experience pain in a similar fashion, yet, it could be argued that the same person's perception of a specific pain in a specific setting remains similar. Nevertheless, the pain perceived in a situation may impact the pain perceived in the same situation in the future; we encountered this issue by splitting the participants into a group that received the intervention first and one that received the comparator first.

The BUZZY device, first invented for needle-related medical practices, has shown to be effective in reducing the pain and anxiety levels of children undergoing medical, needle injections; yet, its real-world effectiveness in dental injections is understudied. Recently, Faghihian *et al*. (19) and Sahiti *et al*. (17) demonstrated an additional level of pain reduction, associated with using the BUZZY device, in comparison to cold alone or counter simulation alone. Yet, our study hints that this additional level of pain reduction is not superior to using anesthetic gels, as per routine in dental injections. It could be argued that the vibrating device itself, along the vibrations and the sounds it produces, may be perceived as pain and increase the children's anxiety, thereby cancelling out the effects that it might have through stimulating temperature and vibration receptors. Furthermore, the topical anesthetic gels may also decrease the temperature of the site, thereby having a similar effect with the device. These points remain to be studied in the future, since they were not investigated in the present study.

Additionally, our study was limited in some aspects, including the number of participants, high loss to follow up, inclusion of only cooperative patients, and absence of minority populations. Particularly, whether the high loss to follow-up rate was associated with the intervention was not investigated, yet, this is deemed unlikely, since a split-mouth design was used, and the rate was similar between the participants in the intervention first and the ones in the comparator first arms. Nevertheless, further evidence is still warranted, to be used for evidence-driven practices. Future studies are encouraged to account for our limitations, especially the ones described supra.

Conclusion

Our study failed to demonstrate the superiority of BUZZY over anesthetic gels regarding WBS and FLACC measures of pain and anxiety, but demonstrated a decrease in HR associated with BUZZY.

Türkçe özet: *Pediatrik diş hekimliğinde infiltratif anestezi ile ilişkili ağrı ve anksiyete için topikal anestezik jelle BUZZY ile dışsal soğuk ve titreşim yönteminin karşılaştırıkması: çift kör, split mouth, randomize, kontrollü çalışma. Amaç: Enjeksiyon ağrısını azaltmanın bir yolu, omurilik kapı kontrol sistemleriyle birlikte BUZZY ile dışsal soğuk veya titreşim uygulamaktır. Bu yöntemin çocukların infiltratif anestezi sırasında ağrı ve anksiyetelerini azaltmada etkinliğini değerlendirmeyi amaçladık. Denekler ve Yöntem: Bu, çift kör, randomize, split mouth, kontrollü bir çalışmaydı. Maksillalarının her iki tarafında çürümüş birinci daimi molar dişi olan 6 ila 12 yaş arasındaki otuz çocuk çalışmaya dahil edildi. Çocukların ağızlarının her iki tarafı, infiltratif anesteziden önce rastgele olarak ya BUZZY ya da topikal anestezik jel gruplarına ayrıldı. İnfiltratif anestezi sırasında ağrı ve anksiyete, Baker-Wong (BWS), FLACC (Yüz, Bacak, Aktivite, Ağlama, Teselli Edilebilirlik) ve kalp atış hızı (HR) ölçekleri ile ölçüldü. Sonuçlar: Yaşa ve başlangıç HR'sine göre ayarlanan genelleştirilmiş tahmin denklemi (GEE), BUZZY ile ilişkili olarak anlamlı derecede daha düşük işlem içi HR'ler olduğunu gösterdi (aOR [95%CI]: 0.02 [0.00, 0.91], p=0.04). Yaşa göre düzeltilmiş GEE'ler, BWS (aOR [95%CI]: 0.59 [0.30, 1.14], p=0.12) ve FLACC (aOR [95%CI]: 0.82 [0.62, 1.09], p=0.17) puanlarının çalışma kolları arasında karşılaştırılabilir olduğunu ortaya koydu. Sonuç: Çalışmamız, ağrı ve anksiyetenin BWS ve FLACC ölçümleri açısından BUZZY'nin anestezik jeller karşısındaki üstünlüğünü gösteremedi, ancak BUZZY ile ilişkili olarak HR'de bir azalma gösterdi. Anahtar kelimeler: pediatrik diş hekimliği, diş anksiyetesi, davranış kontrolü, ağrı, titreşim*

has reviewed the pertinent raw data on which the results and conclusions of this study are based. RF, MMT, SZ, SLA have approved the final version of this paper. SZ guarantees that all individuals who meet the Journal's authorship criteria are included as authors of this paper.

References

1. Melzack R, Wall PD. Pain mechanisms: A new theory: A gate control system modulates sensory input from the skin before it evokes pain perception and response. Science 1965;150:971-9. [CrossRef]

2. Mohiuddin I, Setty JV, Srinivasan I, Desai JA. Topical application of local anaesthetic gel vs ice in pediatric patients for infiltration anaesthesia. Journal of Evolution of Medical and Dental Sciences 2015;4:12934-41. [CrossRef]

3. Nahra H, Plaghki L. Innocuous skin cooling modulates perception and neurophysiological correlates of brief co2 laser stimuli in humans. European Journal of Pain 2005;9:521-30. [CrossRef]

4. Moayedi M, Davis KD. Theories of pain: From specificity to gate control. J Neurophysiol 2013;109:5-12. [CrossRef]

5. Hegde KM, Neeraja R, Srinivasan I, DR MK, Melwani A, Radhakrishna S. Effect of vibration during local anesthesia administration on pain, anxiety, and behavior of pediatric patients aged 6–11 years: A crossover split-mouth study. Journal of dental anesthesia and pain medicine 2019;19:143-9. [CrossRef]

6. İnal S, Kelleci M. The effect of external thermomechanical stimulation and distraction on reducing pain experienced by children during blood drawing. Pediatric Emergency Care 2020;36:66-9. [CrossRef]

7. Shilpapriya M, Jayanthi M, Reddy VN, Sakthivel R, Selvaraju G, Vijayakumar P. Effectiveness of new vibration delivery system on pain associated with injection of local anesthesia in children. Journal of Indian Society of Pedodontics and Preventive Dentistry 2015;33:173-6. [CrossRef]

8. Yilmaz G, Alemdar DK. Using buzzy, shotblocker, and bubble blowing in a pediatric emergency department to reduce the pain and fear caused by intramuscular injection: A randomized controlled trial. Journal of Emergency Nursing 2019;45:502-11. [CrossRef]

9. Raslan N, Masri R. A randomized clinical trial to compare pain levels during three types of oral anesthetic injections and the effect of dentalvibe on injection pain in children. International Journal of Paediatric Dentistry 2018;28:102-10. [CrossRef]

10. Albouni MA, Kouchaji C, Al-Akkad M, Voborna I, Mounajjed R. Evaluation of the injection pain with the use of vibraject during local anesthesia injection for children: A randomized clinical trial. J Contemp Dent Pract 2022;23:749-54. [CrossRef]

11. Bilsin E, Güngörmüş Z, Güngörmüş M. The efficacy of external cooling and vibration on decreasing the pain of local anesthesia injections during dental treatment in children: A randomized controlled study. J Perianesth Nurs 2020;35:44-7. [CrossRef]

12. Nagpal D, Amlani DV, Rathi P, Hotwani K, Singh P, Lamba G. Effect of audio distraction with thermomechanical stimulation on pain perception for inferior alveolar nerve block in children: A randomized clinical trial. J Dent Anesth Pain Med 2023;23:327-35. [CrossRef]

13. Smolarek PC, da Silva LS, Martins PRD, Hartman KDC, Bortoluzzi MC, Chibinski ACR. Evaluation of pain, disruptive behaviour and anxiety in children aging 5-8 years old undergoing different modalities of local anaesthetic injection for dental treatment: A randomised clinical trial. Acta Odontol Scand 2020;78:445-53. [CrossRef]

14. Lescop K, Joret I, Delbos P, Briend-Godet V, Blanchi S, Brechet C, Galivel-Voisine A, Coudol S, Volteau C, Riche V-P. The effectiveness of the buzzy® device to reduce or prevent pain in children undergoing needle-related procedures: The results from a prospective, open-label, randomised, non-inferiority study. International journal of nursing studies 2021;113:103803. [CrossRef]

15. Moadad N, Kozman K, Shahine R, Ohanian S, Badr LK. Distraction using the buzzy for children during an iv insertion. Journal of pediatric nursing 2016;31:64-72. [CrossRef]

16. Faghihian R, Rastghalam N, Amrollahi N, Tarrahi M. Effect of vibration devices on pain associated with dental injections in children: A systematic review and meta-analysis. Australian Dental Journal 2021;66:4-12. [CrossRef]

17. Sahithi V, Saikiran KV, Nunna M, Elicherla SR, Challa RR, Nuvvula S. Comparative evaluation of efficacy of external vibrating device and counterstimulation on child's dental anxiety and pain perception during local anesthetic administration: A clinical trial. J Dent Anesth Pain Med 2021;21:345-55. [CrossRef]

18. Yesilyurt C, Bulut G, Taşdemir T. Pain perception during inferior alveolar injection administered with the wand or conventional syringe. British dental journal 2008;205:E10. [CrossRef]

19. Faghihian R, Esmaeili M, Asadi H, Nikbakht MH, Shadmanfar F, Jafarzadeh M. The effect of external cold and vibration on infiltration-induced pain in children: A randomized clinical trial. International Journal of Dentistry 2022;2022. [CrossRef]

Original research

In silico prediction of differentially expressed genes and functionally grouped networks in patients with inflamed pulp for screening pulpitis biomarkers

Azizeh Asadzadeh[1] (iD),
Fatemeh Shams Moattar[2] (iD),
Azam Moshfegh[2] (iD)

Purpose
Pulpitis is one of the most common oral inflammatory diseases. There are many limitations in the traditional methods of diagnosing pulpitis. By replacing new diagnostic ways based on biomarkers, it is possible to quickly and accurately identify this disease. Biological indicators have greatly helped not only in the screening of infectious diseases but also in early and appropriate treatment. In this research, differentially expressed genes (DEGs) related to pulpitis were analyzed, and prognostic biomarkers were introduced.

Materials and Methods
In this *in silico* study, we applied the GSE77459 dataset as the gene expression profile of pulpitis. Web tool, GEO2R was used to separate up-regulated and down-regulated DEGs. |logFC|>2 and adjusted p-value < 0.05 was set as the cut-off criterion. For the pathway enrichment study of obtained genes, EnrichR was implemented. After constructing a protein-protein interaction (PPI) network, hub genes that are involved in pulpitis were selected. Finally, functionally grouped networks by ClueGO software (v2.5.10) were generated.

Results
GEO2R analysis of the GSE77459 dataset showed 672 up-regulated genes and 239 down-regulated genes with GB_ACC code. Based on Cytoscape results, the 15 top hubba nodes were ranked including PTPRC, ITGAM, CCL2, ICAM1, MMP9, CXCL8, TLR2, CD86, CXCR4, IL1A, CD44, CCL3, ITGAX, CXCL10, and CCR7. Functionally grouped networks determined that these genes were mainly enriched in chemokine-mediated signaling pathway, morphogenesis of endothelium, and neuroinflammatory response

Conclusion
In our research, 15 genes were introduced as diagnostic biomarkers in pulpitis and their functionally grouped networks were constructed. However, the obtained results need to be validated using in vitro and in vivo methods.

Keywords: Dental pulp, inflammation, gene ontology, DEGs, PPI, Pulpitis

Introduction

Under the dentin is the innermost and vital part of the tooth called the dental pulp (1). This jelly-like center is a mass of connective tissue and the presence of proteins such as albumin, transferrin, tenascin, and other proteoglycans is necessary for its proper function (1, 2). Large nerve trunks and blood vessels in the central area of the pulp play a major role in signaling processes and nerve message transmission. In addition, dentin formation, dentin nutrition, and tooth defense are important functions related to the dental pulp (1-3).

Delay in the treatment of tooth decay leads to damage in the hard tissue of the tooth and various stimuli cause pathological changes in the

dental pulp and surrounding periapical tissues which eventually leads to pulpitis. As a result of uncontrolled inflammation caused by invading bacteria, irreversible pulpitis occurs (4). Based on the degree of pulp inflammation and the importance of tooth preservation, dentists choose different strategies for the treatment of pulpitis such as covering the pulp, staged decay drilling, and pulpotomy (5, 6). To preserve the infected tooth, it is very important to quickly recognize and prescribe appropriate treatment for patients. Traditional methods of diagnosing pulpitis are based on clinical findings and the results of X-rays and pulp vital tests, which have limitations and need to be refined (7).

One of the interesting topics in medical science is the identification of molecular biomarkers for early diagnosis of diseases (8, 9). Diagnostic biomarkers are important in drug selection, treatment response, prevention, and other aspects of biomedicine (10). The use of computer-based methods with high throughput has accelerated the process of analysis. One of the ways to identify molecular biomarkers is using microarray technology and the study of differentially expressed genes (DEGs) between two states (healthy and diseased states) (11, 12). To draw the interaction network of DEGs that reflects specific conditions, and physical interactions on a wide scale, a protein-protein interaction network (PPIN) is used. Cytoscape software constructs a network of all the differentially expressed genes along with the determination of degree, betweenness, and closeness. The number of links of a given node determines its degree centrality. Nodes with a higher degree are considered hub genes (8, 13). To investigate the biological pathways related to these hub genes, functionally grouped network analysis in ClueGO software can be used (14).

There is a lot of evidence that shows the important role of differentially expressed mRNAs (DEMs), miRNAs (DEMIs), and lncRNAs (DELs) in a variety of cellular and pathological processes along with pulpitis. With the RT-qPCR technique, the difference in the expression levels of many mRNAs such as, HMOX1, LOX, ACTG1, STAT3, GNB5 has been proven (15). Previous studies have shown that some miRNAs for example miR-155, miR-21, miR-142, miR-223, miR-486, miR-675 were significantly upregulated in patients with inflamed pulp (16). Further, Huang *et al.* (17) showed that 752 lncRNAs were significantly altered in inflamed pulp samples compared to normal pulp samples, they reported 338 overexpressed lncRNAs and 414 down-regulated lncRNAs. However, detailed research on functionally grouped networks based on key differentially expressed genes seems necessary to study key pathways related to pulpitis. In our research, due to the importance of discovering critical pathways related to pulpitis and an improved method in the early detection of this disease, first key differentially expressed genes related to pulpitis were introduced, and then, functionally grouped network for detected biomarkers was constructed.

Materials and Methods

Microarray data extraction

The workflow chart of data processing and analysis in this study is shown in Figure 1. Microarray data related to patients with inflamed pulp was extracted from a public database called Gene Expression Omnibus (GEO). Based on the key-
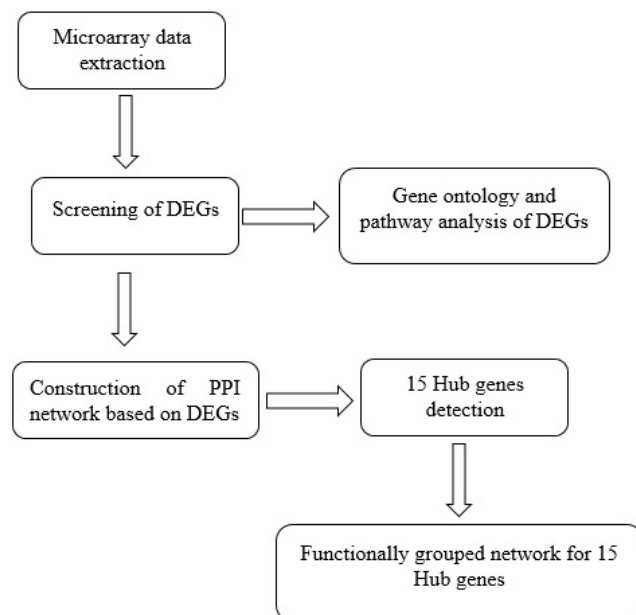
Figure 1. *Flowchart of data processing and analysis.*

words including pulpitis, Homo sapiens in the type of organism part, series in the entry type part, and expression profiling by an array in the study type section, searches were limited.

Screening of DEGs

Screening of DEGs between samples from inflamed pulps, and samples from normal pulps were analyzed via GEO2R (https://www.ncbi.nlm.nih.gov/geo/geo2r). The tool system of GEO2R works using the R language. The normal distribution of data in box plots of this dataset was checked and then, to estimate differentially expressed genes |logFC|>2 and adjusted p-value < 0.05 were regarded as statistically significant.

Gene ontology and KEGG pathway analysis of DEGs

For a more in-depth understanding of the obtained DEGs, Gene ontology and KEGG pathway analysis were carried out by EnrichR. This analysis tool is useful for predicting the most significantly enriched pathways of DEGs in biological processes, molecular functions, cellular components, and human phenotype Ontology.

Construction of PPI network

For PPI network construction, based on the genes that had a significant increase and decrease in expression, STRING v9.1 software in https://string-db.org was used. After selection Homo sapiens in organism type search, DEGs were inserted as multiple proteins. Finally, protein-protein interaction network with a high confidence score ≥ 0.7 was formed. The output file was imported into Cytoscape (v3.9.1) software for more analysis.

Hub genes detection

CytoHubba with free access is a functional section in the menu bar of Cytoscape software that is very helpful in dis-

covering hub protein in protein-protein interaction networks. The basis for identifying key genes in the CytoHubba plugin is the degree, maximum neighborhood component, and other topological analysis parameters. In this research, 15 hub nodes were obtained using this plugin.

Functionally grouped networks for Hub genes

The key genes obtained from the previous step were considered for functionally grouped network studies. The ClueGO software (v2.5.10) was used for this target. This functional software provides a network for hub genes using various original and reliable sources. To deeply investigate the relationship between these genes and pulpitis formation, the pathways with p-values less than 0.05 were filtered.

Results

Microarray data extraction and Screening of DEGs

In our study, accession number GSE77459 was selected as the gene expression profile dataset with inflamed pulp samples for further analysis. GSE77459 which has been studied by the GPL17692 platform (Affymetrix Human Gene 2.1 ST Array) contains 6 samples of irreversible inflamed pulps and 6 samples of normal pulps. Differentially expressed genes that were detected from GSE77459 by GEO2R include 672 upregulated genes and 239 downregulated genes with GB_ACC code. The box plot and volcano plot of this dataset were presented in Figures 2A and 2B.
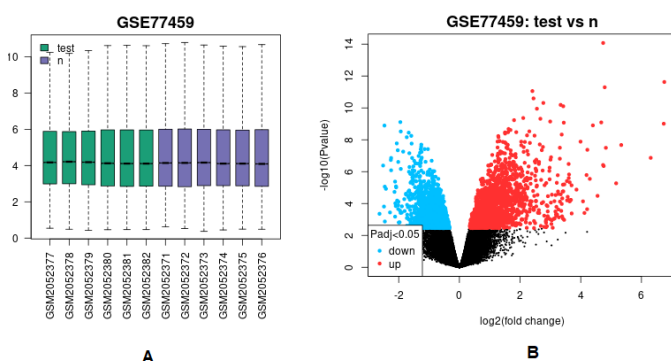
Figure 2. *A: The box plot of GSE77459; B: Volcano plot of GSE77459.*

Gene ontology and pathway analysis of DEGs

Based on GO biological process, the differentially expressed genes were enriched in Cytokine-Mediated Signaling Pathway (GO:0019221), Inflammatory Response (GO:0006954), Neutrophil Chemotaxis (GO:0030593), Granulocyte Chemotaxis (GO:0071621), Neutrophil Migration (GO:1990266), Cellular Response To Lipopolysaccharide (GO:0071222). Kyoto encyclopedia of genes and genomes (KEGG) analysis showed, Cytokine-cytokine receptor interaction, Viral protein interaction with cytokine and cytokine receptor, Chemokine signaling pathway, TNF signaling pathway, Staphylococcus aureus infection, and Cell adhesion molecules are major pathways in which DEGs are involved. The P-value, adjusted P-value, odds Ratio, and Combined score of each pathways are shown in Table 1 and 2.

Construction of PPI network and hub genes detection

The protein network generated by STRING v9. 1 was visualized with Cytoscape software. This network consists of 564 nodes and 6704 edges (Figure 3). After calculating the score of each node by the CytoHubba plugin, 15 hub genes were screened. The 15 top hubba nodes were ranked based on the degree including PTPRC, ITGAM, CCL2, ICAM1, MMP9, CXCL8, TLR2, CD86, CXCR4, IL1A, CD44, CCL3, ITGAX, CXCL10, and CCR7. In this selection, the criterion above 102 was considered. The gene symbols, scores, and ranks of each gene are shown in Table 3.

Functionally grouped network for Hub genes

Functional annotation of the hub genes is shown in Figure 4. hub genes were analyzed by ClueGO software (v2.5.10). The output file was a network with 3 groups (PV < 0.05). chemokine-mediated signaling pathway, morphogenesis of endothelium, and neuroinflammatory response were 3 major groups in this network.

Discussion

The presence of microorganisms in the pulp space causes pulpitis (18). The progress of infection in the dental pulp stimulates the pain receptors causing a pain response which is the main reason for emergency visits to dentists (19). Early diagnosis of inflamed pulp is very important to provide appropriate treatment. Biological markers are measurable parameters and are important indicators for checking normal conditions. Like any other inflammation, pulpitis is accompanied by changes in biological molecules (20-22). These biological differences between healthy and inflamed dental pulp can be the basis of rapid diagnosis. Due to the lack of a reliable reference standard in the diagnosis of pulpitis, the identification of new biomarkers, along with previous methods, can be a suitable strategy for the diagnosis of inflamed pulp before reaching the stage of experiencing progressive and devastating pain (22). In this study, differentially expressed genes (DEGs), PPI networks, and hub genes were investigated by analyzing and comparing the expression matrix of genes in the inflamed pulp. Finally, prognostic biomarkers and functionally grouped networks were introduced.

In our study, in order to compare differentially expressed genes between healthy and inflamed dental pulp, the gene expression profile dataset with accession number GSE77459 was analyzed and 672 upregulated genes and 239 downregulated genes were identified. Among differentially expressed genes, The 15 top hubba nodes were detected as diagnostic biomarkers including PTPRC, ITGAM, CCL2, ICAM1, MMP9, CXCL8, TLR2, CD86, CXCR4, IL1A, CD44, CCL3, ITGAX, CXCL10, and CCR7.

The activity of most obtained genes is related to inflammatory responses. Tyrosine phosphatase receptor type C (PTPRC) is a transmembrane glycoprotein that has important roles in the regulatory processes of cell growth, differentiation, mitosis, and transformation. PTPRC is also known as CD45 (23, 24). An increase in CD45 indicates activation of one or more inflammatory conditions (25). Integrin alpha

Table 1. *Gene ontology results of DEGs.*

Term	P-value	Adjusted P-value	Odds Ratio	Combined Score	Genes
Cytokine-Mediated Signaling Pathway (GO:0019221)	5.89E-34	1.51E-30	11.64114	890.7257	CNTFR;CXCL6;CSF3;PLVAP;CXCL9; SPI1;CSF3R;CXCL8;CXCL1;CXCL13; CXCL3;CXCL2;CXCL5;OASL;GHR;IL6R; PF4V1;CCR2;FCER1G;SYK;IL18;OSMR; TNFRSF1B;EREG;HCK;IL1A;CEACAM1; AIM2;KIT;IL3RA;BIRC3;CSF2RB;IL2RG; CSF2RA;CCL4;STAT4;CCL3;CCL2; CD300LF;LYN;EGR1;IL33;CCL23; CCL21;CCL20;OSM;LILRB1;PPBP; CXCL10;CXCL11;LEP;PTPN6;PF4
Inflammatory Response (GO:0006954)	1.96E-28	2.51E-25	10.68248	681.5376	CXCL6;CXCL9;CXCL8;C5AR1; FPR1; CXCR4;PIK3CD;FPR3;CXCL1; HPR;F11R; CXCL13;CXCL3;ITGAL;CXCL2; CXCL5;CCL4;CCL3;CCL2;CCR7; PF4V1;CMKLR1;CCR2;CD96; CCL23;CCL21;CCL20;SLC11A1; NFAM1;IL18;CYBB;PPBP;FOS; TACR1;SELE;IL1A;CXCL10; CXCL11;KIT;CHI3L1;ACKR1; S100A9;CD44;S100A8;TLR2;PF4
Neutrophil Chemotaxis (GO:0030593)	2.81E-27	2.40E-24	28.47076	1740.634	CXCL6;CXCL9;CXCL8;PIK3CD; CXCL1;CXCL13;CXCL3;CXCL2; TREM1;CXCL5;CXCR1;CCL4; CCL3;CCL2;PF4V1;EDN1;CCL23; FCER1G;SYK;CCL21;CCL20;PPBP; CXCL10;CXCL11;JAML;S100A9; S100A8;PF4
Granulocyte Chemotaxis (GO:0071621)	1.15E-26	7.37E-24	26.56862	1586.856	CXCL6;CXCL9;CXCL8;PIK3CD; CXCL1;CXCL13;CXCL3;CXCL2; TREM1;CXCL5;CXCR1;CCL4; CCL3;CCL2;PF4V1;EDN1;CCL23; FCER1G;SYK;CCL21;CCL20;PPBP; CXCL10;CXCL11;JAML;S100A9; S100A8;PF4
Neutrophil Migration (GO:1990266)	6.72E-26	3.44E-23	24.39474	1413.957	CXCL6;CXCL9;CXCL8;PIK3CD;CXCL1;CXCL13;CXCL3; CXCL2;TREM1;CXCL5;CXCR1;CCL4;CCL3;CCL2;PF4V1; EDN1;CCL23;FCER1G;SYK;CCL21;CCL20;PPBP;CXCL10; CXCL11;JAML;S100A9;S100A8;PF4
Cellular Response To Lipopolysaccharide (GO:0071222)	4.09E-24	1.75E-21	14.94729	804.9457	CD86;CD274;CXCL6;CXCL9;CXCL8;CD80;SERPINE1; TNFAIP3;CXCL1;PTPN22;CXCL13;CXCL3;CXCL2;CXCL5; PLCG2;CCL3;SIRPA;CCL2;PF4V1;LYN;IL18;LILRB1; NR1D1;PPBP;TNFRSF1B;CXCL10;HCK;IL1A;CXCL11; CARD16;CD68;PF4

M (ITGAM) also known as CD11b, is expressed in myeloid and lymphoid cells. Expression of CD11b increase in monocytes in inflammatory response (26). C-C chemokine ligand 2 (CCL2) is produced in response to pro-inflammatory cytokines and increased in inflamed dental pulp (27). Among Glycosylated proteins on the surface of endothelial cells and immune cells that are up-regulated in inflamed tissue is intercellular adhesion molecule 1 (ICAM1) which binds to integrins (28, 29). Matrix metalloproteinase 9 (MMP9) is involved in the proteolysis of the extracellular matrix as well as the migration of leukocytes (30). Sharma *et al.* (31) reported that MMP-9 is a potential prognostic biomarker in patients with irreversible pulpitis. C-X-C Motif Chemokine Ligand 8 (CXCL8) acts as a primary cytokine in the inflammation site for neutrophil recruitment. In a study conducted by Karapanou *et al.* (32) the concentration of CXCL8 in gingival crevicular fluid (GCF) samples in pulpal inflammation was investigated and the increase of this inflammatory factor was confirmed (33). Gram-positive bacteria in the pulp area cause the activation and increase of Toll-Like Re-

Table 2. *KEGG pathway assessment of DEGs.*

Term	P-value	Adjusted P-value	Odds Ratio	Combined Score	Genes
Cytokine-cytokine receptor interaction	5.85E-26	1.47E-23	8.588493	498.9977	CNTFR;CXCL6;IL1RN;CSF3;CXCL9;CSF3R;CXCL8; CXCR4;CSF2RB;CXCL1;CXCL13;CXCL3; IL2RG; CSF2RA;CXCL2;CXCL5;TNFSF13B;GHR; CXCR1;CXCR3;CCL4;TNFSF10;CCL3; TNFRSF17;CCL2;CCR7;IL6R;PF4V1; CCR2;IL33;CCL23;CCL21;CCL20;IL1R2; IL10RA;LIF;IL18;OSM;IL16;PPBP;OSMR; TNFRSF1B;IL1A;CXCL10;CXCL11;LEP;IL3RA;PF4
Viral protein interaction with cytokine and cytokine receptor	8.24E-25	1.04E-22	18.35683	1017.994	CXCL6; CXCL9;CXCL8;CXCR4;CXCL1;CXCL13;CXCL3;IL2RG; CXCL2;CXCL5;CXCR1;CXCR3;CCL4;TNFSF10;CCL3;CCL2;CCR7; IL6R;PF4V1;CCR2;CCL23;CCL21;CCL20;IL10RA;IL18;PPBP; TNFRSF1B;CXCL10;CXCL11;PF4
Chemokine signaling pathway	7.21E-22	4.54E-20	9.972527	485.4778	CXCL6;CXCL9;CXCL8;ADCY4;PIK3CD;CXCR4;CXCL1;ARRB2; CXCL13;CXCL3;CXCL2;CXCL5;PIK3R5;CXCR1;CXCR3;CCL4; PLCG2;RAC2;CCL3;CCL2;CCR7;PF4V1;CCR2;LYN;CCL23;CCL21; CCL20;PPBP;FGR;CXCL10;HCK;CXCL11;ELMO1;DOCK2; PLCB2;PF4
TNF signaling pathway	1.45E-18	7.29E-17	12.82573	526.8552	CXCL6;PIK3CD;TNFAIP3;CXCL1;CXCL3;PTGS2;CXCL2;CXCL5; ICAM1;SOCS3;CASP10;CCL2;JUNB;MAP2K6;EDN1;MLKL; RIPK3;CCL20;LIF;FOS;TNFRSF1B;SELE;MMP9;CXCL10; BCL3;BIRC3
Staphylococcus aureus infection	6.95E-16	2.50E-14	12.68297	442.6667	ITGAM;SELPLG;C5AR1;CFI;PTAFR;FPR1;FPR3;ITGAL;FCAR; ICAM1;C2;C4B;C3;C4A;HLA-DMA;HLA-DMB;FCGR2A; HLA-DRA;HLA-DOA;FCGR1A;HLA-DOB;HLA-DQA1
Cell adhesion molecules	2.05E-15	6.47E-14	9.02434	305.1966	CD86;CD274;ITGAM;SELPLG;CD80;NRXN1;ICAM2;F11R; ITGAL;ICAM1;SPN;CDH5;HLA-DMA;HLA-DMB;CTLA4; HLA-DOA;ICOS;HLA-DOB;HLA-DQA1;HLA-B;SELE;CLDN5; PTPRC;SELL;CNTN1;HLA-DRA
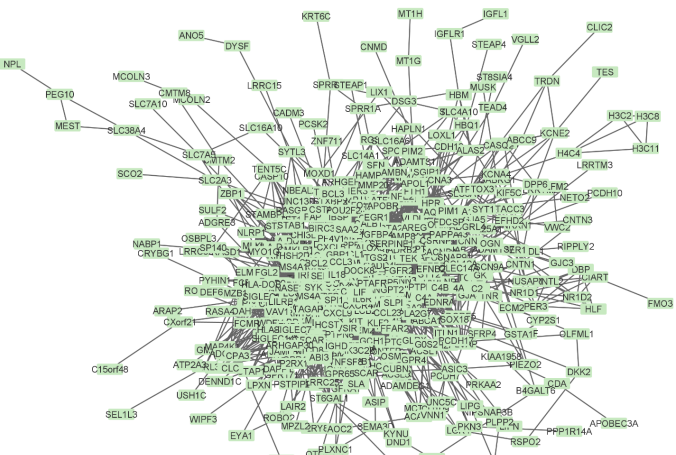
Figure 3. *Protein-protein interaction network of DEGs.*

Figure 4. *Functionally grouped network for Hub genes.*

ceptor 2 (TLR2) expression in adult mice with infected pulp (34). Cluster of Differentiation 86 (CD86) is expressed by macrophages and B lymphocytes which play an essential role in the inflammation (35).

So far, many studies have been conducted on pulpitis biomarkers. Chen *et al.* (36) merged two datasets and reported hub nodes from the common genes of two profiles. In their study, 8 diagnostic biomarker candidates were reported which include PTPRC, CD86, CCL2, IL6, TLR8, MMP9, CXCL8, and ICAM1. In our research, the hub genes of one microarray gene expression dataset related to pulpitis were

subjected to ClueGO software (v2.5.10) for functionally grouped network determination. Based on this network, our hub genes) PTPRC, ITGAM, CCL2, ICAM1, MMP9, CXCL8, TLR2, CD86, CXCR4, IL1A, CD44, CCL3, ITGAX, CXCL10, and CCR7 (were mainly enriched in the chemokine-mediated signaling pathway, morphogenesis of endothelium, and neuroinflammatory response. Detection of target proteins in new drug development is the major challenge. These hub genes can be useful not only in the screening of Pulp inflammation, they can provide some new ideas for further research such as therapeutic drug development for clinical application.

Table 3. *Ranks, Score, gene symbol of the top 15 hub genes that screened with CytoHubba plugin.*

ranks	1	2	3	4	5	6	7	8	9	10	11	12	13	14	15
Score	173	152	134	132	129	126	122	120	110	109	105	105	105	104	102
gene symbol	PTPRC	ITGAM	CCL2	ICAM1	MMP9	CXCL8	TLR2	CD86	CXCR4	IL1A	CD44	CCL3	ITGAX	CXCL10	CCR7
Description	protein tyrosine phosphatase receptor type C	Integrin Subunit Alpha M	C-C chemokine ligand 2	Intercellular Adhesion Molecule 1	Matrix Metallo peptidase 9	C-X-C Motif Chemokine Ligand 8	Toll Like Receptor 2	Cluster of Differentiation 86	C-X-C Motif Chemokine Receptor 4	Interleukin 1 alpha	Cluster of Differentiation 44	C-C Motif Chemokine Ligand 3	(Integrin Subunit Alpha X	C-X-C Motif Chemokine Ligand 10	C-C chemokine receptor type 7

Conclusion

In this study after analyzing the GSE77459 dataset in the GEO database, the 15 biomarker were detected. Functionally grouped networks show these genes were mainly enriched in pathways related to inflammatory responses. However, the obtained results need to be validated by in vitro and in vivo methods.

Türkçe özet: *Pulpitis biyobelirteçlerini taramak için iltihaplı pulpalı hastalarda diferansiyel olarak eksprese edilen genlerin ve fonksiyonel olarak gruplandırılmış ağların silico tahmini Amaç: Pulpitis en sık görülen oral inflamatuar hastalıklardan biridir. Pulpitis tanısının geleneksel yöntemlerinde birçok sınırlama vardır. Biyobelirteçlere dayalı yeni tanı yöntemlerinin değiştirilmesiyle bu hastalığın hızlı ve doğru bir şekilde tanımlanması mümkün olmaktadır. Biyolojik göstergeler sadece bulaşıcı hastalıkların taranmasında değil, aynı zamanda erken ve uygun tedavide de büyük ölçüde yardımcı olmuştur. Bu araştırmada pulpitis ile ilgili diferansiyel olarak eksprese edilen genler (DEG'ler) analiz edilmiş ve prognostik biyobelirteçler tanıtılmıştır. Gereç ve yöntem: Bu in silico çalışmasında, pulpitisin gen ekspresyon profili olarak GSE77459 veri setini uyguladık. Web aracı GEO2R, yukarı regüle edilmiş ve aşağı regüle edilmiş DEG'leri ayırmak için kullanıldı. |logFC|>2 ve düzeltilmiş p değeri < 0,05 kesme kriteri olarak belirlendi. Elde edilen genlerin yol zenginleştirme çalışması için EnrichR uygulandı. Bir protein-protein etkileşimi (PPI) ağı oluşturulduktan sonra pulpitiste rol oynayan merkez genler seçildi. Son olarak, ClueGO yazılımı (v2.5.10) tarafından işlevsel olarak gruplandırılmış ağlar oluşturuldu. Bulgular: GSE77459 veri setinin GEO2R analizi, GB_ACC kodlu 672 yukarı regüle edilmiş gen ve 239 aşağı regüle edilmiş gen gösterdi. Cytoscape sonuçlarına göre, en iyi 15 hubba düğümü PTPRC, ITGAM, CCL2, ICAM1, MMP9, CXCL8, TLR2, CD86, CXCR4, IL1A, CD44, CCL3, ITGAX, CXCL10 ve CCR7 dahil olmak üzere sıralandı. Fonksiyonel olarak gruplandırılmış ağlar, bu genlerin esas olarak kemokin aracılı sinyal yolunda, endotel morfogenezinde ve nöroinflamatuar yanıtta zenginleştiğini belirledi. Sonuç: Araştırmamızda pulpitiste tanısal biyobelirteç olarak 15 gen tanıtılmış ve bunların fonksiyonel olarak gruplandırılmış ağları oluşturulmuştur. Ancak elde edilen sonuçların in vitro ve in vivo yöntemler kullanılarak doğrulanması gerekir. Anahtar Kelimeler: diş pulpası; iltihaplanma; Gen ontolojisi; DEG'ler; ÜFE; Pulpitis.*

References

1. Arola DD, Gao S, Zhang H, Masri R. The Tooth: Its Structure and Properties. Dent Clin North Am 2017;61:651-68. [CrossRef]

2. Mazzoni A, Breschi L, Carrilho M, Nascimento FD, Orsini G, Ruggeri Jr A, et al.. A review of the nature, role, and function of dentin non-collagenous proteins. Part II: enzymes, serum proteins, and growth factors. Endodontic topics 2009;21:19-40. [CrossRef]

3. Galler KM, Weber M, Korkmaz Y, Widbiller M, Feuerer M. Inflammatory Response Mechanisms of the Dentine-Pulp Complex and the Periapical Tissues. Int J Mol Sci 2021;22:1480. [CrossRef]

4. Donnermeyer D, Dammaschke T, Lipski M, Schäfer E. Effectiveness of diagnosing pulpitis: A systematic review. International Endodontic Journal 2023;56:296-325. [CrossRef]

5. Kratunova E, Silva D. Pulp therapy for primary and immature permanent teeth: an overview. Gen Dent 2018;66:30-8.

6. Chandra R, Tripathi S, Jain J, Meherotra A, De R, Dixit M. Vital Pulp Therpay. J Adv Med Dent Scie Res 2023;11:62-81.

7. Abu-Tahun I, Rabah'ah A, Khraisat A. A review of the questions and needs in endodontic diagnosis. Odontostomatol Trop 2012;35:11-20.

8. Liu R, Wang X, Aihara K, Chen L. Early diagnosis of complex diseases by molecular biomarkers, network biomarkers, and dynamical network biomarkers. Med Res Rev 2014;34:455-78. [CrossRef]

9. Tappia PS, Ramjiawan B. Biomarkers for Early Detection of Cancer: Molecular Aspects. Int J Mol Sci 2023; 24:5272. [CrossRef]

10. Burke HB. Predicting Clinical Outcomes Using Molecular Biomarkers. Biomark Cancer 2016;8:89-99. [CrossRef]

11. Kong J, Wang F, Teodoro G, Cooper L, Moreno CS, Kurc T, et al.., editors. High-performance computational analysis of glioblastoma pathology images with database support identifies molecular and survival correlates. EEE Int Conf Bioinformatics Biomed 2013;229-36. [CrossRef]

12. Liu X, Liu ZP, Zhao XM, Chen L. Identifying disease genes and module biomarkers by differential interactions. J Am Med Inform Assoc 2012;19:241-8. [CrossRef]

13. Su G, Morris JH, Demchak B, Bader GD. Biological network exploration with Cytoscape 3. Curr Protoc Bioinformatics. 2014; 47:8.13.1-24. [CrossRef]

14. Bindea G, Mlecnik B, Hackl H, Charoentong P, Tosolini M, Kirilovsky A, et al.. ClueGO: a Cytoscape plug-in to decipher functionally grouped gene ontology and pathway annotation networks. Bioinformatics 2009;25:1091-3. [CrossRef]

15. Zhang D, Zheng C, Zhu T, Yang F, Zhou Y. Identification of key module and hub genes in pulpitis using weighted gene co-expression network analysis. BMC Oral Health 2023;23:2. [CrossRef]

16. Jiang Y, He Y, Chen Y, Zeng J, Huang W, Huang L, et al.. Overexpression of MicroRNA-155 aggravates pulpitis by targeting kinesin superfamily Proteins-5C based on illumina high-throughput sequencing. Int Endod J 2023;56:837-53. [CrossRef]

17. Huang X, Chen K. Differential Expression of Long Noncoding RNAs in Normal and Inflamed Human Dental Pulp. J Endod 2018;44:62-72. [CrossRef]

18. Fouad A. The microbial challenge to pulp regeneration. Adv Dent Res 2011;23:285-9. [CrossRef]

19. Yu C, Abbott PV. An overview of the dental pulp: its functions and responses to injury. Aust Dent J 2007;52:S4-S6. [CrossRef]

20. Karrar RN, Cushley S, Duncan HF, Lundy FT, Abushouk SA, Clarke M, et al.. Molecular biomarkers for objective assessment of symptomatic pulpitis: A systematic review and meta-analysis. Int Endod J 2023;56:1160-77. [CrossRef]

21. Brizuela C, Meza G, Mercadé M, Inostroza C, Chaparro A, Bravo I, et al.. Inflammatory biomarkers in dentinal fluid as an approach to molecular diagnostics in pulpitis. Int Endod J 2020;53(9):1181-91. [CrossRef]

22. Rechenberg D-K, Galicia JC, Peters OA. Biological markers for pulpal inflammation: a systematic review. PloS one 2016;11:e0167289. [CrossRef]

23. Al Barashdi MA, Ali A, McMullin MF, Mills K. Protein tyrosine phosphatase receptor type C (PTPRC or CD45). J Clin Pathol 2021;74:548-52. [CrossRef]

24. He R-j, Yu Z-h, Zhang R-y, Zhang Z-y. Protein tyrosine phosphatases as potential therapeutic targets. Acta pharmacologica sinica 2014;35:1227-46. [CrossRef]

25. Rheinländer A, Schraven B, Bommhardt U. CD45 in human physiology and clinical medicine. Immunol Lett 2018;196:22-32. [CrossRef]

26. Roberts A, Fürnrohr B, Vyse T, Rhodes B. The complement receptor 3 (CD11b/CD18) agonist Leukadherin-1 suppresses human innate inflammatory signalling. Clin Exp Immunol 2016.;185:361-71. [CrossRef]

27. Hirsch V, Wolgin M, Mitronin AV, Kielbassa AM. Inflammatory cytokines in normal and irreversibly inflamed pulps: a systematic review Arch Oral Biol 2017;82:38-46. [CrossRef]

28. Hubbard AK, Rothlein R. Intercellular adhesion molecule-1 (ICAM-1) expression and cell signaling cascades. Free Radic Biol Med 2000;28:1379-86. [CrossRef]

29. Frank PG, Lisanti MP. ICAM-1: role in inflammation and in the regulation of vascular permeability. Am J Physiol Heart Circ Physiol 2008;295:H926-H7. [CrossRef]

30. Vandooren J, Van den Steen PE, Opdenakker G. Biochemistry and molecular biology of gelatinase B or matrix metalloproteinase-9 (MMP-9): the next decade. Crit Rev Biochem Mol Biol 2013;48(3):222-72. [CrossRef]

31. Sharma R, Kumar V, Logani A, Chawla A, Mir R, Sharma S, et al.. Association between concentration of active MMP-9 in pulpal blood and pulpotomy outcome in permanent mature teeth with irreversible pulpitis–a preliminary study. Int Endod J 2021;54(4):479-89. [CrossRef]

32. Karapanou V, Kempuraj D, Theoharides TC. Interleukin-8 is increased in gingival crevicular fluid from patients with acute pulpitis. J Endod 2008;34:148-51. [CrossRef]

33. Russo RC, Garcia CC, Teixeira MM, Amaral FA. The CXCL8/IL-8 chemokine family and its receptors in inflammatory diseases. Expert Rev Clin Immunol 2014;10:593-619. [CrossRef]

34. Lee PR, Lee J-H, Park JM, Oh SB. Upregulation of toll-like receptor 2 in dental primary afferents following pulp injury. Exp Neurobiol 2021;30:329. [CrossRef]

35. Newton S, Ding Y, Chung C-S, Chen Y, Lomas-Neira JL, Ayala A. Sepsis-induced changes in macrophage co-stimulatory molecule expression: CD86 as a regulator of anti-inflammatory IL-10 response. Surg Infect 2004;5:375-83. [CrossRef]

36. Chen M, Zeng J, Yang Y, Wu B. Diagnostic biomarker candidates for pulpitis revealed by bioinformatics analysis of merged microarray gene expression datasets. BMC Oral Health 2020;20:1-13. [CrossRef]

In vitro evaluation of shear bond strength of polymethyl methacrylate/montmorillonite modified Biodentine with dental resin composite

Purpose
The aim of this study was to evaluate the bond strength between Biodentine, modified with polymethyl methacrylate/Montmorillonite nanoclay, and resin composite at different stages of Biodentine's setting time.

Materials and Methods
Nanoclay was prepared and organo-modified with polymethyl methacrylate. The characterization of polymethyl methacrylate/Montmorillonite nanoclay, Biodentine, and modified Biodentine was assessed by X-ray diffraction analysis, Fourier-transform infrared spectroscopy, and scanning electron microscopy coupled with energy-dispersive X-ray spectroscopy. A total of sixty acrylic molds were constructed; thirty specimens were filled with Biodentine, and the other thirty with nanoclay-modified Biodentine. Each group was subdivided according to different stages of Biodentine's setting time: 12 minutes, 2 hours, and 2 weeks. Universal adhesive, followed by flowable resin composite, was applied. The micro-shear bond strength was tested using a universal testing machine. Data were analyzed using one-way ANOVA followed by Tukey's post hoc test, in addition to two-way ANOVA. The significance level was set at $p \leq 0.05$.

Results
The characterization results revealed the successful preparation of polymethyl methacrylate/Montmorillonite nanoclay and modified Biodentine. The micro-shear bond strength results showed that modified Biodentine had significantly higher micro-shear bond strength than unmodified Biodentine at 12 minutes. However, no statistically significant difference was found between the unmodified and modified Biodentine groups at 2 hours and 2 weeks.

Conclusion
The incorporation of 10% modified nanoclay by weight into Biodentine could enhance the bond strength with resin composite when placed after 12 minutes of Biodentine's setting time.

Keywords: Biodentine, montmorillonite nanoclay, resin-modified nanoclay, micro-shear bond strength, pulp capping materials

Fagr Hassan Elmergawy[1] (iD),
Ola M. Elborady[2] (iD),
Dina M. Wahied[1] (iD)

Introduction

Pulp capping materials have been used for pulp protection against chemical, thermal, and other noxious stimuli. They are placed as a protective layer on the floor of deep cavities or after traumatic exposure. These biomaterials should be bioactive to allow for the regeneration of dentin at the exposed pulp areas.

Calcium hydroxide ($Ca(OH)_2$) had been regarded as the gold standard for pulp capping due to its high pH which leads to stimulation of the pulp cells to form dentin bridge and its antibacterial effect. However, $Ca(OH)_2$ showed

ORCID IDs of the authors: F.H.E. 0000-0003-1514-4851; O.M.E. 0000-0002-4168-5697; D.M.W. 0000-0002-8006-6901

[1]Dental biomaterials Department, Faculty of Dentistry, October University for Modern Sciences and Arts

[2]Institute of Nanoscience and Nanotechnology, Kafr El-Sheikh University, Qism Kafr El-Sheikh

Corresponding Author: Fagr Hassan Elmergawy

E-mail: fmergawy@msa.edu.eg

high solubility, poor sealing ability, lack of adhesion with tooth structure, tunnel defects in the formed dentin bridge as well as necrosis and inflammation in pulp tissues. To overcome these drawbacks calcium-silicate based pulp capping materials have been introduced (1, 2). Mineral tri-oxide aggregate (MTA) is the first calcium silicate bioactive material introduced in 1993 (3). MTA is capable of apatite formation by either using calcium aluminates or calcium silicates. MTA exhibits a higher rate of clinical success compared to Ca(OH)$_2$, owing to the formation of thicker and less porous dentin bridge with fewer signs of inflammation. Yet, MTA shows some disadvantages such as its long setting time, difficulty in handling, tooth discoloration, high cost as well as incompatibility with other dental materials when layered. (1, 3, 4)

Second generation calcium silicate based materials were introduced in an attempt to overcome the drawbacks of MTA, among which is the Biodentine. (4) Biodentine is a repair material that was introduced in 2011 as a bioactive dentin substitute due to its resemblance to dentin regarding its mechanical properties. Biodentine is composed of tri-calcium and di-calcium silicates, calcium carbonate, in addition to iron oxide and zirconium oxide (5). Biodentine has an accelerated setting time and higher viscosity, in addition to its easier manipulation, and less tooth discoloration than MTA. Moreover, it shows very promising bioactivity which comes mainly from being formed of tri-calcium silicate and calcium carbonate matrix along with zirconium oxide and iron oxide (6, 7). Owing to its promising properties, it has not been used only as a pulp capping material but also used as a retrograde filling, perforation repair, treatment of immature necrotic teeth, pulpotomy, and apexification (7, 8). However, one of the main drawbacks of Biodentine is the poor bond strength with the overlying resin composite restoration due to its water based chemistry which affects the micromechanical retention with overlying resin composite, impairing the longevity of the final restoration (3).

Nanoclays are promising nanoparticles that attracted many researchers due to their biocompatibility, good mechanical properties as well as high abundance (9). Montmorillonite (MMT) is a type of nanoclay that is formed of alumino-silicate sheets of approximately one nanometer thickness that are stacked over one another forming complex crystallites (10). Organo-modification of nanoclays involves the grafting of bulkier organic polymers onto MMT sheets to increase its compatibility with resin based materials.

To our knowledge, no previous studies have been done to modify Biodentine with resin or nanoclay in an attempt to increase bond strength with resin composite. Thereby, the aim of this study was the addition of polymethyl methacrylate modified MMT nanoclay to Biodentine and to evaluate its effect on shear bond strength with resin composite restoration over different stages of Biodentine setting time. The null hypothesis states that there would be no statistically significant effect of adding organo-modified nanoclay on shear bond strength between Biodentine and overlaid composite at different stages of setting time.

Materials and Methods

Materials

Materials used for the synthesis of MMT modified with polymethyl methacrylate (PMMA/MMT), as well as Biodentine, universal adhesive system and flowable resin composite are listed in Table 1.

Table 1. *Materials used in this study, their chemical composition and manufacturer.*

Material	Chemical composition	Manufacturer
Tetraethyl orthosilicate (TEOS)	$(C_2H_5O)_4Si$	Alpha Chemika (India)
Aluminum nitrate	$Al(NO_3)_3$	Alpha Chemika (India)
Magnesium nitrate	$Mg(NO_3)_2$	Alpha Chemika (India)
Calcium nitrate	$Ca(NO_3)_2$	Sigma-Aldrich (Germany)
Sodium nitrate	$NaNO_3$	LOBA Chemie (India)
Acrylamido- methyl Propane sulfonic acid (AMPS)	$C_7H_{13}NO_4S$	Acros organics (USA)
Ammonium persulfate (APS)	$(NH_4)_2S_2O_8$	LOBA Chemie (India)
Methyl methacrylate	$C_4H_6O_2$	LOBA Chemie (India)
Carbon tetrachloride	CCl_4	Acros organics (USA)
Ethanol	C_2H_5OH	LOBA Chemie (India)
Methanol	CH_3OH	LOBA Chemie (India)
Biodentine	Tri-calcium silicate, di-calcium silicate, calcium carbonate, iron oxide and zirconium oxide	Septodont (France)
All bond universal adhesive	Bis-GMA, 10-MDP, HEMA, ethanol and water	Bisco (USA)
Flowable resin composite	Bis-GMA and TEGDMA Methacrylate-based nanohybrid resin composite with 76wt% filler loading	VOCO GmbH. (Germany)

PMMA/MMT nanoclay preparation

PMMA/MMT was prepared following a method mentioned in a previous study (10), where TEOS, Al(NO$_3$)$_3$, Mg(NO$_3$)$_2$, Ca(NO$_3$)$_2$, and NaNO$_3$ were used as sources of SiO$_2$, Al$_2$O$_3$, MgO, CaO, and Na$_2$O respectively. MMT nanoclay was first synthesized from sol-gel technique, where a solution of 57% SiO$_2$, 33% Al$_2$O$_3$, 5.4% MgO, 4% CaO and Na$_2$O was mixed in 250ml of acidified distilled water of pH 2. Afterward, 26.26g

of TEOS and 30 ml of ethanol were added to the solution, and mixed till a powder is precipitated. The formed powder was washed with distilled water using a centrifugal machine, dried at 80°C for 24hrs and ground into fine powder.

PMMA was grafted onto MMT nanoclay via in-situ graft polymerization methodology adopted from Atai *et al* (11, 12) (Figure 1). An aqueous solution of distilled water containing 0.5 wt% MMT was prepared and kept at 50°C for 12 hours with continuous stirring using a magnetic stirrer. Then 2.5g of AMPS (2-acrylamido-2methyl-1 Propane sulfonic acid) was added to the aqueous solution and mixed for 2hrs. Afterward, 2g of the initiator (Ammonium persulfate), in addition to 50ml of methacrylic acid and 2ml of CCl_4 (the chain transfer agent) were added to the solution. The temperature was then elevated to 70°C to allow for full polymerization and gel formation. Precipitation was done by dropping the formed gel into methanol solution. The precipitate was washed using distilled water and ethanol by centrifugal machine. Purification of the powder was performed by the dialysis method adopted from Sample-Lord and Shackelford (13). The prepared sample powder was then dried and ground into fine powder and stored in a sealed container till use.

Sample size estimation

Statistical power analysis was performed to determine the sample size using Power and Sample Size Calculation Software (Version 3.1.2, Vanderbilt University, Nashville, Tennessee, USA). Sample size was calculated to be 10 for each experimental condition (n=10) with power value of 90% and type I error probability of 0.05.

Specimens preparation

A total of sixty acrylic circular molds with a depth of 2mm and internal diameter of 10mm were prepared using self-cured acrylic resin (Acrostone Cold Cure Acrylic Resin, Acrostone Co., England). Thirty acrylic molds were fully filled with unmodified Biodentine (Biodentine™, Septodont, Saint-Maur-des-Fossıs, Creteil, France). Samples were stored at 37°C and 100% humidity in an incubator at three time intervals (12min for initial setting time, 2hrs and 2 weeks for final setting time). Another thirty acrylic molds were packed with

10wt% PMMA/MMT modified Biodentine, stored at the same condition and aging periods (12min, 2hrs and 2 weeks).

Unmodified Biodentine was prepared according to the manufacturer's instructions, where the powder was mixed with five drops of Biodentine liquid in an amalgamator for 30 seconds. The prepared Biodentine paste was packed into the acrylic molds using a plastic condenser, then a glass slab was used to gently press over the Biodentine to create a smooth surface. Biodentine modified with 10% PMMA/MMT by weight was prepared. Samples of both unmodified and modified Biodentine were stored in an incubator as mentioned above before the application of adhesive bonding agent. After each incubation period, specimens were randomly selected to apply the adhesive bonding agent and resin composite build up.

A universal adhesive (All bond universal, Bisco, USA) was applied in a self-etch mode using a bristle brush on the surface of each tested material, rubbed for 20 seconds and dried by gentle air for 5 seconds. Before light curing, five transparent cylindrical shaped silicon tubes of 1mm internal diameter and 2mm length were placed on the surface of each tested specimen and then the adhesive resin was polymerized by a light cure unit (VivaDent Bluephase, Ivoclar, USA) for 20 seconds. Flowable resin composite (Polofil NHT Flow, VOCO GmbH. Germany) was carefully injected in a inside each tube in a single bulk to avoid air bubbles formation and light cured. Polyethylene tubes were then removed by a sharp razor blade. Specimens were stored for 48 hours at 37°C at a relative humidity of 100% before testing.

Chemical analysis and phase identification

Chemical analysis of PMMA/MMT nanoclay as well as Biodentine before and after modification with PMMA/MMT was done by Fourier Transform Infrared Spectroscopy (FTIR) (IRAffinity-1S.SHIMADZU. Japan), with a wavelength of 4000 to 400 cm^{-1}. Phase identification was tested by X-ray diffraction analysis (XRD) (PXRD-6000 SCHIMADZU. Japan) with a voltage of 40KV and a current of 30mA with CuKα radiation (λ=1.54056A°).

Scanning electron microscope (SEM) and energy dispersive X-Ray spectroscopy (EDX) assessment

Surface morphology of Biodentine before and after modification with PMMA/MMT was performed by SEM (Quanta FEG-250, FEI. USA) coupled with energy dispersive X-Ray spectroscopy (EDX) for elemental composition analysis. Disc shaped specimens (4mm in diameter and 2 mm in height) were mounted on stubs, gold coated using a vacuum sputter coater and their upper surfaces were examined by the SEM.

Micro-shear bond (µSBS) strength testing

All tested samples were subjected to shear bond strength by a Universal testing machine (Model 3345; Instron Industrial Products, Norwood, USA) with a load cell of 5 kN. Samples were mounted to the lower fixed compartment of testing machine and load was applied at resin-liner interface using a metallic loop attached to the upper movable compartment of testing machine operated at crosshead speed
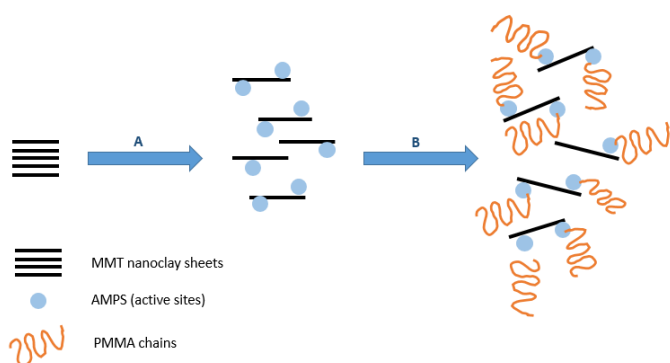
Figure 1. *Schematic representation of grafting of PMMA onto MMT nanoclay sheets; step (A) represents swelling behavior of nanoclay sheets in distilled water in the presence of AMPS. Step (B) represents graft polymerization of PMMA chains in the presence of the initiator and chain transfer agent.*

of 0.5 mm/min. The load required to de-bonding was recorded in Newtons.

Statistical analysis

Mean values and standard deviation for each group were tested for normality using Shapiro-Wilk tests. One-way ANOVA then Tukey's post hoc test were used to evaluate the effect of unmodified and PMMA/MMT modified Biodentine within each setting time interval and the effect of setting time intervals within each group on micro-shear bond strength test. A two-way ANOVA test was used to test the interactions between the tested variables. The significance level was set at $P \leq 0.05$. Statistical analysis was performed with (IBM SPSS Statistics Version 23 Armonk, NY, USA) for Windows.

Results

FTIR analysis results

Results of FTIR of PMMA/MMT showed peaks corresponding to aluminum silicates and magnesium silicates at 447 cm-1 and 537 cm-1 respectively (Figure 2). In addition, bands of aluminum oxide and silicon oxide were aligned at 900 cm-1 and 1045 cm−1 respectively (14-18). Bands were detected at the regions of 2900 that were attributed to C-H bonds of the organic modifier PMMA. Another band was observed at approximately 1700 cm-1 which is associated to the stretching of the carbonyl group (C=O) belonging to PMMA (19-23).
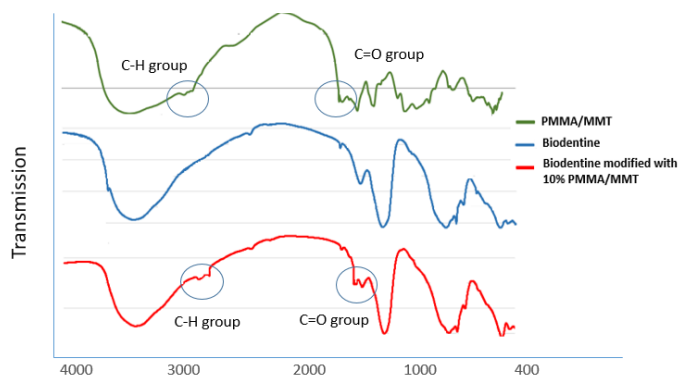
Figure 2. *FTIR analysis of PMMA/MMT nanoclay, Biodentine and PMMA/MMT modified Biodentine.*

FTIR analysis of Biodentine and modified Biodentine revealed bands at 500cm-1 that corresponded to silica vibrations. Broad bands at 1400 and 1600 cm-1, as well as bands at 870, and 700 cm-1 attributed to carbonate groups were also presented (24, 25) Modified Biodentine showed new bands corresponding to C-H and C=O of PMMA.

XRD analysis results

XRD results of PMMA/MMT (Figure 3) showed the characteristic peak of MMT (d001) at 2θ=7.4°(26). Typical peaks of quartz were also detected at 2θ=25.5° (27). XRD results of Biodentine showed peaks corresponding to calcium carbonates and calcium silicates at approximately 2θ= 24.5°and

28° respectively (28). However, Biodentine modified with PMMA/MMT showed peaks corresponding to MMT(d001) at 2θ=7.7°. As well as peaks of quartz at approximately 2θ=25.5°.
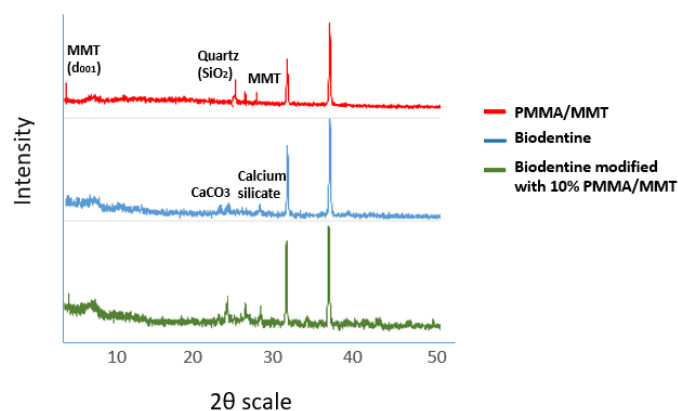
Figure 3. *XRD patterns of PMMA/MMT nanoclay, Biodentine and PMMA/MMT modified Biodentine.*

Scanning electron microscopy

SEM images of Biodentine (Figure 4A) showed Biodentine crystals with large spaces between them, while Biodentine modified with PMMA/MMT (Figure 4B) showed nanoclay particles (yellow arrows) on the surface of Biodentine and in between the crystals.
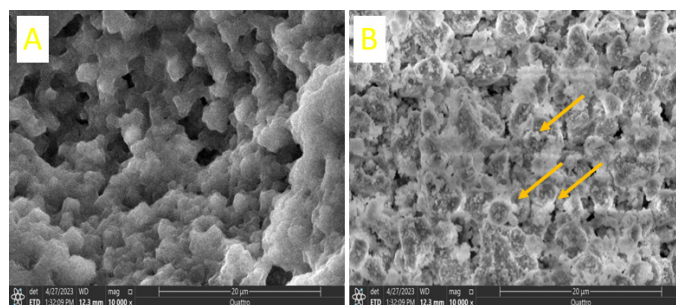
Figure 4. *SEM images (10000X) of A: Biodentine, B: PMMA/MMT modified Biodentine.*

EDX analysis results

EDX analysis (Figure 5-A) revealed the typical composition of Biodentine with high percentages of calcium (50.21%), oxygen (36.77%), carbon (6.75%) and silicon (6.25%), whereas in EDX analysis of PMMA/MMT modified Biodentine, aluminum (0.48%), sodium (0.23%) and magnesium (0.07%) attributed to MMT nanoclay were detected as shown in (Figure 5-B).
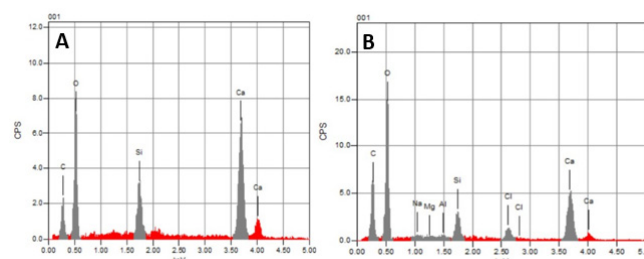
Figure 5. *EDX analysis of A: Biodentine, B: PMMA/MMT modified Biodentine.*

Micro-shear bond strength (µSBS) results

Statistical analysis of micro-shear bond strength results (Figure 6 and Table 2) revealed significantly lower µSBS values (MPa) for the unmodified Biodentine group at 12 minutes compared to 2 weeks where p <0.001. However, no statistically significant difference was found between 12 minutes with 2 hours and between 2 hours and 2 weeks within unmodified Biodentine groups. No statistically significant differences were found between PMMA/MMT modified BD groups between the three-time intervals. Pairwise comparisons showed significant difference between unmodified and modified Biodentine groups at 12 minutes, where (p=0.002), however, no statistically significant difference was found between unmodified and modified Biodentine groups at 2hours and 2weeks, where (p=0.176 and 0.289) respectively. The results of two-way ANOVA showed that type of Biodentine exhibited a statistically significant effect on micro-shear bond strength at p=0.0463. While different setting time intervals showed a statistically significant effect at p<0.001. Moreover, the interaction between the two tested variables showed statistically significant effect at p=0.0137.

Table 2. *Micro-shear bond strength (µSBS) data in MPa for tested groups.*

Groups	12 min	2 hours	2 weeks	p value
Unmodified Biodentine	5.95[a]±1.35	7.19[ab]±1.54	8.59[b]±0.88	<0.001
PMMA/MMT Biodentine	7.67[a]±0.98	7.92[a]±1.28	8.02[a]±0.97	0.756
P-value	0.002	0.176	0.289	

Different letter within each row indicates significant difference by Tukey's post hoc test (P-value<0.001).
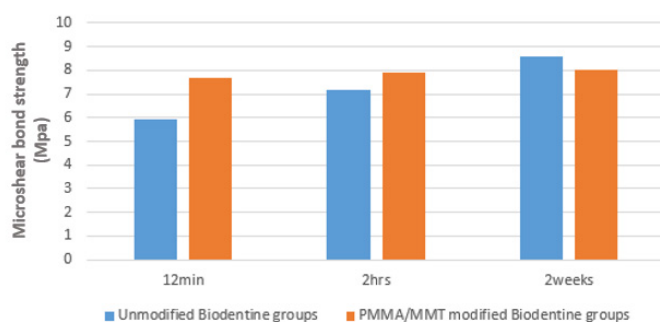
Figure 6. *Bar chart representing micro-shear bond strength of the different tested groups.*

Discussion

Biodentine is a tri-calcium silicate based bioactive material that was advertised in markets as "Bioactive dentin substitute" since it has mechanical properties comparable to that of dentin. Moreover, it has a superior ability to stimulate the odontoblasts differentiation leading to the formation of reparative dentin, excellent bioactive property as well as biocompatibility. However, Biodentine has water-based chemistry which has greatly compromised the micromechanical bond with overlying resin composite (29-31). To overcome this drawback, polymethyl methacrylate (PMMA) modified Montmorillonite (MMT) nanoclay (PMMA/MMT) was used in this study to modify Biodentine in an attempt to improve its bond strength with resin composite due to the good chemical interaction between PMMA and Bis-GMA in resin composite matrix (32).

MMT was synthesized by sol-gel technique due to its ability to control the structural morphology of the final product, utilize relatively low temperature and produce very fine powder with high chemical homogeneity (33, 34). Then PMMA was incorporated inside MMT using in-situ graft polymerization method (Figure 1) which was reported to be an easy and reliable technique that allows the penetration of polymeric chains into nanoclay sheets and also promotes covalent bonding between polymer and nanoclay (35, 36).

FTIR analysis for PMMA/MMT (Figure 2) was in agreement with that reported in literature; where peaks contributing to distinctive functional groups of Si-O-Al, Si-O-Mg as well as Si-O-Si of the tetrahedral layer of MMT were observed (37, 38). The appearance of C-H band as well as C=O band could further confirm the success of organo-modification and incorporation of PMMA into nanoclay sheets (38, 39). Bands of functional groups containing carbon were detected in FTIR analysis of PMMA/MMT modified Biodentine suggesting the success of incorporation of PMMA/MMT into Biodentine.

XRD results of PMMA/MMT exhibited the characteristic peaks of MMT (d_{001}), quartz and Montmorillonite which were in accordance with the chemical structure reported in literature(40) (Figure 3). Peaks of MMT (d_{001}) and quartz were also observed in the XRD pattern of PMMA/MMT modified Biodentine confirming the incorporation of PMMA/MMT into Biodentine. FTIR and XRD findings were further justified by SEM images and EDX analysis. SEM shows clusters of PMMA/MMT nanoclay on modified Biodentine surface (Figure 4-B). Moreover, the EDX analysis confirmed the presence of aluminum, sodium and magnesium in modified Biodentine which are the main constituent elements of MMT, thus confirming the incorporation of PMMA/MMT in Biodentine (Figure 5-B).

Biodentine has different stages for setting, the initial setting stage is when the tri-calcium silicate reacts with water forming calcium silicate gel and calcium hydroxide and it takes nearly 12 minutes, then afterward nucleation and expansion of this gel over the tri-calcium silicate occur filling the spaces between tri-calcium silicate till crystallization of the hydrated calcium silicates gel. Crystallization continues till complete maturation of the cement occurs which might take 12 weeks up to 1 month (7, 41).

The literature was unclear regarding the time after which resin composite should be placed over Biodentine. Some studies suggested immediate placement of resin composite after Biodentine setting (42-44). However, one study claimed that resin composite should be placed after 2 hours of Biodentine setting and they suggested that the changes in Biodentine became minimal after nearly 120 minutes (8)**.** Other studies reported that final composite restoration should be placed at least 14 days after setting to allow sufficient maturation of Biodentine (7, 45-47). Accordingly, the time intervals chosen in this study for placement of resin composite and testing the bond strength were; after 12 minutes (as claimed by the manufacturer), 2 hours and 2 weeks.

Regarding the type of adhesive systems used with Biodentine, some studies suggest the advantage of using etch and rinse methodology over self-etch (48, 49). However, other studies reported that self-etch strategies showed higher bond strength (42). While other studies reported that the choice of the adhesive strategy doesn't affect the bond strength (45, 50-52). In this study, universal bonding in self-etch mode was used to simplify the application process and reduce the technical errors (53).

Micro-shear bond strength (SBS) test was performed to evaluate the bond strength between Biodentine and resin composite because of its simplicity, ease of specimen preparation and lower incidence of pretest failure. Micro- shear mode testing was employed in this study rather than macro-shear testing as it was reported that conventional macro shear bond test resulted in non-uniform stress distribution with heterogeneous stress patterns when assessed by finite element stress analysis (54). Acrylic resin molds were used as it is an easy and fast way for standardization and central holes with 10 mm × 2 mm were done allowing better retention of the overlying resin composite (45).

The null hypothesis in this study was rejected as there was a statistically significant difference between the shear bond strength of the modified Biodentine and the unmodified one after 12 minutes of Biodentine setting (as shown in Figure 6 and Table 2). Addition of PMMA modified nanoclay to Biodentine might have increased the bond strength with resin composite, as PMMA chains within the nanoclay could interact with BisGMA of resin composite matrix creating stronger network with the monomers in resin composite.

Besides, the incorporation of nanoclays in between Biodentine crystals could act as crack deflectors resisting crack propagation, thus increasing the bond strength (55). Moreover, the use of self-etch adhesives with freshly mixed Biodentine was reported to cause deeper penetration of the adhesive system into the unset Biodentine leading to stronger micro-mechanical retention (46). This was in agreement with previous studies that recommended immediate placement of resin composite restoration on fresh Biodentine (42-44, 56).

The results also revealed that unmodified Biodentine group after 2 weeks showed significantly higher shear bond strength than after 12 minutes. This could be attributed to the fact that calcium hydroxide released during the hydration setting reaction of Biodentine could react chemically with 10-MDP monomers present in self-etch adhesives, thereby enhancing their chemical bonding. Moreover, the initial water-based nature of Biodentine could have a detrimental effect on the bond strength when resin composite is placed immediately. This was in accordance with other studies that suggested that the bond strength continues to increase by time and it should not be placed immediately after setting (7, 45-47). However, no significant difference was found between different setting times of PMMA/MMT modified Biodentine. This could be due to the incorporation of PMMA/MMT that increased the initial bond strength compared to unmodified Biodentine as mentioned above and changed the mode of interaction with resin composite.

It is worth noting that Theracal LC (a resin modified light-cured calcium silicate base material) showed higher bond strength to resin composite compared to Biodentine. This was attributed to the similarity between the resin chemistry of Theracal and resin composite promoting true chemical adhesion and creating strong interface (57).

The current study findings are of important clinical relevance; as strong bond between resin composite and underlying base material is essential to increase the longevity of the final restoration and enhance its stability and performance. However, the current study has some limitations; this is an in vitro study with limited sample size and the simulation of in vivo conditions is yet unsolved. The concentration of nanoclay used was 10% by weight only, yet the effect of different concentrations needs to be examined. Moreover, the effect of modified Biodentine on other properties such as solubility, bioactivity and water sorption are of great importance and it is recommended to be considered in further researches. Evaluation of the biological properties and assessment of the biocompatibility of the nanoclay modified Biodentine should be taken in consideration in further researches. Bond strength durability after different aging conditions was not considered in this study and it is also recommended to be investigated in further studies.

Conclusion

Within the limitations of this study, it was concluded that incorporation of 10% PMMA/MMT by weight to Biodentine improved shear bond strength with resin composite when placed after 12 minutes of Biodentine setting time.

Türkçe özet: *Polimetil Metakrilat/Montmorillonit Modifiye Biodentine'nin Dental Rezin Kompozit ile Kayma Bağlanma Dayanımının İn Vitro Değerlendirilmesi. Amaç: Bu çalışmanın amacı, polimetil metakrilat/ montmorillonit nanokil ile modifiye edilen Biodentine ile rezin kompozit arasındaki bağlanma dayanımını, Biodentine'in farklı sertleşme aşamalarında değerlendirmektir. Gereç ve Yöntemler: Nanokil hazırlandı ve polimetil metakrilat ile organik olarak modifiye edildi. Polimetil metakrilat/montmorillonit nanokilin, Biodentine'in ve modifiye Biodentine'in karakterizasyonu; X-ışını kırınım analizi, Fourier dönüşümlü kızılötesi spektroskopisi ve enerji dağılımlı X-ışını spektroskopisi ile eşleştirilmiş taramalı elektron mikroskobu kullanılarak yapıldı. Toplam altmış akrilik kalıp hazırlandı; otuz örnek Biodentine ile, diğer otuz örnek ise nanokil ile modifiye Biodentine ile dolduruldu. Her grup, Biodentine'in sertleşme sürecinin farklı aşamalarına göre üç alt gruba ayrıldı: 12 dakika, 2 saat ve 2 hafta. Evrensel adeziv uygulandıktan sonra akışkan rezin kompozit yerleştirildi. Mikro-kayma bağlanma dayanımı, üniversal test cihazı kullanılarak test edildi. Veriler tek yönlü ANOVA ve ardından Tukey'nin post hoc testi ile analiz edildi; ayrıca iki yönlü ANOVA uygulandı. Anlamlılık seviyesi p ≤ 0,05 olarak belirlendi. Bulgular: Karakterizasyon sonuçları, polimetil metakrilat/montmorillonit nanokilin ve modifiye Biodentine'in başarılı bir şekilde hazırlandığını ortaya koydu. Mikro-kayma bağlanma dayanımı testleri, modifiye Biodentine'in 12. dakikada, modifiye edilmemiş Biodentine'e kıyasla anlamlı derecede daha yüksek bağlanma dayanımına sahip olduğunu gösterdi. Ancak, 2 saat ve 2 hafta grupları arasında istatistiksel olarak anlamlı bir fark bulunmadı. Sonuç: Biodentine'e ağırlıkça %10 oranında modifiye nanokil eklenmesi, Biodentine'in sertleşme sürecinin 12. dakikasında uygulandığında, rezin kompozit ile bağlanma dayanımını artırabilir. Anahtar Kelimeler: biodentine, montmorillonit nanokil, rezin-modifiye nanokil, mikro-kayma bağlanma dayanımı, pulpa örtüleme materyalleri*

study. FHE, DMW participated in gathering the data for the study. FHE, OME participated in the analysis of the data. DMW wrote the majority of the original draft of the paper. FHE, DMW participated in writing the paper. FHE, OME, DMW has had access to all of the raw data of the study. FHE, OME, DMW has reviewed the pertinent raw data on which the results and conclusions of this study are based. FHE, DMW have approved the final version of this paper. FHE guarantees that all individuals who meet the Journal's authorship criteria are included as authors of this paper.

Conflict of Interest: The authors declared that they have no conflict of interest.

Financial Disclosure: The authors declared that they have received no financial support.

References

1. Nie E, Yu J, Jiang R, Liu X, Li X, Islam R. Effectiveness of direct pulp capping bioactive materials in dentin regeneration: a systematic review. Mater, 2021;14:1-14. [CrossRef]

2. Kaul S, Kumar A, Jasrotia A, Gorkha K, Kumari S, Jeri SY. Comparative analysis of biodentine, calcium hydroxide, and 2% chlorhexidine with resin-modified glass ionomer cement as indirect pulp capping materials in young permanent molars. J Contemp Dent Pract, 2021;22:511-6. [CrossRef]

3. Singla MG, Wahi P. Comparative evaluation of shear bond strength of Biodentine, Endocem mineral trioxide aggregate, and TheraCal LC to resin composite using a universal adhesive: an in vitro study. Endodontology, 2020;32:14-9. [CrossRef]

4. Camilleri J, Laurent P, About I. Hydration of biodentine, theracal lc, and a prototype tricalcium silicate–based dentin replacement material after pulp capping in entire tooth cultures. J Endod, 2014;40:1846-54. [CrossRef]

5. Kadali NS, Alla RK, AV R, MC SS, Mantena SR, RV R. An overview of composition, properties, and applications of Biodentine. IJDM, 2021;3:120-6. [CrossRef]

6. Arandi NZ and Thabet M. Minimal intervention in dentistry: A literature review on Biodentine as a bioactive pulp capping material. Biomed Res Int, 2021;2021:1-13. [CrossRef]

7. Mustafa RM, Al-Nasrawi SJ, Aljdaimi AI. The effect of biodentine maturation time on resin bond strength when aged in artificial saliva. Int J Dent, 2020;22. [CrossRef]

8. Buła KA, Palatyńska-Ulatowska A, Klimek L. Biodentine management and setting time with Vicat and Vickers evaluation; a survey-based study on clinicians' experience. Arch Mater Sci Eng, 2020;103. [CrossRef]

9. Calabria-Holley J, Papatzani S, Naden B, Mitchels J, Paine K. Tailored montmorillonite nanoparticles and their behaviour in the alkaline cement environment. Appl Clay Sci, 2017;143:67-75. [CrossRef]

10. Elmergawy FH, Nassif MS, El-Borady OM, Mabrouk M, El-Korashy DI. Physical and mechanical evaluation of dental resin composite after modification with two different types of Montmorillonite nanoclay. J Dent, 2021;112:103731. [CrossRef]

11. Atai M, Solhi L, Nodehi A, Mirabedini SM, Kasraei S, Akbari K. PMMA-grafted nanoclay as novel filler for dental adhesives. Dent Mater, 2009;25:339-47. [CrossRef]

12. Solhi L, Atai M, Nodehi A, Imani M, Ghaemi A, Khosravi K. Poly(acrylic acid) grafted montmorillonite as novel fillers for dental adhesives: synthesis, characterization and properties of the adhesive. Dent Mater, 2012;28:369-77. [CrossRef]

13. Sample-Lord KM, Shackelford CD. Dialysis Method to Control Exchangeable Sodium and Remove Excess Salts From Bentonite. GTJ, 2016;39:206-16. [CrossRef]

14. Madejova J, Komadel P. Baseline studies of the clay minerals society source clays: infrared methods. Clays Clay Miner, 2001;49:410-32. [CrossRef]

15. Krupskaya VV, Zakusin SV, Tyupina EA, Dorzhieva OV, Zhukhlistov AP, Belousov PE. Experimental study of montmorillonite structure and transformation of its properties under treatment with inorganic acid solutions. Minerals, 2017;7:49. [CrossRef]

16. Bishop JL, Pieters CM, Edwards JO. Infrared spectroscopic analyses on the nature of water in montmorillonite. Clays Clay Miner, 1994;42:702-16. [CrossRef]

17. Yusoh K, Kumaran SV, Ismail FS. Surface Modification of Nanoclay for the Synthesis of Polycaprolactone (PCL)–Clay Nanocomposite. MATEC Web Conf, 2018;150:1-6. [CrossRef]

18. Abdullah M, Afzaal M, Ismail Z, Ahmad A, Nazir M, Bhat A. Comparative study on structural modification of Ceiba pentandra for oil sorption and palm oil mill effluent treatment. Desalin Water Treat, 2015;54:3044-53. [CrossRef]

19. Abdallah W, Yilmazer U. Novel thermally stable organomontmorillonites from phosphonium and imidazolium surfactants. Thermochim Acta, 2011;525:129-40. [CrossRef]

20. Zandsalimi K, Akbari B, Mehrnejad F, Bagheri R. Compatibilization of clays and hydrophobic polymers: the case of montmorillonite and polyetheretherketone. Polym Bull, 2019;1: 1 -23. [CrossRef]

21. Günister E, Pestreli D, Ünlü CH, Atıcı O, Güngör N. Synthesis and characterization of chitosan-MMT biocomposite systems. Carbohydr Polym, 2007;67:358-65. [CrossRef]

22. Thakur G, Singh A, Singh I. Chitosan-montmorillonite polymer composites: Formulation and evaluation of sustained release tablets of aceclofenac. Sci Pharm, 2016;84:603-17. [CrossRef]

23. Tommasini FJ, Ferreira LdC, Tienne LGP, Aguiar VdO, Silva MHPd, Rocha LFdM. Poly (methyl methacrylate)-SiC nanocomposites prepared through in situ polymerization. Mater Res, 2018;21. [CrossRef]

24. Kleczewska J, Bieliński D, Nowak J, Sokołowski J, Łukomska-Szymańska M. Dental composites based on dimethacrylate resins reinforced by nanoparticulate silica. Polym Polym Compos, 2016;24:411-8. [CrossRef]

25. Alotaibi J, Saji S, Swain M. FTIR characterization of the setting reaction of biodentine. Dent Mater J, 2018;34:1645-51. [CrossRef]

26. Chuayjuljit S, Thongraar R, Saravari O. Preparation and properties of PVC/EVA/organomodified montmorillonite nanocomposites. J Reinf Plast Compos, 2008;27:431-42. [CrossRef]

27. Marsh A, Heath A, Patureau P, Evernden M, Walker P. Alkali activation behaviour of un-calcined montmorillonite and illite clay minerals. Appl Clay Sci,2018;166:250-61. [CrossRef]

28. Li Q, Hurt AP, Coleman NJ. The application of 29Si NMR spectroscopy to the analysis of calcium silicate-based cement using Biodentine as an example. J Funct Biomater, 2019;10:25. [CrossRef]

29. Kaur M, Singh H, Dhillon JS, Batra M, Saini M. MTA versus Biodentine: review of literature with a comparative analysis. JCDR, 2017;11:ZG01. [CrossRef]

30. Carretero V, Giner-Tarrida L, Peñate L, Arregui M. Shear bond strength of nanohybrid composite to biodentine with three different adhesives. Coat, 2019; 9:783. [CrossRef]

31. Malkondu Ö, Kazandağ MK, Kazazoğlu E. A review on biodentine, a contemporary dentine replacement and repair material. Biomed Res Int, 2014;2014. [CrossRef]

32. Zhong H, Zhou XG, Cai Q, Yang XP. Poly (methyl methacrylate) Grafted Silica Nanoparitcles Via ATRP for Bis-GMA/TEGDMA Dental Restorative Composite Resins. Adv Mat Res, 2013;647:46-52 [CrossRef]

33. Ulatowska-Jarza A, Andrzejewski D, Maruszewski K, Podbielska H, Strek W. Advantages of sol-gel technologies for biomedical applications. Optical and Imaging Techniques for Biomonitoring IV 1999, SPIE, p. 50-8 [CrossRef]

34. Carter CB, Norton MG. Sols, gels, and organic chemistry. Ceramic Materials: Science and Engineering 2007, Springer, p. 400-11. [CrossRef]

35. Jawaid M, Qaiss A, Bouhfid R. Nanoclay reinforced polymer composites 2016, Springer, p. 3-8 [CrossRef]

36. Malas A. Rubber nanocomposites with graphene as the nanofiller. Progress in Rubber Nanocomposites 2017, Woodhead publishing, p. 179-229. [CrossRef]

37. García-Padilla Á, KarianaMoreno-Sader MA-M, Realpe-Jimenez Á, Soares JB. Synthesis and Characterization of Starch/Na-MMT Nanocomposites. Contemp Eng Sci, 2018;11:1633-41. [CrossRef]

38. Alshabanat M, Al-Arrash A, Mekhamer W. Polystyrene/montmorillonite nanocomposites: study of the morphology and effects of sonication time on thermal stability. J Nanomater, 2013;2013:1-13. [CrossRef]

39. Cervantes-Uc JM, Cauich-Rodríguez JV, Vázquez-Torres H, Garfias-Mesías LF, Paul DR. Thermal degradation of commercially available organoclays studied by TGA–FTIR. Thermochim Acta, 2007;457:92-102. [CrossRef]

40. Damian G, Damian F, Szakács Z, Iepure G, Aştefanei D. Mineralogical and Physico-Chemical Characterization of the Oraşu-Nou (Romania) Bentonite Resources. Minerals, 2021;11:938. [CrossRef]

41. Mayya A, George AM, Mayya A, D'souza SP, Mayya SS. Impact of maturation time on the shear bond strength of an alkasite restorative material to pure tricalcium silicate based cement: An in-vitro experimental study. J Int Oral Health, 2022;14:494. [CrossRef]

42. Çolak H, Tokay U, Uzgur R, Uzgur Z, Ercan E, Hamidi MM. The effect of different adhesives and setting times on bond strength between Biodentine and composite. J Appl Biomater Funct Mater, 2016;14:217-22. [CrossRef]

43. Palma PJ, Marques JA, Falacho RI, Vinagre A, Santos JM, Ramos JC. Does delayed restoration improve shear bond strength of different restorative protocols to calcium silicate-based cements?. Mater, 2018;11:2216. [CrossRef]

44. Palma PJ, Marques JA, Antunes M, Falacho RI, Sequeira D, Roseiro L. Effect of restorative timing on shear bond strength of composite resin/calcium silicate–based cements adhesive interfaces. Clin Oral Investig, 2021;25:3131-9. [CrossRef]

45. Carretero V, Giner-Tarrida L, Peñate L, Arregui M. Shear bond strength of nanohybrid composite to biodentine with three different adhesives. Coat, 2019;9:783. [CrossRef]

46. Ha H-T. The effect of the maturation time of calcium silicate-based cement (Biodentine™) on resin bonding: an in vitro study. Appl Adhes Sci, 2019;7:1-13. [CrossRef]

47. Singla MG, Wahi P. Comparative evaluation of shear bond strength of Biodentine, Endocem mineral trioxide aggregate, and TheraCal LC to resin composite using a universal adhesive: An: in vitro: study. Endodontology, 2020;32:14-9. [CrossRef]

48. Meraji N, Camilleri J. Bonding over dentin replacement materials. J Endod, 2017;43:1343-9. [CrossRef]

49. Cengiz E, Ulusoy N. Microshear bond strength of tri-calcium silicate-based cements to different restorative materials. J Adhes Dent, 2016;18:231-7.

50. Aksoy S, Ünal M. Shear bond strength of universal adhesive systems to a bioactive dentin substitute (Biodentine) at different time intervals. SDS, 2017;1:116-22. [CrossRef]

51. Hashem DF, Foxton R, Manoharan A, Watson TF, Banerjee A. The physical characteristics of resin composite–calcium silicate interface as part of a layered/laminate adhesive restoration. Dent Mater, 2014;30:343-9. [CrossRef]

52. Odabaş ME, Bani M, Tirali RE. Shear bond strengths of different adhesive systems to biodentine. Sci. World J, 2013;2013:1-5 [CrossRef]

53. Kudva A, Raghunath A, Nair PM, Shetty HK, D'Costa VF, Jayaprakash K. Comparative evaluation of shear bond strength of a bioactive material to composite resin using three different universal bonding agents: An in vitro study. J Conserv Dent, 2022;25:54. [CrossRef]

54. Ismail AM, Bourauel C, ElBanna A, Salah Eldin T. Micro versus macro shear bond strength testing of dentin-composite interface using chisel and wireloop loading techniques. Dent J, 2021;9:140. [CrossRef]

55. Chan M-l, Lau K-t, Wong T-t, Ho M-p, Hui D. Mechanism of reinforcement in a nanoclay/polymer composite. Compos B: Eng, 2011;42:1708-12. [CrossRef]

56. Nekoofar MH, Motevasselian F, Mirzaei M, Yassini E, Pouyanfar H, Dummer PM. The micro-shear bond strength of various resinous restorative materials to aged biodentine. Iran Endod J, 2018;13:356.

57. Deepa VL, Dhamaraju B, Bollu IP, Balaji TS. Shear bond strength evaluation of resin composite bonded to three different liners: TheraCal LC, Biodentine, and resin-modified glass ionomer cement using universal adhesive: An in vitro study. J Conserv Dent, 2016;19:166. [CrossRef]

Original research

In vitro fracture resistance of implant-supported terminal zirconia cantilevered frameworks

Purpose
This study aims to investigate the in vitro fracture loads of three different terminal cantilever forms of implant-supported zirconia frameworks.

Materials and Methods
A total of 30 implant-supported zirconia frameworks (Aconia, China) were CAD/CAM-fabricated and divided into three groups, each with a distal abutment cantilever form design of 5mm: Group A had square cantilevers, Group B had oval cantilevers, and Group C had oval-square cantilevers. Universal testing machine was used to apply vertical loads to the samples, and the fracture loads were recorded. Variance analysis and Tukey's post-hoc tests were applied for statistical evaluation.

Results
There was no significant difference between the mean fracture loads of Group B (587.8±112.2 N) and Group C (591.3 ±81.3 N), but both of these groups exhibited significantly lower fracture loads compared to Group A (893.8±145 N, p<0.001 for each).

Conclusion
Within the scope of this experimental study, it can be concluded that implant-supported terminal square shaped cantilever zirconia frameworks, each measuring 5 mm from the distal abutment, are more likely to exhibit greater resistance to vertical loads compared to their oval and oval-square counterparts.

Keywords: Fixed partial denture, zirconia, implant, fracture load, dental prosthesis

Tabark Shihab Al Bayati[1] ID,
Saja Ali Muhsin[2] ID

ORCID IDs of the authors: T.S. 0009-0003-3576-6591; S.A.M. 0000-0003-0272-7409

[1]*Department of Dental Techniques, College of Health and Medical Techniques, Middle Technical University, Ministry of Higher Education and Scientific Research, Baghdad, Iraq*

[2]*Department of Dental Techniques, College of Health and Medical Techniques, Middle Technical University, Ministry of Higher Education and Scientific Research, Baghdad, Iraq*

Corresponding Author: Saja Ali Muhsin

E-mail: assist.prof.dr.sajaalimuhsin@gmail.com

Introduction

Cantilevered Fixed Partial Dentures (CFPDs) are among the alternative options available for patients with distal extension edentulous ridges. The evaluations vary, and some researchers have expressed concerns about the risks associated with CFPDs (1). Implant restorations may experience mechanical failure due to the potential interference of cantilevers with biomechanics (2). Patients with critical anatomical features, such as high ridge bone resorption structures near the maxillary sinus floor and inferior alveolar nerves, are recommended to opt for an implant-retained prosthesis. However, the demand for CFPDs has surged due to factors such as cost-effectiveness, patient comfort, and acceptance (3).

Loads on distal extensions can cause bending because of the hinging action of the restorations (4). Despite the absence of a consensus on the maximum permissible cantilever span, suggestions include considering anterior-posterior extension and the use of various prosthodontic materials (5). The Shorter Dental-Arch concept (SDA) may provide an alternative treatment option to reduce restoration bending and stress on implant/bone contacts caused by cantilever loads. Therefore, it is advisable to keep the distal extensions as short as possible (6).

Recently, the utilization of zirconia (Zr) dental restorations has witnessed a substantial increase. This surge can be attributed to their enhanced biocompatibility and mechanical attributes, including fracture strength and toughness, as well as physical properties such as dimensional stability and tooth color matching (7,3). Several authors have suggested that occlusal forces may have the potential to damage the cantilever structure by acting as a lever. However, there exists a lack of empirical consensus in the literature concerning classic titanium and Zr substructures due to their limited study, primarily in vitro and retrospective research studies (8). Zr ceramics find application in single crowns, implant abutments, frameworks, and fixed partial dentures (FPD) (9). The formation of inherent flaws and microcracks is an outcome of the intrinsic brittleness of ceramics, which continues to pose a fundamental challenge in the use of metal-free ceramic restorations (10). Over time, microcracks may propagate, ultimately leading to restorative fracture and failure (11). Zr dental restorations have demonstrated an increased resistance to crack propagation and microcrack formation. This heightened resistance may be attributed to the conversion of the tetragonal phase to the monoclinic phase through transformation toughening (12).

Computer-aided design and computer-aided manufacturing (CAD/CAM) represents an additional production method that plays a pivotal role in dentistry (13,14). The production of an ideal metal-ceramic restoration involves a myriad of intricate techniques that are method-sensitive, time-consuming and costly. With the advent of state-of-the-art CAD/CAM technology, it is now feasible to precisely fabricate Zr abutments for implant-supported fixed dental prostheses (FDPs) (15,16). Nonetheless, despite their remarkable mechanical capabilities, Zr FPDs are not exempt from challenges (17). FPDs located in posterior regions should ideally be able to withstand masticatory pressures without mechanical failure (18). This is of paramount importance for posterior restorations in terms of biofunctionality, as they are designed for functional mastication rather than purely aesthetic considerations (19). Molars are particularly susceptible to complex occlusal stresses, which can range from 300 to 800N. In certain patients exhibiting parafunctional behaviors, occlusal loads can escalate to 1000N (20). In terms of the implications and survival rates of Zr FPDs, the data is contingent on study designs and specific circumstances (21).

The use of implant-supported CAD/CAM fabricated cantilevered Zr frameworks (ISCZFs) in distal extension-free end saddle zones has arisen out of necessity (22,23). Currently, there is limited and insufficient evidence regarding the strength of ISCZFs concerning the size and dimensions of the cantilever (24,25). The indirect fabrication of restorations through CAD/CAM empowers dentists and practitioners to design a wide range of restorations, from simple inlays/onlays to single crowns, fixed partial dentures (FPDs), and even maxillofacial prostheses. CAD/CAM technology comes with no constraints, resulting in restorations that are long-lasting, aesthetically pleasing, biocompatible, possess greater marginal and internal adaptability, and are efficiently manufactured (26). However, the milling method involving diamond burs for the cutting blocks under torque may initially cause tiny, non-visible fractures that could propagate and eventually lead to restoration failure (27).

Many in-vitro studies related to implant-supported restorations excluded the use of cementation during testing procedures to ensure uniform stress distribution along the occlusal surface. Cement retention is often associated with occlusal integrity (28). Removing any excess cement material entirely from the subgingival area can be challenging (29). During the fabrication process, the flowable cement material may have lined the inner surface of the implant-supported crown, resulting in a tight fit between the restoration and the abutment. Cementless fixation (CLF) involves a recessed device on the occlusal surface of the abutment that uniformly distributes stresses along the occlusal surface (30). Consequently, CLF has been proposed as a novel retentive method for implant prostheses that do not rely on cement or screws. However, there have been few studies investigating the biomechanical aspects of the CLF implant crown, leaving the optimal design for reducing stress distribution on the CLF implant restoration uncertain.

In the present in-vitro study, the fracture load of the cross-sectional dimension of the cantilever on ISCZF was considered as the standard. The ultimate fracture strength of the specimens was assessed using a universal mechanical tester and incremental loading until failure. This method, known for its simplicity and accuracy, has been employed in previous studies to evaluate cantilever prostheses (31,32). The objective of this in-vitro study is to examine the fracture load of three different forms of terminal Zr cantilevers. According to the null hypothesis, the different forms of the terminal cantilevers would not have an impact on the fracture load of ISCZFs.

Materials and Methods

Sample preparation

In this in-vitro study, CAD/CAM ISCZF specimens (n=33) were fabricated using Aconia Zirconia blank (HT+, Sichuan, China). The specimens were then divided into three main groups (n=11) based on the forms of the terminal cantilever: Group A (Oval-shaped cantilever), Group B (Square-shaped cantilever), and Group C (Oval-square shaped cantilever).

The study utilized a Dentium arch (Dentium, Cypress CA, USA) to secure two mono-screw implants measuring 5mm in diameter and 10mm in height (De-Tech mono-screw implant, Ankara, Turkey). Digital implant-supported cantilever zirconia frameworks (ISCZFs) were designed for the study groups using Exocad dental (3.0 Galway 2018, Germany), and fabricated using the In lab imes-icore CORITEC 350i PRO milling device (GmbH & Co, Germany). The frameworks were milled from Aconia Zirconia blank HT+. Two identical cemented-retained mono-titanium abutments were used in the preparation of Zr implant-supported frameworks.

For the Co-Cr base model, a 3D-printed version was created using Bego Co-Cr (BEGO GmbH & Co, Germany) and the Riton Dual-150 DMLS Dental Laboratory Fit Laser Metal 3D Printer (Guangzhou, China) (33,34). All frameworks were designed with dimensions corresponding to the forms of the cantilever, as shown in Figure 1, and were sintered at 1520°C for 8h using ZITIN-TECH (Zhengzhou, China), to achieve full strength. The dimensions of all terminal cantilevers were confirmed using a digital caliper (Shanghai, China).

Fracture strength test

As per the ISO standardization for dental ceramics (6872:1995), each framework with a terminal cantilever underwent testing for ultimate fracture load using a Universal Testing Machine (Instron 1195, England). Failure was identified through naked-eye observation, discerning an audible crack or a sudden drop in the applied force at the terminal end of each specimen. The static load testing involved a traditional load-to-failure approach until fracture occurred (35).

A vertically oriented tapered-shaped plate, with a crosshead speed of 2mm/min, was directed to contact the framework 2mm away from the terminal end of the cantilever (see Figure 2). The maximum load values leading to fracture were recorded in newtons (N), and failure was determined by a sharp decrease in the applied force at the terminal cantilever.

Statistical analysis

The fracture load data for the three-shaped terminal cantilever was recorded and subjected to statistical analysis using IBM SPSS 22.0 (IBM SPSS Inc., Armonk, NY, USA). Analysis of variance (ANOVA) and post-hoc Tukey HSD test were employed to assess the differences between the fracture loads of the ISCZFs. The established statistical significance threshold was set at $p < 0.05$.

Results

The study results are presented in Table 1 and Figure 3. Oval-shaped terminal cantilever specimens failed at a mean load of 587.8±112.2N, square-shaped terminal cantilevers at 893.8±145N, and oval-square terminal cantilevers fractured at 591.3±81.3N.

The one-way ANOVA test indicated a statistically significant strength effect for the square-shaped terminal cantilever ($p < 001$). However, a non-significant interaction was observed between the oval and oval-square terminal cantilevers.

Specimens failed due to a fracture of the terminal cantilever without abutment copy damage or plastic deformation. In all oval and oval-squared terminal cantilevers, the distal abutment wall broke, leading to catastrophic crack propaga-
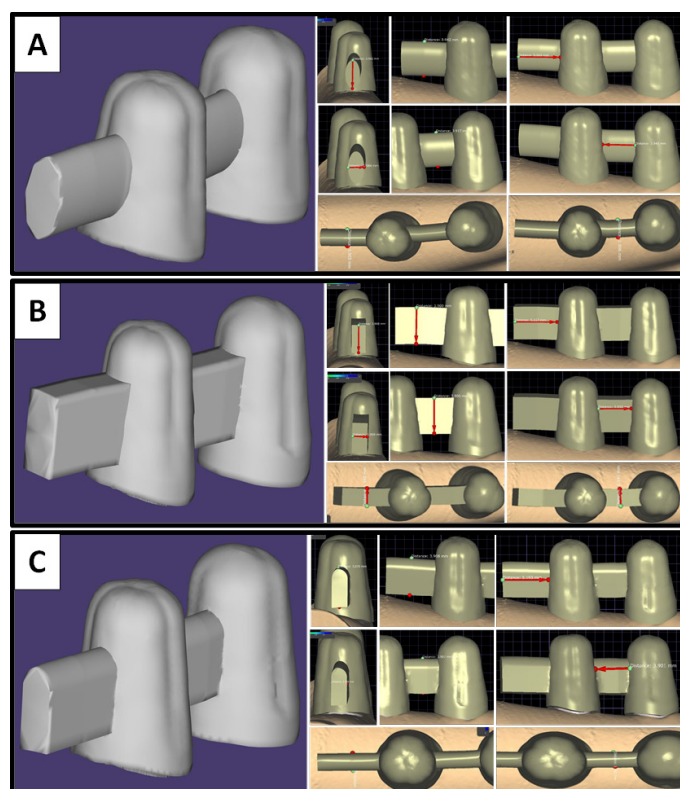
Figure 1. The CAD design and dimensions of the Zr framework terminal cantilevers, A, oval-shaped; A, Square-shaped; and C, Oval-square shaped cantilever
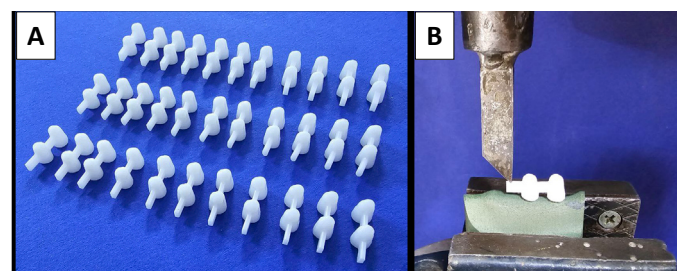
Figure 2. RPD Zr frameworks, A, Three different terminal cantilever designs; B, Terminal cantilever under load fracture testing chisel
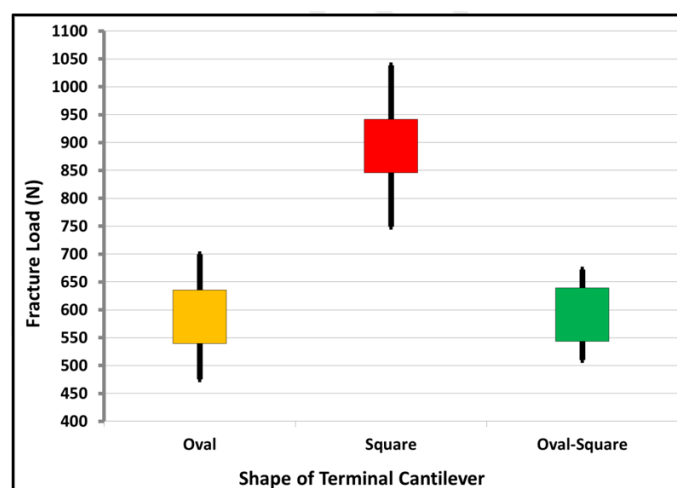
Figure 3. Box plot represent an ultimate fracture load for three shaped terminal cantilevers.

Table 1. *Analysis of variance and post-hoc Tukey HSD test showing the mean fracture load differences for three groups.*

Groups		Mean Difference	Std. Error	P-Value	Sig.	95% Confidence Interval	
						Lower Bound	Upper Bound
Oval	Square	-306.0000*	49.36945	.000	S	-427.7091	-184.2909
	Oval-Square	-3.4545	49.36945	.997	NS	-125.1636	118.2545
Square	Oval-Square	302.5455*	49.36945	.000	S	180.8364	424.2545

tion at the cantilever connector section. Fissures extended around the length of the distal abutment copy wall, reaching the connecting region. In contrast, the squared Zr specimens shattered at the very end of the terminal cantilever (see Figure 4 and Figure 5).
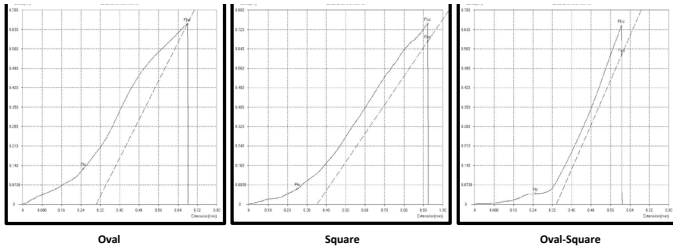
Figure 4. *The mode of failure for shaped terminal cantilevers, A, Oval; B, Square; and C, Oval-square*
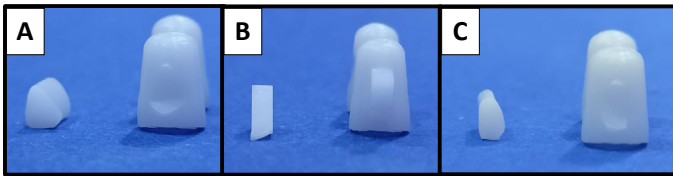
Figure 5. *Fractographical chart for the studied cantilevers.*

Discussion

The testing method, although based on static applied forces, can provide an early assessment of the mechanical properties of cantilevered restorations. Zr materials are prone to crack propagation and fracture due to their brittleness nature. Therefore, it is essential to identify some material's mechanical characteristics in advance, including fracture strength and fractographic analysis (32). Moreover, the use of implant mimics for testing the fracture resistance and stress distribution for implant-supported cemented crowns is well acknowledged (33).

A typical load-to-failure technique was employed to test Zr implant-supported frameworks with variable dimensions of a terminal cantilever. The null hypothesis has been partially rejected. In the case of the square-shaped terminal cantilever, different cantilever forms having the same fracture load were rejected. However, it is accepted in terms of oval and oval-square cross-sectional area cantilevers since non-significant interaction was found between both oval and oval-square terminal cantilevers.

The failure of terminal cantilevered implant-supported frameworks made of Zr occurred at the thinnest region of the abutment wall. Figures 4 and 5 show the failures that occurred within the abutment walls, likely at internal stress concentrators as a result of abutment copy design. Tensile forces cause cracks to propagate and fracture within the thinnest ceramic part of 1mm thickness. Future research should investigate the impact of thickening the abutment copy wall. The distal abutment wall shattered all oval and oval-squared terminal cantilevers, resulting in catastrophic crack propagation to the cantilever connector region.

Despite the lack of long-term successful clinical evidence and complication rates of Zr FPDs, one systematic review advocated for the use of posterior Zr FPDPs (35). The inter-

occlusal space available for restorative material is likely to influence the cantilever dimension. As a result, the cantilever shape must fit inside the given area. It seems that certain connector specifications enable the terminal cantilever to overcome higher loads and have superior fracture resistance (2). This study applied a static load with gradual displacement increases till failure, following the experimental methods over a 3D-printed Cobalt-Chromium (Co-Cr) mandibular testing model. Although this study's static load up to failure testing does not reflect the clinical conditions, it can be considered a preliminary determination for ultimate fracture force. It might denote the sort of fracture force that is applicable to terminal cantilevered Zr restorations, and further studies are needed to highlight the effect of terminal cantilever cross-section on the performance of FPDs.

The current study's cantilever form was a basic Zr beam. To overcome the problem of stresses at the site of failure, future research will properly include the importing of a 3D study component of framework design into modeling and finite element analysis (FEM/FEA) by reinforcing the areas of weakness within the framework. Zr thermocycling loading in a wet environment should also be established to determine how this material is expected to perform in an oral environment, as well as include cementation and the use of the original components of the implant system.

This study was conducted without veneering porcelain, as the overlaying veneering porcelain may weaken the specimens. Recent treatment procedures have incorporated unique Zr with partial designs to reduce or eliminate veneering porcelain fractures. Furthermore, in the current design, Zr FPDFs were mounted on third-party 3D non-titanium implant-printed counterparts with no cementation. The critical fracture force of the frameworks might be lower due to the use of non-original components that cause misfits at the implant-abutment contact (28,29).

Conclusion

This in-vitro data suggests that the use of a 5mm square-shaped short terminal cantilever with Zr frameworks should be limited to the two distal implant-supported occluding units. It appears that employing a cantilevered implant-supported restoration could be a viable alternative in partial edentulous rehabilitations. The success of implant-retainer Zr cantilevers replacing posterior teeth relies on a computerized prosthetic approach that considers the design of the cantilever area. Consequently, for prosthetic construction dependent on the position and shape of the terminal cantilever, a comprehensive examination of the implant-supported case is necessary.

Türkçe özet: *İmplant destekli terminal zirkonya kantilever alt yapıların in vitro kırılma direnci. Amaç: Bu çalışma, implant destekli zirkonya alt yapıların üç farklı şekilli kantilever formunun in vitro kırılma yüklerini araştırmayı amaçlamaktadır. Gereç ve Yöntem: Toplam 30 adet implant destekli zirkonya alt yapı (Aconia, Çin) CAD/CAM ile üretildi ve her biri 5 mm'lik distale uzanan farklı kantilever kesit tasarımına sahip üç gruba ayrıldı: Grup A'da kare, Grup B'de ise oval ve Grup C'de oval-kare şekilli numuneler hazırlandı. Numunelere dikey yükler uygulamak için evrensel test cihaı kullanıldı ve kırılma yükleri kaydedildi. İstatistiksel değerlendirmede varyans analizi ve Tukey post-hoc testleri uygulandı. Bulgular: Grup B (587,8±112,2 N) ve Grup C'nin (591,3 ±81,3 N)*

ortalama kırılma yükleri arasında anlamlı bir fark yoktu, ancak her iki grup da Grup A'ya (893,8±145 N) kıyasla anlamlı derecede daha düşük kırık yükleri sergiledi (her biri için p<0,001). Sonuç: Bu deneysel çalışma kapsamında, her biri distal dayanaktan 5 mm uzanan kare şekilli zirkonya implant destekli terminal kantileverlerin, oval ve köşeli alt yapılara kıyasla dikey yüklere karşı daha fazla direnç gösterme ihtimalinin daha yüksek olduğu sonucuna varılabilir. Anahtar kelimeler: sabit bölümlü protez, zirkonya, implant, kırık yükü, diş protezi

References

1. Norström Saarva, V.; Bjerkstig, G.; Örtorp, A.; Svanborg, P., A three-year retrospective study on survival of ceramic-veneered zirconia (Y-TZP) fixed dental prostheses performed in private practices. Int J Dent 2017; 2017. https://doi.org/10.1155/2017/9618306 [CrossRef]

2. De Andrade, G. S.; Kalman, L.; Giudice, R. L.; Adolfi, D.; Feilzer, A. J.; Tribst, J. P. M., Biomechanics of implant-supported restorations. Braz Dent Sci. 2023; 26. https://doi.org/10.4322/bds.2023.e3637 [CrossRef]

3. Tang, Y.; Yu, H.; Wang, J.; Qiu, L., Implant Survival and Complication Prevalence in Complete-Arch Implant-Supported Fixed Dental Prostheses: A Retrospective Study with a Mean Follow-up of 5 Years. Int J Oral Maxillofac Implants. 2023; 38. https://doi.org/10.11607/jomi.9808 [CrossRef]

4. D'Amico, C.; Bocchieri, S.; Sambataro, S.; Surace, G.; Stumpo, C.; Fiorillo, L., Occlusal load considerations in implant-supported fixed restorations. Prosthesis. 2020; 2:252-65. https://doi.org/10.3390/prosthesis2040023 [CrossRef]

5. Walter, L.; Greenstein, G., Utility of measuring anterior-posterior spread to determine distal cantilever length off a fixed implant-supported full-arch prosthesis: a review of the literature. J Am Dent Assoc. 2020;151:790-95. https://doi.org/10.1016/j.adaj.2020.06.016 [CrossRef]

6. Haroyan-Darbinyan, E.; Romeo-Rubio, M.; Del Río-Highsmith, J.; Lynch, C. D.; Castillo-Oyagüe, R., Thermo-mechanical behavior of alternative material combinations for full-arch implant-supported hybrid prostheses with short cantilevers. J Dent. 2023; 132: 104470. https://doi.org/10.1016/j.jdent.2023.104470 [CrossRef]

7. Alshamrani, A.; Alhotan, A.; Kelly, E.; Ellakwa, A., Mechanical and Biocompatibility Properties of 3D-Printed Dental Resin Reinforced with Glass Silica and Zirconia Nanoparticles: In Vitro Study. Polym. 2023; 15:2523. https://doi.org/10.3390/polym15112523 [CrossRef]

8. Branco, A. C.; Colaço, R.; Figueiredo-Pina, C. G.; Serro, A. P., Recent Advances on 3D-Printed Zirconia-Based Dental Materials:

9. Solá-Ruiz, M. F.; Leon-Martine, R.; Labaig-Rueda, C.; Selva-Otalaorrouchi, E.; Agustín-Panadero, R., Clinical outcomes of veneered zirconia anterior partial fixed dental prostheses: A 12-year prospective clinical trial. J Prosthet Dent. 2022; 127: 846-51. https://doi.org/10.1016/j.prosdent.2020.09.046 [CrossRef]

10. Liu, C.; Liao, Y.; Jiao, W.; Zhang, X.; Wang, N.; Yu, J.; Liu, Y. T.; Ding, B., High Toughness Combined with High Strength in Oxide Ceramic Nanofibers. Adv Mater. 2023. 2304401. https://doi.org/10.1002/adma.202304401 [CrossRef]

11. Zhang, Y.; Kelly, J. R., Dental ceramics for restoration and metal veneering. Dent Clin. 2017; 61:797-819. https://doi.org/10.1016/j.cden.2017.06.005 [CrossRef]

12. Abbas, M.; Ramesh, S.; Tasfy, S.; Lee, K. S.; Gul, M.; Aljaoni, B., Effect of sintering additives on the properties of alumina toughened zirconia (ATZ). MRS Commun. 2023; 1-9. https://doi.org/10.1557/s43579-023-00400-y [CrossRef]

13. Lancellotta, V.; Pagano, S.; Tagliaferri, L.; Piergentini, M.; Ricci, A.; Montecchiani, S.; Saldi, S.; Chierchini, S.; Cianetti, S.; Valentini, V., Individual 3-dimensional printed mold for treating hard palate carcinoma with brachytherapy: A clinical report. J Prosthet Dent. 2019; 121(4):690-93. https://doi.org/10.1016/j.prosdent.2018.06.016 [CrossRef]

14. Meirowitz, A.; Bitterman, Y.; Levy, S.; Mijiritsky, E.; Dolev, E., An in vitro evaluation of marginal fit zirconia crowns fabricated by a CAD-CAM dental laboratory and a milling center. BMC Oral Health. 2019; 19:1-6. https://doi.org/10.1186/s12903-019-0810-9 [CrossRef]

15. Reuss, J. M.; Reuss, D.; Rutten, L.; Mateo, B.; Vilaboa, B. R.; Vilaboa, D. R., Facially Driven Rehabilitation of a Cleft Lip and Palate Patient with an Implant-Supported Complete Fixed Dental Prosthesis: Outcome of a Multidisciplinary Approach. Int J Prosthodont. 2023; 36. https://doi.org/10.11607/ijp.7622 [CrossRef]

16. Shokry, T. E., Evaluation of Fracture Resistance of Long Span Implant Supported Fixed Dental Prostheses Fabricated from Different CAD/CAM Materials. Al-Azhar J Dent Sci. 2023; 26:15-25. https://doi.org/10.21608/ajdsm.2022.115225.1286 [CrossRef]

17. Hu, M.-L.; Lin, H.; Zhang, Y.-D.; Han, J.-M., Comparison of technical, biological, and esthetic parameters of ceramic and metal-ceramic implant-supported fixed dental prostheses: A systematic review and meta-analysis. J Prosthet Dent. 2020; 124:26-35. e2. https://doi.org/10.1016/j.prosdent.2019.07.008 [CrossRef]

18. Yin, S.; Cizek, J.; Chen, C.; Jenkins, R.; O'Donnell, G.; Lupoi, R., Metallurgical bonding between metal matrix and core-shelled reinforcements in cold sprayed composite coating. Scr Mater. 2020; 177:49-53. https://doi.org/10.3390/ma12142252 [CrossRef]

19. Budală, D. G.; Lupu, C. I.; Vasluianu, R. I.; Ioanid, N.; Butnaru, O. M.; Baciu, E.-R., A Contemporary Review of Clinical Factors Involved in Speech-Perspectives from a Prosthodontist Point of View. Medicina. 2023; 59:1322. https://doi.org/10.3390/medicina59071322 [CrossRef]

20. Dorado, S.; Arias, A.; Jimenez-Octavio, J. R., Biomechanical Modelling for Tooth Survival Studies: Mechanical Properties, Loads and Boundary Conditions—A Narrative Review. Mater. 2022; 15:7852. https://doi.org/10.3390/ma15217852 [CrossRef]

21. Matta, R. E.; Eitner, S.; Stelzer, S. P.; Reich, S.; Wichmann, M.; Berger, L., Ten-year clinical performance of zirconia posterior fixed partial dentures. J Oral Rehabil. 2022; 49:71-80. https://doi.org/10.1111/joor.13276/v1/review1 [CrossRef]

22. Horsch, L.; Kronsteiner, D.; Rammelsberg, P., Survival and complications of implant-supported cantilever fixed dental prostheses with zirconia and metal frameworks: A retrospective cohort study. Clin Implant Dent Relat Res. 2022. https://doi.org/10.1111/cid.13125 [CrossRef]

23. Karasan, D.; Canay, S.; Sailer, I.; Att, W., Zirconia Cantilever Fixed Dental Prostheses Supported by One or Two Implants: An In Vitro Study on Mechanical Stability and Technical Outcomes. Int J Oral Maxillofac Implants. 2022; 37. https://doi.org/10.11607/jomi.8953 [CrossRef]

24. Takaba, M.; Tanaka, S.; Ishiura, Y.; Baba, K., Implant-supported fixed dental prostheses with CAD/CAM-fabricated porcelain crown and zirconia-based framework. J Prosthodont on Complex Restorations. 2016; 225-31. https://doi.org/10.1111/jopr.12001 [CrossRef]

25. D'Albis, G.; D'Albis, V.; Susca, B.; Palma, M.; Al Krenawi, N., Implant-supported zirconia fixed partial dentures cantilevered in the lateral-posterior area: A 4-year clinical results. J Dent Res Dent Clin Dent Prospects. 2022; 16: 258-63. https://doi.org/10.34172/joddd.2022.041 [CrossRef]

26. Lee, B.; Oh, K. C.; Haam, D.; Lee, J.-H.; Moon, H.-S., Evaluation of the fit of zirconia copings fabricated by direct and indirect digital scanning procedures. J Prosthet Dent. 2018; 120: 225-31. https://doi.org/10.1016/j.prosdent.2017.08.003 [CrossRef]

27. Alao, A.-R.; Stoll, R.; Zhang, Y.; Yin, L., Influence of CAD/CAM milling, sintering and surface treatments on the fatigue behavior of lithium disilicate glass ceramic. J Mech Behav Biomed Mater. 2021; 113: 104133. https://doi.org/10.1016/j.jmbbm.2020.104133 [CrossRef]

28. Sancho-Puchades, M.; Crameri, D.; Özcan, M.; Sailer, I.; Jung, R.; Hämmerle, C.; Thoma, D., The influence of the emergence profile on the amount of undetected cement excess after delivery of cement-retained implant reconstructions. Clin Oral Implants Res. 2017; 28: 1515-22. https://doi.org/10.1111/clr.13020 [CrossRef]

29. Gehrke, P.; Bleuel, K.; Fischer, C.; Sader, R., Influence of margin location and luting material on the amount of undetected cement excess on CAD/CAM implant abutments and cement-retained zirconia crowns: an in-vitro study. BMC Oral Health. 2019; 19: 1-12. https://doi.org/10.1186/s12903-019-0809-2 [CrossRef]

30. Al-Sanea, A.; Mutlu, I.; Kişioğlu, Y.; Mohamed, E., The Effect of V-Thread and Square Thread Dental Implants on Bone Stresses. J Biomim Biomater Biomed Eng. 2023; 60: 83-96. https://doi.org/10.4028/p-3qasy2 [CrossRef]

31. Novais, M.; Silva, A. S.; Mendes, J.; Barreiros, P.; Aroso, C.; Mendes, J. M., Fracture Resistance of CAD/CAM Implant-Supported 3Y-TZP-Zirconia Cantilevers: An In Vitro Study. Mater. 2022; 15: 6638. https://doi.org/10.3390/ma15196638 [CrossRef]

32. Ghavami-Lahiji, M.; Firouzmanesh, M.; Bagheri, H.; Kashi, T. S. J.; Razazpour, F.; Behroozibakhsh, M., The effect of thermocycling on the degree of conversion and mechanical properties of a microhybrid dental resin composite. Restor Dent Endod. 2018; 43. https://doi.org/10.5395/rde.2018.43.e26 [CrossRef]

33. Gomes, R. S.; Bergamo, E. T. P.; Bordin, D.; Cury, A. A. D. B., The substitution of the implant and abutment for their analogs in mechanical studies: In vitro and in silico analysis. Mater Sci Eng: C. 2017; 75: 50-54. https://doi.org/10.1016/j.msec.2017.02.034 [CrossRef]

34. Stamenković, D.; Popović, M.; Rudolf, R.; Zrilić, M.; Raić, K.; Đuričić, K. O.; Stamenković, D., Comparative Study of the Microstructure and Properties of Cast-Fabricated and 3D-Printed Laser-Sintered Co–Cr Alloys for Removable Partial Denture Frameworks. Mater. 2023; 16: 3267. https://doi.org/10.3390/ma16083267 [CrossRef]

35. Sadid-Zadeh, R.; Lin, K.; Li, R.; Nagy, K., Fracture strength of screw-retained zirconia crowns assembled on zirconia and titanium implants. J Prosthodont. 2023. https://doi.org/10.1111/jopr.13683 [CrossRef]

Original research

The antimicrobial effect of R-limonene and its nano emulsion on *Enterococcus faecalis - In vitro* study

Purpose
This study aimed to evaluate the effectiveness of R-limonene and its nano emulsion formulation against *Enterococcus faecalis (E. faecalis)* in infected root canals.

Materials and Methods
A nano emulsion containing 20% R-limonene was prepared using the phase inversion method. *E. faecalis* was cultivated, and MIC/MBC values were determined through the macrodilution method. Standardized *E. faecalis* suspensions were used to infect the root canals ex vivo. Subsequently, R-limonene, nano emulsion containing 20% R-limonene, calcium hydroxide, and sterile saline were applied to the infected root canals for 7 days at the determined MIC/MBC dose. The root canals were sampled, and droplets were plated onto Mueller-Hinton agar plates, and viable bacteria (Colony Forming Units, CFU/mL) were counted. Statistical analyzes were performed based on the data.

Results
Statistically similar efficacy was observed between test materials on the root canal samples. All test materials were significantly more effective than the saline control (p<0.05), however, none of the test materials completely eliminated *E. faecalis* from root canals.

Conclusion
Although the effects of R-limonene on *E. faecalis* in infected root canals appeared to be like calcium hydroxide, with its broad antibacterial spectrum, gutta-percha softening and cleansing benefits, it was considered that it could considered among antimicrobials that could be used especially in endodontic retreatments alone or in synergistic combinations.

Keywords: Antimicrobial effect, calcium hydroxide, Enterococcus faecalis, nano emulsion, R-limonene

Introduction

Enterococcus faecalis (*E. faecalis*) is an enteric facultative Gram-positive cocci frequently associated with persistent endodontic infections (1). In addition to several virulence factors displayed by this species, *E. faecalis* isolates expressed varied resistance patterns to some agents used as intracanal medications including calcium hydroxide pastes (2). The proton pump of the *E. faecalis* cell wall, the dentin buffering capacity in the clinical samples, the bacteria's deep penetration into dentin tubules, and the biofilm formation characterize the behavior of this bacterial species in the face of calcium hydroxide in root canal treatment. Therefore, conventional calcium hydroxide cannot penetrate well into dentinal tubules resulting in limited effectiveness of this material on this microorganism. This finding leads researchers to explore new and different forms and combinations of antimicrobial agents and various application methods.

Ilke Doga Seker[1] ,
Tayfun Alacam[2] ,
Gulcin Akca[3] ,
Aysel Yilmaz[4] ,
Sevgi Takka[4]

ORCID IDs of the authors: I.D.S. 0000-0001-9531-240X; T.A. 0000-0002-1456-0223; G.A. 0000-0002-8877-4144; A.Y. 0000-0001-8874-1521; S.T. 0000-0001-6451-0497

[1]Department of Endodontics, Faculty of Dentistry, Gazi University, Ankara, Türkiye

[2]Department of Endodontics, Faculty of Dentistry, Lokman Hekim University, Ankara, Türkiye

[3]Department of Medical Microbiology, Faculty of Dentistry, Gazi University, Ankara, Türkiye

[4]Department of Pharmaceutical Technology, Faculty of Pharmacy, Gazi University, Ankara, Türkiye

Corresponding Author: Tayfun Alacam

E-mail: talacam@gazi.edu.tr

Medicinal plants have been found to have various therapeutic properties such as antimicrobial, anti-inflammatory, sedative/anxiolytic, analgesic, antioxidant, anticoagulant, anti-cariogenic, antiseptic, and antitumor effects (3-5). These properties make them functional in a wide range of endodontic applications, such as irrigation solutions, intracanal drugs, chelating agents, gutta-percha solvents, storage media for traumatic injuries, and repair materials in vital pulp therapy (6). Limonene, a cyclic monoterpene, and the primary component of essential oils in citrus plants has been identified as one of the most important active compounds with antimicrobial effects (7). A previous study showed that *Citrus limonum* essential oil, which has a high content of limonene (73%), was effective against endodontic pathogens, including *E. faecalis* (8). The use of *Citrus limonum* and R-limonene in endodontics is promising because of their antimicrobial, antioxidant, anti-inflammatory, and gutta-percha solvent effects. The antimicrobial mechanism of R-limonene involves disrupting the integrity of the cytoplasmic membrane of microorganisms, causing leakage of cellular components, and inhibiting respiratory enzymes (9, 10). Using R-limonene in the form of a nano emulsion carrier system can further enhance its penetration into microorganism cells and dentinal tubules. Due to its smaller size and its existence as a kinetically stable system, nano emulsions may exhibit improved functional properties compared to conventional emulsions. A nano emulsion carrier system prepared with a mixture of D-limonene and terpene has been shown to significantly increase the antimicrobial activity of the compounds (11).

E. faecalis is a microorganism commonly found in unsuccessful endodontic treatments. If any form of R-limonene will provide a plus benefit as an antimicrobial on this microorganism, the use of R-limonene in retreatment cases will gain a dual benefit along with its organic dissolving property on gutta-percha. This study aimed to investigate the antibacterial effects of R-limonene and its nano emulsion containing 20% R-limonene on root canals infected with *E. faecalis* and to compare these effects against calcium hydroxide. The null hypothesis of this study states there is no difference between pure R-limonene and its nano emulsion formulations and their effects compared to calcium hydroxide on *E.faecalis* infected root canals.

Materials and Methods

Ethical statement

The study protocol was approved by the Gazi University Faculty of Dentistry Clinical Research Ethics Committee with the number 21071282-050.99/06 and dated 12/03/2020.

Chemicals used in the study

(R)-(+)-Limonene was purchased from Alfa Aesar (97%, Stab., Kandel, Germany). Calcium hydroxide, Polysorbate 80 (Tween 80) and 1,2-Propanediol (Propylene Glycol) were purchased from Merck KGaA (Darmstadt, Germany). All other chemicals and reagents were of analytical grade.

Sample size determination

Power analysis was performed according to one-way ANOVA (analysis of variance) for the sample size of the number of viable bacteria after treatment with the test (R-limonene, nano emulsion containing 20% R-limonene) or control materials (calcium hydroxide, saline solution) to be compared. In calculating the sample size, the probability of Type I error ($\alpha=0.05$) and the power of the test ($1-\beta$) were considered as 0.95. When literature studies (12) were examined, it was seen that the average difference of 0.6 points was significant and therefore the effect size was taken as 0.6 points. Using the G Power 3.1.9.2 (Heinrich Heine-Universität, Düsseldorf, Germany) program, it was calculated that the total sample size should be 64 teeth, with 16 teeth in each group [($\alpha=0.05$), ($1-\beta=0.95$)].

Preparation of R-limonene nano emulsions

R-limonene nano emulsions were prepared using the phase inversion method with some modifications (10, 13, 14). The water phase consisted of sterile distilled water and propylene glycol in a mass ratio of 2:1, while the oil phase included R-limonene and Tween-80. Experiments were performed in triplicate, and nano emulsions were evaluated for their external phase detection, droplet size and zeta potential measurements, microscopic examination, viscosity, flow properties, and stability.

The external phase of the nano emulsions was determined using the dyeing method and it was found that all the prepared nano emulsions formed an oil-in-water emulsion. Droplets smaller than 200 nm were obtained in all formulations, and the mean diameter of the droplets decreased as the surfactant concentration increased. Zeta potential values also decreased with increasing surfactant concentration. A nano emulsion containing 20% (w/w) R-limonene/10% (w/w) Tween-80 formulation was chosen for further testing.

The stability of nano emulsion containing 20% R-limonene was evaluated at 4, 25, and 40 °C for one week, during which time no significant changes in overall physical appearance, droplet size, or zeta potential were observed. Microscopic examination revealed that oil droplets were homogeneously distributed in the water phase. The viscosity of nano emulsion containing 20% R-limonene was determined as 8.128±0.17 mPa.s and exhibited pseudoplastic flow properties.

Determination of the minimum inhibitory and bactericidal concentration (MIC/MBC)

In this study, the standard bacterial strain *E. faecalis* (ATCC 29212) was used. Preliminary experiments indicated the effectiveness of R-limonene in agar diffusion tests (data not shown). Therefore, it was decided to determine the minimum inhibitory concentration (MIC) and minimum bactericidal concentration (MBC) of both R-limonene and its nano emulsion containing 20% R-limonene. A serial macrodilution method was used to determine MI/MBC, and the relevant data are summarized in Table 1.

Endodontic experiment setup

This study is based on the approach of Turner *et al.* (12). Accordingly, 64 recently extracted human maxillary molar teeth were collected, and the palatal roots were resected and coronally abraded to length of 11 mm. The working length was determined as 1 mm shorter than the length at which the tip of the #10 K-file (Dentsply Sirona, Ballaigues, Switzerland) ap-

peared at the apical foramen and was adjusted to 10 mm (Figure 1). The canals were prepared using ProTaper Gold (PTG; Dentsply Sirona, Ballaigues, Switzerland) nickel-titanium rotary files, and the preparation was completed with PTG F2. During preparation, sodium hypochlorite (Wizard, Rehber Chemistry, Istanbul, Turkey) irrigation (10 mL, 1%) was performed using sterile endodontic needles and a 5 mL syringe. The standardized roots were rinsed in an ultrasonic bath (Eurosonic Micro, Euronda, Vicenza, Italy) first with water for 5 minutes, then with 17% ethylenediaminetetraacetic acid (EDTA; Wizard, Rehber Chemistry, Istanbul, Turkey) for 4 minutes, sodium hypochlorite (1%) for 4 minutes, and finally with water for 5 minutes, respectively. After sterilization in an autoclave (15 min at 121°), three layers of clear nail polish were applied to all outer root surfaces, and the apical regions of the roots were covered with composite resin (Charisma, Kulzer, Hanau, Germany). The roots were then placed in sterile Eppendorf tubes upright.

Infection of root canals

Using brain heart infusion (BHI; Merck KGaA, Darmstadt, Germany) broth, the *E. faecalis* bacterial suspension was adjusted according to the 0.5 McFarland standard (1.5×10^8 CFU/mL). Each root canal was infected and incubated for 21 days at 37 °C, sealed in 2 ml of bacterial suspension within separate Eppendorf tubes. The canals were recontaminated with bacterial suspension in a fresh medium every 3 days. The viability (culturing) and purity (gram staining, microscopic examination) of the bacteria were also controlled periodically.

Medication of root canals

After 21 days, the canals were rinsed with 5 mL saline using a sterile endodontic needle and dried with sterile paper points. Roots were distributed into 2 test groups and 2 control groups, each containing 16 roots. In the first group, the determined MIC/MBC value of R-limonene (210,3 mg/mL; dilution in Tween 80) was applied using a 27-gauge dental needle and syringe (Set Inject; Set Medical Instruments, Istanbul, Turkey).

In the second group (nano emulsion containing 20% R-limonene), the R-limonene concentration was 195,29 mg/mL. In the third group, a mixture of calcium hydroxide powder (Merck KGaA, Darmstadt, Germany) and distilled water (15) was applied using a sterile lentulo spiral filler (Dentsply Sirona). The fourth group was washed only with sterile saline solution, as the control groups. The canal openings were closed with dental wax, and then all samples were incubated in Eppendorf tubes at 37 °C for 7 days with the closed caps. After seven days, the canals were rinsed with 5 mL of sterile saline solution and dried using sterile paper points (DiaDent, Chongju, Korea). The root canals were sampled using a sterile PTG F3 file, and the dentinal chips were collected into a sterile Eppendorf tube containing 1 mL of BHI broth, followed by vortexing for 30 seconds. Ten-fold serial dilutions were prepared, and inoculations were made on Mueller-Hinton agar (MHA; Merck KGaA, Darmstadt, Germany) plates. The plates were incubated at 37 °C for 24 hours. Colonies that grew at the end of the incubation were counted, and the result for each sample, in terms of viable bacteria count in CFU/mL was recorded.

Statistical analysis

Descriptive statistics for the number of viable bacteria were calculated for R-limonene, nano emulsion containing 20% R-limonene, calcium hydroxide and saline solution. Normality assumptions were examined using the Shapiro-Wilk test. Since the assumption of normal distribution was not provided, the non-parametric Kruskal-Wallis test was used to compare the materials. Pairwise comparisons were made using Dunn's test with Bonferroni correction. All analyzes were performed using SPSS v23 software (IBM Corp. SPSS Statistics for Windows, Armonk, NY, USA) and the upper limit for the significance level was taken as 0.05.

Results

The number of viable bacteria counts, and statistical analysis results are given in Table 2 and Table 3. The Shapiro-Wilk test showed that the viable bacterial count did not follow a normal distribution, and Figure 2 revealed the presence of outliers and/or skewness in the data.

Table 1. *Minimum Inhibitory Concentration and Minimum Bactericidal Concentration (MIC/MBC) values .*

Type of Microorganism	Type of test medicament	Concentration range	MIC/MBC
E. faecalis	R-limonene	841.2 mg/mL – 1.64 mg/mL	210.3 mg/mL
	Nano emulsion containing 20% R-limonene	195.29 mg/mL – 0.38 mg/mL	48.82 mg/mL

Figure 1. *The diagram depicting the workflow of the experiment.*

Table 2. *Comparison of materials in terms of the number of viable bacteria.*

Material	Median$^\Psi$	IQR	χ^2	P
R-limonene	3.39×10^6 a	6.33×10^6		
Nano emulsion containing 20% R-limonene	4.16×10^6 a	1.25×10^7	37.09	<0.001
Calcium hydroxide	2.08×10^6 a	2.32×10^6		
Saline solution	1.38×10^8 b	4.85×10^7		

$^\Psi$: *Within the same column, different letters indicate groups statistically differing from each other based on post hoc comparisons by Dunn's test (P<.05).*
IQR: Interquartile Range; χ2 (Kruskal-Wallis Test Statistics Value)

Table 3. *Descriptive statistics on the number of viable bacteria.*

Measurement	Group	M	SD	Min	Max	SW
Number of viable bacteria	R-limonene	5.56×10^6	7.25×10^6	1.08×10^5	2.64×10^7	.732*
	Nano emulsion containing 20% R-limonene	6.31×10^6	6.31×10^6	2.56×10^3	1.61×10^7	.819*
	Calcium hydroxide	1.61×10^6	1.17×10^6	1.80×10^2	3.58×10^6	.878*
	Saline solution	1.43×10^8	3.93×10^7	9.20×10^7	2.52×10^8	.905

$p<0.05$ (The data is not from the Normal Distributions); M: Mean; SD: Standard Deviation; SW: Shapiro-Wilk
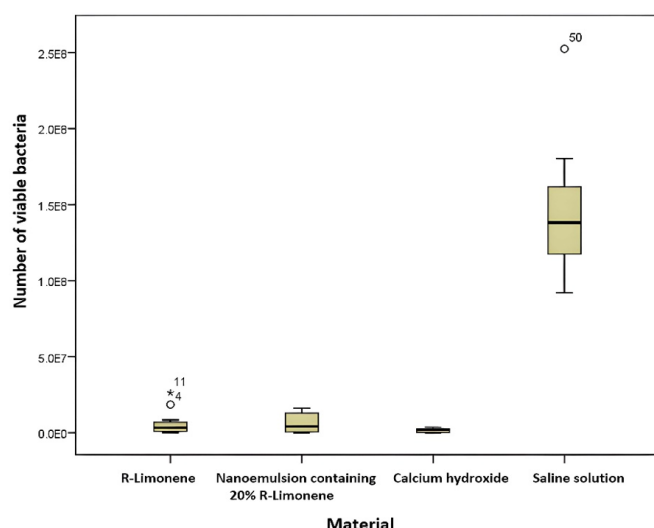
Figure 2. *Distribution graph at the material level in terms of viable bacteria count values.*

Figure 3. *Graphs of the binary comparison test of the materials over the viable bacteria count values.*

Statistical analysis of the materials according to the number of viable bacteria showed that the measurement values of the saline solution were significantly higher than the other materials ($p<0.05$). On the other hand, there was no statistically significant difference between the nano emulsion containing 20% R-limonene, R-limonene, and calcium hydroxide materials. Pairwise comparisons revealed that each group had significantly lower bacterial count compared to the saline control, and a significant difference was found between each group and the saline solution (Figure 3).

Discussion

There has been increased interest in herbal products recently in dentistry due to their high therapeutic efficacy and fewer adverse effects. Limonene is the main compound contained in all citrus-derived essential oils. It is widely used as a flavoring in commercial applications such as the food and beverage industry, due to its transparency and pleasant citrus fragrance. It is listed in the code of federal regulations as generally considered safe (GRAS) for food preservation (16). In addition, limonene has aroused the interest of many researchers due to its wide spectrum of antimicrobial activities, making it a promising antimicrobial agent (17, 18), as a green solvent for the extraction of natural products (19), and its ability to serve as a substitute solvent for chloroform for softening gutta-percha during endodontic retreatment cases (20).

To minimize the oxidation degradation and hydrophobicity of limonene, nano emulsion technology has been widely used for its encapsulation (11, 21). Nano emulsions are very efficient in terms of improving the stability and decreasing the disruption of encapsulated compounds (22). Furthermore, it is believed that the same encapsulated component displays higher antimicrobial activity compared to the bulk form. This might be due to tiny droplets of the formulation that can easily penetrate bacterial cells and destabilize the lipid envelope of the treated microorganisms (23, 24).

The purpose of this study was to compare the antibacterial properties of R-limonene and its nano emulsion containing 20% R-limonene on *E. faecalis* in infected root canals. It was first planned to develop nano emulsion formulation containing 20% R-limonene using the phase inversion method, known for being cost-effective, time-efficient, and does not require high energy. Initially, it was thought that an emulsion formulation with a droplet size of "nm" would be effective in terms of antibacterial activity, and it was aimed to develop stable and nano-sized emulsions with the phase inversion method. The results of the macrodilution method showed that the nano emulsion containing 20% R-limonene exhibited a lower MIC/MBC against *E. faecalis* compared to R-limonene. This difference can be attributed to the improved transport mechanism of the nano-sized emulsion form of R-limonene to the cell membrane of target microorganisms. Additionally, R-limonene is susceptible to oxidative degradation, which results in direct loss of activity. Therefore, the protection offered by the nano emulsion form of R-limonene against oxidative stress contributed to the increased antimicrobial activity observed in this study. On the other hand, the hydrophobic nature of R-limonene may have prevented

its homogeneous dispersion in the macrodilution method, which could be the reason for the less antimicrobial effect.

MIC/MBC values were determined for R-limonene and nano emulsion containing 20% R-limonene, and these values were then applied to infected canals at the prepared concentration. While using R-limonene and nano emulsion containing 20% R-limonene in the root canals in this study, care was taken to include R-limonene in a similar mass ratio to understand which form of R-limonene would be more effective. The least number of viable bacteria was observed in calcium hydroxide. Subsequently, R-limonene, nano emulsion containing 20% R-limonene, and saline solution were observed, respectively. The number of viable bacteria in the saline group was significantly higher than the other materials in infected root canals.

On the other hand, it was observed that both R-limonene and its nano emulsion containing 20% R-limonene demonstrated similar efficacy against *E. faecalis* on infected root canal dentin as that of calcium hydroxide. According to these results, the fact that there was no difference between calcium hydroxide and pure R-limonene and the nano emulsion form on infected root canals confirmed the null hypothesis. Findings regarding the number of viable bacteria for nano emulsion similar to that of R-limonene were consistent with results reported by Sonu *et al.* (25) who reported that the nano emulsion of limonene and limonene dissolved in dimethyl sulfoxide had an antimicrobial effect on *Bacillus cereus, Escherichia coli, E. faecalis,* and *Salmonella typhi* microorganisms, but there was no difference between them. Although the nano emulsion containing 20% R-limonene was superior in terms of MIC/MBC value, it lost its advantage when exposed to structural materials such as dentin, hydroxyapatite, and collagen found in infected root canals. The preparation method of nano emulsion, the amount of surfactant and active agent concentration, pH, ionic strength, temperature, and sampling technique problems arising from the complexities of root canal anatomy, as well as the penetration factor of microorganisms into dentinal tubules, and subsequent culturing, may be the causes of variation in the number of microorganisms among the groups. An increase in the sample size in future studies would mitigate the effects of variations and may provide more supporting evidence for the benefit of using nano emulsions in infected teeth during the endodontic treatment.

The retreatment requires the complete removal of the filling material from the root canal space, usually made by the association of gutta-percha and some endodontic cement (26). The effectiveness of this procedure is guaranteed by the total removal of the sealer and the gutta-percha from an inadequately shaped and filled root canal system because it is critical to uncover remnants of necrotic tissue or bacteria, and they have to be exposed to a more efficient chemo-mechanical disinfection procedure (27). Organic solvents have to be applied during retreatment to reduce the resistance of filling materials inside the root canal, thus facilitating their removal (28). The orange oil solvent is traditionally used for cleansing and removing various types of cement, pastes, and impression materials from instruments, mixing plates, devices, patient skin, tissues, etc., but it is widely indicated as a solvent during endodontic retreatments. Orange oil was found to be more biocompatible than eucalyptol, xy-

lol, chloroform, and halothane (29). The main ingredient of *Citrus limonum* essential oil is monoterpenoids, especially limonene. Orange oil solvent efficiency was found similar to chloroform, so it is recommended as a suitable alternative to this product. This facilitates chemo-mechanical preparation, and the irrigating solutions can access all ramifications of the entire root canal system during retreatment by decreasing the residual microbial population (30). Thus, citrus oil has discrete effectiveness in the antimicrobial, antioxidant, anti-inflammatory activity, and solvent action on remnants of gutta-percha in endodontic retreatment. Given the association of *E. faecalis* in cases of chronic failure in endodontically treated teeth, a medication especially for this species may be of value (8).

Using normal saline to eliminate calcium hydroxide was one of the limitations of this study. It is not possible to be sure that some remnants of calcium hydroxide were not included in the collected debris, which should be considered in future studies. One of the other limitation of our study is that it was conducted under *in vitro* conditions. The effectiveness of antiseptic substances is affected by factors such as the density of the active substance, incubation time, ambient temperature, root canal condition, pH, pollution level, and the amount of organic matter in the environment. Considerations should include the resistance of microorganisms, the interaction between microorganisms, host factors, inactivation by bacteria in the canal, and the ability of the drug to penetrate the dentin tissue and canal details. Since microorganisms diffuse into the dentin canals, intracanal drugs must also be capable of penetrating the dentin canals or spreading their activity deeply. The wetting properties of antiseptics are also gaining importance. Additionally, biofilms and bacterial aggregation are general mechanisms for the survival of bacteria and are virulence factors that play an important role in development. In addition to the antibacterial effect in irrigation and disinfection of root canals, the prevention of bacterial adhesion should also be considered. The fact that R-limonene, nano emulsion containing 20% R-limonene, and calcium hydroxide showed similar results suggests that R-limonene could serve as an alternative to intracanal medicaments used in root canals, considering its other properties. The organic solvent feature, gutta-percha dissolving capability, and antibacterial effects all indicate that this natural product holds promise for use in endodontics.

Conclusion

Within the limitations of this *in vitro* experiment, it can be concluded that both R-limonene and its nano emulsion containing 20% R-limonene demonstrated similar efficacy against *E. faecalis* on infected root canal dentin as that of calcium hydroxide. Although we have determined that the nano emulsion form does not provide a plus advantage over its pure form in terms of its antibacterial effect on *E. faecalis*, the use of the nano emulsion form may be preferable in retreatment cases, for its gutta-percha dissolving efficacy, existing broad-spectrum antibacterial effects, and protection against oxidative stress. Furthermore, due to its anti-inflammatory, and antioxidant properties, R-limonene can be incorporated into the content of endodontic medicaments, irrigation solutions, and sealers.

Türkçe Özet: *R-Limonen ve nanoemülsiyonunun Enterococcus fae-calis üzerindeki antimikrobiyal etkisi- In vitro çalışma. Amaç: Bu çalış-ma, enfekte kök kanallarında Enterococcus faecalis'e (E. faecalis) karşı R-limonen'in ve onun nanoemülsiyon formülasyonunun etkinliğini değerlendirmeyi amaçlamaktadır. Gereç ve yöntem: %20 R-limonen içeren nanoemülsiyon, faz inversiyon yöntemi kullanılarak hazırlandı. E. faecalis kültüre edildi ve MIC/MBC değerleri makrodilüsyon yöntemi ile belirlendi. Standartlaştırılmış E. faecalis süspansiyonları kök kanal-larını enfekte etmek için ex vivo olarak kullanıldı. Daha sonra, R-limo-nen, %20 R-limonen içeren nanoemülsiyon, kalsiyum hidroksit ve ster-il salin, belirlenen MIC/MBC dozunda enfekte kök kanallarına 7 gün boyunca uygulandı. Kök kanallarından alınan örnekler, Mueller-Hinton agar plaklarına ekildi ve canlı bakteriler (CFU/mL) sayıldı. Verilere dayalı olarak istatistiksel analizler yapıldı. Bulgular: Test materyalleri arasın-da istatistiksel olarak benzer etkinlik gözlendi (p>0.05). Tüm test ma-teryalleri, salinden (p<0.05) önemli ölçüde daha etkiliydi, ancak hiçbir test materyali E. faecalis'i kök kanallarından tamamen elimine edeme-di. Sonuç: R-limonen'in enfekte kök kanallarında E. faecalis üzerinde-ki etkileri kalsiyum hidroksite benzer görünse de geniş antibakteriyel spektrumu, guta-perka yumuşatma etkisi ve temizleyici etkisi de göz önüne alınarak endodontik tedavilerde tek başına veya sinerjistik kom-binasyonlarla kullanılabilecek antimikrobiyaller arasında bulunabi-leceği düşünülmüştür. Anahtar kelimeler: Antimikrobiyal etki, kalsiyum hidroksit, Enterococcus faecalis, nanoemülsiyon, R-limonen.*

References

1. Sunde PT, Olsen I, Debelian GJ, Tronstad L. Microbiota of periapical lesions refractory to endodontic therapy. J Endod 2002;28:304-10. [CrossRef]
2. Byström A, Claesson R, Sundqvist G. The antibacterial effect of camphorated paramonochlorophenol, camphorated phenol and calcium hydroxide in the treatment of infected root canals. Dent Traumatol 1985;1:170-5. [CrossRef]
3. Sinha DJ, Sinha AA. Natural medicaments in dentistry. Ayu 2014;35:113-8. [CrossRef]
4. Tewari R, Kapoor B, Mishra S, Kumar A. Role of herbs in endodontics. Journal of Oral Research and Review 2016;8:95-9. [CrossRef]
5. Vishnuvardhini S, Sivakumar A, Ravi V, Prasad A, Sivakumar J. Herbendodontics–phytotherapy in endodontics: A review. Biomed Pharmacol J 2018;11:1073-82. [CrossRef]
6. Almadi EM, Almohaimede AA. Natural products in endodontics. Saudi Med J 2018;39:124-30. [CrossRef]
7. Jantrawut P, Boonsermsukcharoen K, Thipnan K, Chaiwarit T, Hwang KM, Park ES. Enhancement of antibacterial activity of orange oil in pectin thin film by microemulsion. Nanomaterials (Basel) 2018;8:545. [CrossRef]
8. Seker ID, Akca G, Alacam T. In vitro evaluation of antimicrobial effects of citrus limonum essential oil on some endodontic pathogens. Ann Med Res 2022;29:427-33. [CrossRef]
9. Zahi MR, El Hattab M, Liang H, Yuan Q. Enhancing the antimicrobial activity of d-limonene nano emulsion with the inclusion of ε-polylysine. Food Chem 2017;221:18-23. [CrossRef]
10. Zhang Z, Vrieskoop F, Yuan Q, Liang H. Effects of nisin on the antimicrobial activity of d-limonene and its nano emulsion. Food Chem 2014;150:307-12. [CrossRef]
11. Donsì F, Annunziata M, Sessa M, Ferrari G. Nanoencapsulation of essential oils to enhance their antimicrobial activity in foods. LWT - Food Science and Technology 2011;44:1908-14. [CrossRef]
12. Turner S, Love R, Lyons K. An in-vitro investigation of the antibacterial effect of nisin in root canals and canal wall radicular dentine. Int Endod J 2004;37:664-71. [CrossRef]
13. Feng J, Wang R, Chen Z, Zhang S, Yuan S, Cao H, Jafari SM, Yang W. Formulation optimization of d-limonene-loaded nano emulsions as a natural and efficient biopesticide. Colloids Surf A Physicochem Eng Asp 2020;596:124746. [CrossRef]
14. Maté J, Periago PM, Palop A. Combined effect of a nano emulsion of d-limonene and nisin on listeria monocytogenes growth and viability in culture media and foods. Food Sci Technol Int 2016;22:146-52. [CrossRef]
15. Alaçam T, Yoldaş HO, Gülen O. Dentin penetration of 2 calcium hydroxide combinations. Oral Surg Oral Med Oral Pathol Oral Radiol Endod 1998;86:469-72. [CrossRef]
16. Sun J. D-limonene: Safety and clinical applications. Altern Med Rev 2007;12:259-64.
17. Chikhoune A, Hazzit M, Kerbouche L, Baaliouamer A, Aissat K. Tetraclinis articulata(vahl) masters essential oils: Chemical composition and biological activities. Journal of Essential Oil Research 2013;25:300-7. [CrossRef]
18. Vuuren Sv, Viljoen AM. Antimicrobial activity of limonene enantiomers and 1, 8-cineole alone and in combination. Flavour Fragr J 2007;22:540-4. [CrossRef]
19. Chemat S, Tomao V, Chemat F. Limonene as green solvent for extraction of natural products. In: Mohammad A, editor. Green solvents i: Properties and applications in chemistry. Dordrecht: Springer Netherlands; 2012. p. 175-86. [CrossRef]
20. Uemura M, Hata G, Toda T, Weine FS. Effectiveness of eucalyptol and d-limonene as gutta-percha solvents. J Endod 1997;23:739-41. [CrossRef]
21. Li PH, Chiang BH. Process optimization and stability of d-limonene-in-water nano emulsions prepared by ultrasonic emulsification using response surface methodology. Ultrason Sonochem 2012;19:192-7. [CrossRef]
22. Weiss J, Gaysinsky S, Davidson M, McClements J. Nanostructured encapsulation systems: Food antimicrobials. In: Barbosa-Cánovas G, Mortimer A, Lineback D, Spiess W, Buckle K, Colonna P, editors. Global issues in food science and technology. San Diego: Academic Press; 2009. p. 425-79.
23. Baker J, Hamouda T, Shih A, Myc A, inventors; University of Michigan, assignee. Non-toxic antimicrobial compositions and methods of use. USA patent US-6559189-B2. 2003.

24. Zahi MR, Liang H, Yuan Q. Improving the antimicrobial activity of d-limonene using a novel organogel-based nano emulsion. Food Control 2015;50:554-9. [CrossRef]

25. Sonu KS, Mann B, Sharma R, Kumar R, Singh R. Physico-chemical and antimicrobial properties of d-limonene oil nano emulsion stabilized by whey protein-maltodextrin conjugates. J Food Sci Technol 2018;55:2749-57. [CrossRef]

26. Wennberg A, Ørstavik D. Evaluation of alternatives to chloroform in endodontic practice. Dent Traumatol 1989;5:234-7. [CrossRef]

27. Ørstavik D, Haapasalo M. Disinfection by endodontic irrigants and dressings of experimentally infected dentinal tubules. Dent Traumatol 1990;6:142-9. [CrossRef]

28. Bodrumlu E, Er O, Kayaoğlu G. Solubility of root canal sealers with different organic solvents. Oral Surg Oral Med Oral Pathol Oral Radiol Endod 2008;106:e67-9. [CrossRef]

29. Rehman K, Khan FR, Aman N. Comparison of orange oil and chloroform as gutta- percha solvents in endodontic retreatment. J Contemp Dent Pract 2013;14:478-82. [CrossRef]

30. Whitworth JM, Boursin EM. Dissolution of root canal sealer cements in volatile solvents. Int Endod J 2000;33:19-24. [CrossRef]

Original research

Comparison of screw and plate osteosynthesis in advancement genioplasty: a finite element analysis study

Purpose
The purpose of this study was to evaluate the distribution of stresses in screw and plate fixation systems during simulated advancement genioplasty using finite element analysis.

Materials and Methods
A cone-beam computed tomography image of a patient was used to create three-dimensional virtual models of mandibular bone. Chin advancement of 8 mm was simulated following a horizontal osteotomy of the chin in a computer-aided design program. The distal segment was stabilized with two titanium mini-screws placed bilaterally in the first model and a single 4-hole titanium pre-bent chin plate placed centrally in the second model. The plate was fixed with four mini-screws, two in the proximal and two in the distal segment. All fixative appliances were submitted to 15 N force applied backwards to the lingual surface of the chin parallel to the occlusal plane and 7 N force applied upwards to the buccal surface of the chin perpendicular to the occlusal plane. The distributions of von Mises stresses and deformations in bone and titanium materials were evaluated.

Results
In the screw fixation system (22.52 MPa) higher stress values were observed compared to the plate fixation system (13.71 MPa). The deformation value was higher for the screw fixation system (0.021 mm) than the plate fixation system (0.0007 mm).

Conclusion
In advancement genioplasty, fixation with a single pre-bent centrally placed chin plate showed slightly better stabilization than fixation with two bilaterally placed bicortical screws. The stress values were within the physical strength limits of bone and titanium for both systems.

Keywords: Genioplasty, bone plate, bone screw, finite element analysis, stress distribution

Introduction

The chin plays an important role in facial aesthetics and overall appearance and creates the basis for judging an individual's character (1). A properly shaped and positioned chin contributes to self-confidence and good social life (2).

Genioplasty is a surgical procedure performed to correct the cosmetic deformities of the chin in three dimensions and has been carried out alone or in association with other orthognathic surgical procedures (3). Hofer (4) first described the horizontal sliding osteotomy of the anterior half of the inferior border of the mandible performed by a submental approach to the chin in 1942. Trauner and Obwegeser (5) first described the intraoral approach to expose the symphysis for horizontal osteotomy of the chin in 1957. Over the years various modifications have been de-

Serap Gulsever[1] (iD),
Sumer Munevveroglu[1] (iD),
Selim Hartomacioglu[2] (iD),
Ipek Necla Guldiken[3] (iD),
Sina Uckan[1] (iD)

[1]Department of Oral and Maxillofacial Surgery, Faculty of Dentistry, Istanbul Medipol University, Istanbul, Turkiye

[2]Department of Mechanical Engineering, Faculty of Technology, Marmara University, Istanbul, Turkiye

[3]Department of Oral and Maxillofacial Surgery, Faculty of Dentistry, Istinye University, Istanbul, Turkiye

Corresponding Author: Serap Gulsever

E-mail: sgulsever@medipol.edu.tr

scribed to lengthen, shorten, advance, set back, widen, or narrow the chin.

Among all movements of the chin, the most frequently performed is the advancement genioplasty (2). Advancement genioplasty is a reliable surgical procedure however; suprahyoid muscles and perimandibular connective tissues attached to the mandible can contribute to mechanical instability and relapse by creating resistance during advancement (1,3). Therefore, the use of a proper fixation technique is important for predictable postoperative results. Today, rigid internal fixation with plates or screws is the standard procedure because of their ease of application and reliability (6-9).

Various studies were conducted to evaluate the most reliable fixation method in terms of skeletal and soft-tissue stability in genioplasty procedures (7-15), however, the discussion about the ideal type of fixation is still going on (16). To our knowledge, the stability of titanium bicortical screw and plate fixation systems have not been evaluated in advancement genioplasty procedures with large bone movements.

The aim of this study was to evaluate the stress distribution in titanium bicortical screws and pre-bent chin plates in simulated advancement genioplasty using finite element analysis (FEA).

Materials and Methods

Data acquisition and 3D model

A cone-beam computed tomography (CBCT) scan of a 26-year-old female patient which was obtained previously using Planmeca ProMax 3D (Planmeca, Roselle, IL, USA) was used to create a three-dimensional (3D) image of the mandibular bone. Images were saved in Digital Imaging and Communications in Medicine (DICOM) format. The DICOM data was imported to MIMICS software (Materialise, Leuven, Belgium), segmented by 222 to 3071 HU (Haunsfield unit) values, and 3D object data was created. This data was imported to reverse engineering software (Geomagic 11.0, Geomagic Company, Morrisville, NC, USA) to clean and repair the data and create a 3D surface model of the mandible. The surface model was imported to SolidWorks 2018 software (Dassault Systemes SolidWorks Corp., Waltham, MA, USA) to create a 3D solid model. Finite element models including the cortical and cancellous bones were employed and the mean cortical bone thickness was defined as 1.5 mm.

Surgical treatment simulation

A surgical treatment plan was simulated with an 8 mm advancement of the chin. The genioplasty technique simulated in the experiment was a horizontal osteotomy of the chin created approximately 5 mm below the inferior margins of the mental foramina and parallel to the horizontal plane. 2.0 mm titanium screws and 2.0 mm pre-bent titanium 4-hole chin plate with 8 mm step (KLS Martin, Tuttlingen, Germany) were measured using a digital caliper and the information obtained was used to create solid 3D models of hardware via SolidWorks software. Using the SolidWorks assembly module, all 3D models were assembled considering the surgical plan, and the assembly model was exported to STEP format. In the first model, two screws (2.0x19 mm) were placed bicortically (Figure 1A); in the second model, a centrally placed

pre-bent chin plate was fixed with two screws (2.0x11 mm) in the chin and another two in the mandible (Figure 1B) virtually. The STEP data was imported to ANSYS 18.1 Workbench software to perform the finite element simulation.

Finite element model

In this finite element study, firstly the model was opened using ANSYS SpaceClaim module to repair the geometric faults (e.g., split edges, extra edges, and inexact edges) and prepared for analysis. Secondly, using ANSYS Mesh module, the 3D mesh model was generated. The locations where critical stresses will occur were subjected to a more stringent mesh process. In the mesh structure; the numbers of the elements and nodes were 165117 and 275006 respectively for the screw fixation model, and 182555 and 300082 for the plate fixation model (Figure 2). Mechanical properties of the materials were defined in the ANSYS Workbench. Poisson's ratio and modulus of elasticity of all materials were obtained from the literature (17) (Table 1). All materials were considered isotropic, homogenous, and linearly elastic. The finite element package of ANSYS Workbench software was used to establish boundary conditions and loading conditions for the components of solid models. The symmetric boundary condition was applied to the symmetric region and the fixed support boundary condition was applied to the posterior region (Figure 3). Two different loads representing the muscle forces that can affect the distal segment during the postoperative bone healing period in a clinical situation were applied to each model. A load of 15 N parallel to the mandibular occlusal plane was applied back-
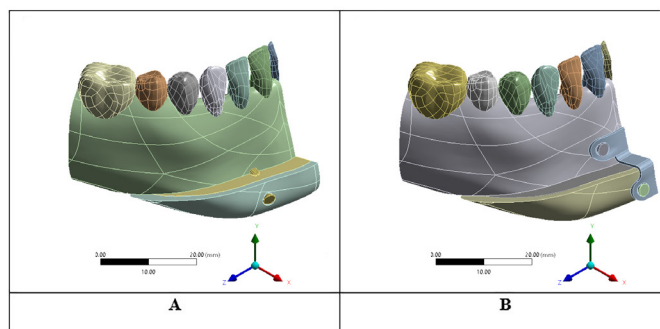
Figure 1. *Mandible models with simulated advancement genioplasty and fixation systems. (A) Screw fixation system; two screws (2.0x19 mm) were placed bicortically. (B) Plate fixation system; centrally placed pre-bent chin plate was fixed with four screws (2.0x11 mm).*
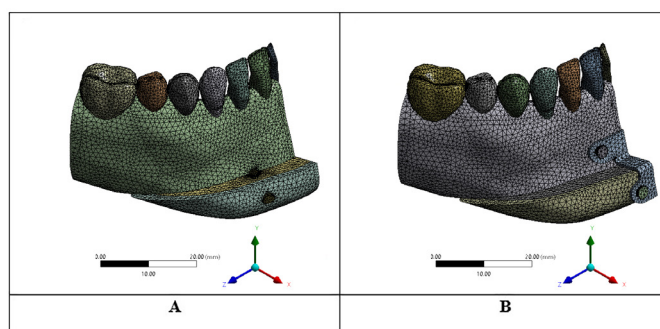
Figure 2. *Finite element mesh generation. (A) Screw fixation (B) Plate fixation.*

Table 1. *Mechanical properties of the materials.*

Structure	Modulus of elasticity (MPa)	Poisson's ratio
Cortical bone	13700	0,3
Medullary bone	1370	0,3
Titanium (Ti-6Al-4V)	110000	0,35

wards to the lingual surface of the chin segment, simulating the forces of the suprahyoid muscles. A load of 7 N perpendicular to the mandibular occlusal plane was applied upwards to the buccal surface of the chin segment, simulating the force of the mentalis muscle (Figure 3). The connections were contacted with frictionless contact and a non-linear solution was generated for each finite element model. The finite element solution took 8 iterations for the screw fixation model and 11 iterations for the plate fixation model (Figure 4).

The stress distribution and the deformation in the bone and fixation appliances were analyzed by the FEM. The distribution of stresses was analyzed with the equivalent von Mises stress criterion.
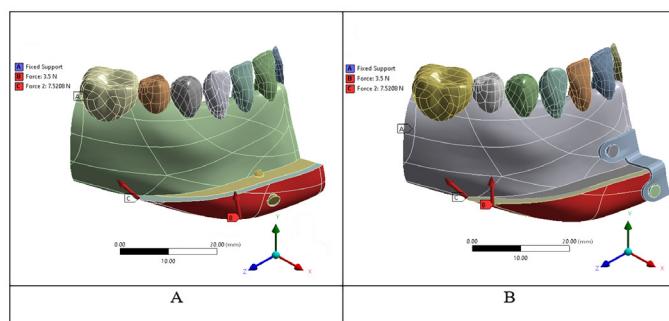
Figure 3. *Loading and boundary conditions in finite element simulations. (A) Screw fixation (B) Plate fixation.*
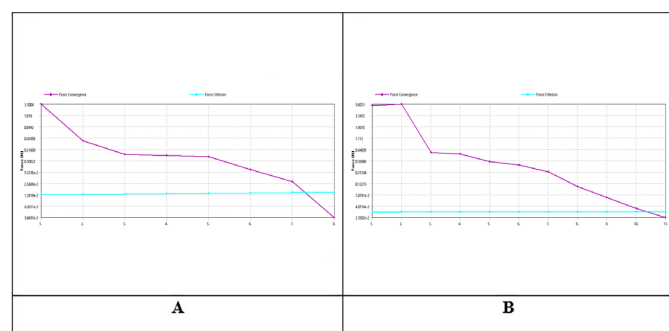
Figure 4. *Solution process and the total number of iterations. (A) Screw fixation (B) Plate fixation.*

Results

Higher stress values were observed for double screw fixation in comparison with a single chin plate fixation (Figure 5). For the screw fixation system, the maximum equivalent stress of 22.52 MPa was observed on the screw, and for the plate fixation system maximum equivalent stress of 13.71 MPa was observed on the plate (Figure 6) (Table 2).

Maximum equivalent stress values observed in the cortical bone of the proximal segment were 14.93 MPa in the screw
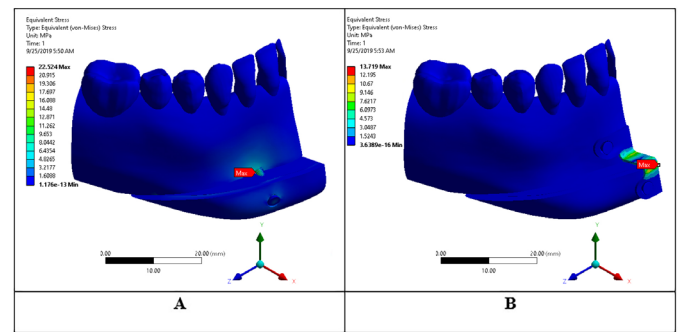
Figure 5. *Distribution of von Mises stresses in the structures. (A) Screw fixation (B) Plate fixation.*
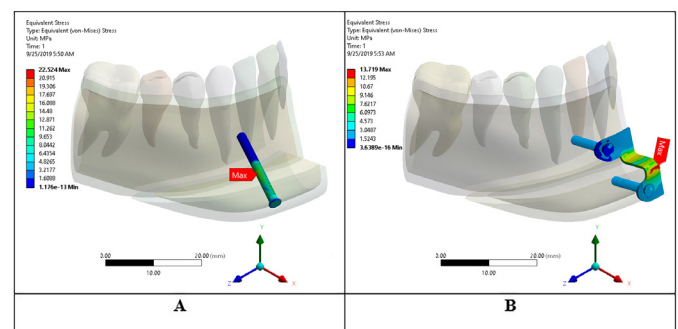
Figure 6. *Distribution of von Mises stresses in the fixation appliances. (A) Screw fixation (B) Plate fixation.*

Table 2. *Maximum equivalent (von Mises) stress values and deformation values.*

Fixation type	Maximum equivalent stress (MPa)	Deformation (mm)
Screw fixation	22.52	0.021
Plate fixation	13.71	0.0007

system and 2.74 MPa in the plate system (Figure 7). Maximum equivalent stress values observed in the cortical bone of the lower segment were 4.41 MPa in the screw system and 11.81 MPa in the plate system (Figure 8). In screw fixation system, the maximum stress (14.93 MPa) was observed in the part of the osteotomy line close to the screw body at the cortical bone of the proximal segment. In the plate fixation system, the maximum stress (11.81 MPa) was observed in the part of the osteotomy line under the plate at the cortical bone of the distal segment.

Maximum deformations were observed in the distal segments in both models. In the screw system, maximum deformation was 0.021 mm and observed in the chin region. In the plate system, maximum deformation was 0.0007 mm and observed in the posterior part of the distal segment (Figure 9) (Table 2).

Discussion

The long-term success of orthognathic surgery procedures resulting in ideal esthetic and function depends on skeletal and soft tissue stability that is obtained by achieving optimal osseous union. As with other maxillofacial osteotomies, two important mechanisms affect the stability of advancement genioplasty carried out by the osteotomy of the lower edge
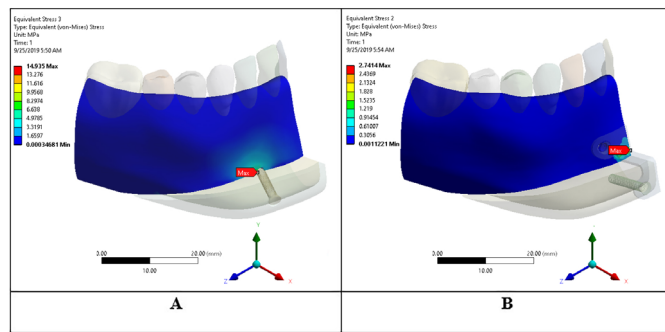
Figure 7. *Distribution of von Mises stresses in the cortical bone of the proximal segment. (A) Screw fixation (B) Plate fixation.*
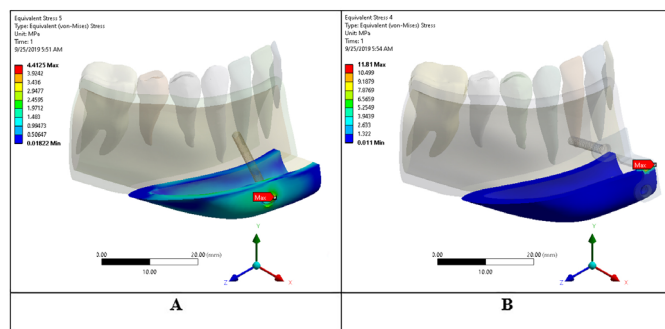
Figure 8. *Distribution of von Mises stresses in the cortical bone of the distal segment. (A) Screw fixation (B) Plate fixation.*
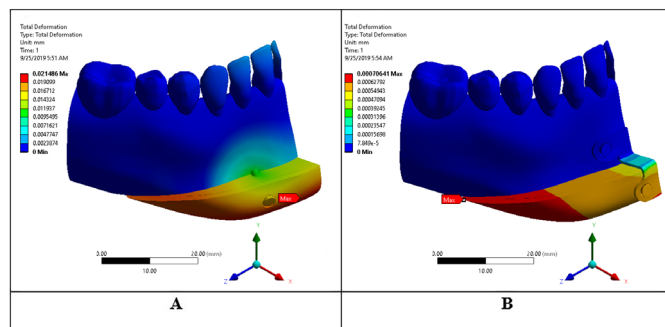
Figure 9. *Distribution of deformation in the structures. (A) Screw fixation (B) Plate fixation.*

of the mandible. The first one is the skeletal instability that may alter the surgical outcome by causing a change in the position of the genial segment before the osseous union. The second one is the osseous remodeling process, during which the advanced genial segment is slowly recontoured and may cause the final result to differ from the immediate postoperative outcome (1,7,18).

Fixation method, magnitude of surgical movement, and other factors such as age, gender, and occurrence of complications are possible factors that may influence the postoperative relapse rate in advancement genioplasty (2). Even though advancement genioplasty is considered a reliable surgical procedure with only minor relapses (2,8,10-12,19), the surgical results may not always be predictable, especially in large vertical and horizontal bony movements. The great propensity of the advanced genial segment to displace downward and posteriorly because of the tendency of the suprahyoid musculature and perimandibular connective tissues to retain the inferior segment in the original anatomic position contributes to potential bony instability and unde-

sired resorption especially when semirigid fixation is used (1,3,12,14,20,21). Additionally, the genial region is also vulnerable to external forces in daily life and sleep. Immobility of the repositioned genial segment should be achieved with a proper fixation technique before osseous union, for predictable results (14).

The literature is replete with studies reporting the use of different fixation techniques in genioplasty but there is still controversy about which of these methods is more successful regarding the skeletal stability, clinical advantages, and long-term results. In some studies, the instability of the bony segment due to the fixation method was held responsible for recurrence (15,21), while others indicated that the amount of recurrence was not related to the fixation method (2,9-11,22,23). At this point, the distinction between short-term bone healing and long-term bone remodeling should be considered. The close approximation of the bony segments by providing maximum stability promotes early osteogenesis and enhances short-term bone healing.

Rigid internal fixation is usually performed with the aid of screws, miniplates, and pre-bent chin plates in genioplasty procedures (14,20,24). Osteosynthesis with bone plates and/or screws has certain technical advantages regarding skeletal stability, especially in cases with complex, asymmetrical, and large chin movements (6,11,12,18,21). Although 3D planning is very helpful in preoperative planning, still the final decision of whether to use plate and/or screw osteosynthesis is often made during surgery in the operating room.

Pre-bent chin plates have become increasingly popular due to their ease of manipulation, and fixation with a single chin plate placed to the midline in the symphysis is often preferred (2,14,20). Screw osteosynthesis is also a viable option in genioplasty procedures, but the applicability of the technique depends on the osteotomy type and the direction of movement of the genial segment and it may be technically more challenging and sensitive than plate osteosynthesis (20). For screw fixation alone, the 2.0 mm bicortical screws are usually employed and a minimum of two screws is needed to achieve initial segmental stability (20,24). After the down-fractured segment is mobilized, it is relatively difficult to prepare the screw holes and insert the screws with maintaining the intraoperative segmental stability. When placing bicortical screws, holding the distal segment may cause undesired displacement of the distal segment that directly affects the postoperative symmetry of the chin. It is not easy to notice an asymmetry at the time of surgery and it may be obvious days or weeks after the operation. When genioplasty is performed to achieve the retro positioning of the chin, fixation with screws is difficult or even impossible because stabilization can be only possible if the screw can reach the far cortex (6,20). In the fixation of multisegmental osteotomies, maintaining the planned positional relationship between the bone fragments seems to be technically more difficult during the insertion of bicortical screws compared to the plates.

The amount of surgical movement is another important factor that could affect the stability of the procedure. The more the chin is advanced, the less the soft tissue follows the advancement due to the more tension on the soft tissues and the muscles (2,12). However, the results of some studies evaluating the effect of the magnitude of genial

advancement on relapse rates indicated no significant correlation between the amount of surgical movement and the amount of long-term relapse in the hard and soft tissues (3,8,10,19). Based on the knowledge that the main technical advantage of rigid fixation is successful applicability in large advancements and three-dimensional repositioning; in this study, the amount of chin advancement was determined as 8 mm, taking into account previous studies using 7 mm (3,8) or 8 mm (12,19) advancement, and the even-numbered step lengths of the pre-bent chin plates of the selected company.

In the present study, a FEA was used to compare the stability of fixation with pre-bent chin plate and screws. FEA is a numerical analysis method widely applied in engineering and is a powerful research tool that can be used to solve biomechanical problems in oral and maxillofacial sciences. Stress analysis obtained from finite element modeling of maxillofacial bony structures can provide information about the complex biomechanical behavior of bone and hardware affected by mechanical loading (25,26).

Although FEA is useful in the evaluation of osteotomy procedures, it has some limitations (27). Finite element modeling involves some assumptions and simplifications about material properties that differ from real clinical conditions. For example, bone is modeled as isotropic and homogeneous whereas, in fact, it is anisotropic and nonhomogeneous (26). In this study, it was assumed that the osteotomy line was smooth and clear and that the contacts between the bone and the osteosynthesis systems were 100%, but these conditions cannot be achieved in a clinical situation. In addition, in this study only the muscle forces acting on the distal segment were considered, however external forces that may affect this region during daily life and at sleep were not considered.

During the postoperative bone healing period, the distal segment is subjected to the retraction forces of the suprahyoid muscles, especially the anterior belly of the digastric muscle, which originates from the digastric fossa on the lingual surface of the mandible, and the geniohyoid muscle, which originates from the inferior mental spine of the symphysis menti. The mentalis muscle originates from the mental protuberance of the mandible near the midline and provides a weak upward-inward movement of the soft tissue complex of the chin. In this study, to represent the muscle forces to which the chin segment would be subjected in a clinical situation, a 15 N load parallel to the occlusal plane was applied backwards simulating the forces of the suprahyoid muscles and a 7 N load perpendicular to the occlusal plane was applied upwards simulating the force of the mentalis muscle. The backward applied loads were determined by considering the study by Ramos *et al.* (28).

There are many papers comparing titanium screw and plate osteosynthesis systems in terms of postoperative stability in other mandibular osteotomies. Although the results of these studies varied, generally it has been indicated that the factors that appear to have the greatest influence on the stability were the magnitude and direction of the bone movement. To the best of our knowledge, the only report that comparatively evaluated the stability of monocortical miniplate and bicortical screw systems in advancement genioplasty is the study by Aktı and Kalaycı (16) in which five different fixation models were evaluated in 5 mm advance-

ment genioplasty using finite element analysis. They reported that better stability and less displacement were observed in the bicortical screw fixation groups, but the plate groups were more favorable in terms of tensile and compression stresses. The present study demonstrated that; plate osteosynthesis showed slightly better stress distribution and less deformation than screw osteosynthesis, and in both fixation systems the maximum stress values in the bone and titanium fixation appliances were far below the yield strength values described for bone and Ti-6Al-4V alloy in the literature (29). Further studies performing fatigue analysis by applying higher forces to the genial segment in advancement genioplasty can be undertaken.

The decision of the fixation method to be used depends on the clinical characteristics of the case, such as the magnitude and the direction of segmental movement or the number of bone segments. Surgeons should be able to make this decision intraoperatively based on the final position of the advanced genial segment and considering the stresses that may affect the postoperative results.

Conclusion

Fixation with a single centrally positioned titanium miniplate is slightly more stable than fixation with two bilaterally positioned titanium bicortical screws in advancement genioplasty. Both osteosynthesis systems can withstand the loads that are exerted by the muscles that attach to the chin in the postoperative remodeling period.

Türkçe özet: *İlerletme genioplastisinde vida ve plak osteosentezinin karşilaştirilmasi: sonlu elemanlar analizi çalişması. Amaç: Bu çalişmanın amacı, ilerletme genioplastisinde vida ve plak fiksasyon sistemlerindeki stres dağılımını sonlu elemanlar analizi ile değerlendirmektir. Gereç ve Yöntem: Bir hastaya ait konik ışınlı bilgisayarlı tomografi görüntüleri kullanılarak mandibular kemiğinin üç boyutlu sanal modelleri oluşturulmuştur. Bilgisayar destekli tasarım programında çene ucunun horizontal osteotomisini takiben 8 mm'lik çene ucu ilerletmesi simüle edilmiştir. Distal segment, ilk modelde bilateral olarak yerleştirilen iki adet titanyum mini vida ile ve ikinci modelde ortaya yerleştirilen tek bir 4 delikli titanyum önceden bükülmüş genioplasti plağı ile stabilize edilmiştir. Plak, iki adet proksimal ve iki adet distal segmentte olmak üzere toplam dört adet mini vida ile fikse edilmiştir. Tüm fiksasyon araçları, çene ucunun lingual yüzeyine oklüzal düzleme paralel olarak lingual yönde uygulanan 15 N'luk ve çene ucunun bukkal yüzeyine oklüzal düzleme dik olarak yukarı yönde uygulanan 7 N'luk kuvvetlere maruz bırakılmıştır. Kemik ve titanyum materyallerdeki von Mises stres dağılımları ve deformasyonlar değerlendirilmiştir. Bulgular: Vida fiksasyon sisteminde (22,52 MPa), plak fiksasyon sistemine (13,71 MPa) göre daha yüksek stres değerleri gözlenmiştir. Deformasyon değeri vida fiksasyon sisteminde (0,021 mm), plak fiksasyon sistemine (0,0007 mm) göre daha yüksek bulunmuştur. Sonuç: İlerletme genioplastisinde, ortaya yerleştirilen tek bir önceden bükülmüş genioplasti plağı ile fiksasyon, bilateral yerleştirilen iki adet bikortikal vida ile fiksasyona göre daha iyi stabilizasyon göstermiştir. Her iki sistemdeki stres değerleri, kemik ve titanyumun fiziksel dayanım sınırları içerisinde kalmıştır. Anahtar kelimeler: Genioplasti, Plak, Vida, Sonlu elemanlar analizi, stres dağılımı*

for the study. SG, SM, SH participated in gathering the data for the study. SG, SM, SH, ING, SU participated in the analysis of the data. SG, SH wrote the majority of the original draft of the paper. SG, SM, SH, ING, SU participated in writing the paper. SG, SM, SH, ING, SU has had access to all of the raw data of the study. SG, SU has reviewed the pertinent raw data on which the results and conclusions of this study are based. SG, SM, SH, ING, SU have approved the final version of this paper. SG guarantees that all individuals who meet the Journal's authorship criteria are included as authors of this paper.

References

1. Brar RS, Gupta R, Gupta S, Chaudhary K, Singh P, Kaur M. Skeletal and Soft-Tissue Stability Following Advancement Genioplasty: A Comparative Analysis between Wire and Miniplate Osteosynthesis. J Pharm Bioallied Sci 2021;13:72–5. [CrossRef]
2. Janssens E, Shujaat S, Shaheen E, Politis C, Jacobs R. Long-term stability of isolated advancement genioplasty, and influence of associated risk factors: a systematic review. J Craniomaxillofac Surg 2021;49(4):269–76. [CrossRef]
3. Mortazavi H, Tabrizi R, Mohajerani H, Ozkan T. Evaluation of stability in advancement genioplasty: An 18-month follow-up. Shiraz Univ Dent J 2010;10:61–4.
4. Hofer O. Operation der prognathie and mikrogenie. Dtsch Zahn-, Mund-, und Kieferheilkunde 1942;9:121–32.
5. Trauner R, Obwegeser H. The surgical correction of mandibular prognathism and retrognathia with consideration of genioplasty. Part I. Surgical procedures to correct mandibular prognathism and reshaping of the chin. Oral Surg Oral Med Oral Pathol 1957;10(7):677–89. [CrossRef]
6. Precious DS, Cardoso AB, Cardoso MCAC, Doucet JC. Cost comparison of genioplasty: when indicated, wire osteosynthesis is more cost effective than plate and screw fixation. Oral Maxillofac Surg 2014;18:439–44. [CrossRef]
7. Shaik M, Koteswar Rao N, Kiran Kumar N, Prasanthi G. Comparison of rigid and semirigid fixation for advancement genioplasty. J Maxillofac Oral Surg 2013;12:260–5. [CrossRef]
8. Talebzadeh N, Pogrel MA. Long-term hard and soft tissue relapse rate after genioplasty. Oral Surg Oral Med Oral Pathol Oral Radiol Endod 2001;91(2):153–6. [CrossRef]
9. Ekram S, Arunkumar KV, Mowar A, Khera A. Evaluation of stability and esthetic outcome following rigid fixation of a new sagittal genioplasty technique - A clinical study. Natl J Maxillofac Surg 2021;12:17–24. [CrossRef]
10. Shaughnessy S, Mobarak KA, Hogevold HE, Espeland L. Long-term skeletal and soft-tissue responses after advancement genioplasty. Am J Orthod Dentofac Orthop 2006;130(1):8–17. [CrossRef]
11. Reyneke JP, Johnston T, Van der Linden WJ. Screw osteosynthesis compared with wire osteosynthesis in advancement genioplasty: a retrospective study of skeletal stability. Br J Oral Maxillofac Surg 1997;35(5):352–6. [CrossRef]
12. Polido WD, Regis LDC, Bell WH. Bone resorption, stability, and soft-tissue changes following large chin advancements. J Oral Maxillofac Surg 1991;49(3):251–6. [CrossRef]
13. Dr. Manoj Kumar Rawat Dr. Mohammed Ibrahim Dr. Hemanadh Kolli Dr.Sriram Choudary Nuthalapati Dr Shilpa Sunil Khanna Dr. Gowri Swaminatham Pendyala Dr. Rahul VC TiwariRawat MK, Ibrahim M, Kolli H, Nuthalapati SC, Khanna SS, Pendyala GS, Tiwari RVC. Comparison Of Two Different Osteosynthesis Technique To Evaluate Skeletal Stability In Advancement Genioplasty: A Retrospective Study. Eur J Molecul Clin Med 2020;7(3):5685–90.
14. Lee GT, Jung HD, Kim SY, Park HS, Jung YS. The stability following advancement genioplasty with biodegradable screw fixation. Br J Oral Maxillofac Surg 2014;52(4):363–8. [CrossRef]
15. Ueki K, Moroi A, Yoshizawa K. Stability of the chin after advancement genioplasty using absorbable plate and screws with template devices. J Craniomaxillofac Surg 2019;47(10):1498–503. [CrossRef]
16. Aktı A, Kalaycı A. İlerletme Genioplastisinde Kullanılan 5 Farklı Fiksasyon Sisteminin Stabilite ve Stres Dağılımlarının Sonlu Elemanlar Analizi ile Değerlendirilmesi. Selcuk Dent J 2020;7(3):364–72. [CrossRef]
17. Carneiro JA, Lima PRL, Leite MB, Toledo Filho RD. Compressive stress–strain behavior of steel fiber reinforced-recycled aggregate concrete. Cem Concr Compos 2014;46:65–72. [CrossRef]
18. DeFreitas CE, Ellis E III, Sinn DP. A retrospective study of advancement genioplasty using a special bone plate. J Oral Maxillofac Surg 1992;50(4):340–6. [CrossRef]
19. Van Sickels JE, Smith CV, Tiner BD, Jones DL. Hard and soft tissue predictability with advancement genioplasties. Oral Surg Oral Med Oral Pathol 1994;77(3):218–21. [CrossRef]
20. Payami A, Manji Z, Greenberg AM. Genioplasty Techniques. In: Greenberg AM, Schmelzeisen R (eds). Craniomaxillofacial Reconstructive and Corrective Bone Surgery. New York: Springer, 2019, p. 625–650. [CrossRef]
21. Precious DS, Armstrong JE, Morais D. Anatomic placement of fixation devices in genioplasty. Oral Surg Oral Med Oral Pathol 1992;73(1):2–8. [CrossRef]
22. Polido WD, Bell WH. Long-term osseous and soft tissue changes after large chin advancements. J Craniomaxillofac Surg 1993;21(2):54–9. [CrossRef]
23. Moragas JSM, Oth O, Büttner M, Mommaerts MY. A systematic review on soft-to-hard tissue ratios in orthognathic surgery part II: Chin procedures. J Craniomaxillofac Surg 2015;43(8):1530–40. [CrossRef]
24. Ward JL, Garri JI, Wolfe SA. The Osseous Genioplasty. Clin Plastic Surg 2007;34(3):485–500. [CrossRef]
25. Aquilina P, Chamoli U, Parr WCH, Clausen PD, Wroe S. Finite element analysis of three patterns of internal fixation of fractures of the mandibular condyle. Br J Oral Maxillofac Surg 2013;51(4):326–31. [CrossRef]
26. Erkmen E, Şimsek B, Yücel E, Kurt A. Three-dimensional finite element analysis used to compare methods of fixation after sagittal split ramus osteotomy: Setback surgery-posterior loading. Br J Oral Maxillofac Surg 2005;43(2):97–104. [CrossRef]
27. Atik F, Ataç MS, Özkan A, Kılınç Y, Arslan M. Biomechanical analysis of titanium fixation plates and screws in mandibular angle fractures. Niger J Clin Pract 2016;19(3):386–90. [CrossRef]
28. Ramos VF, Pinto LAPF, Basting RT. Force and deformation stresses in customized and non-customized plates during simulation of advancement genioplasty. J Craniomaxillofac Surg 2017;45(11):1820–7. [CrossRef]
29. Kayabaşı O, Yüzbasıoğlu E, Erzincanlı F. Static, dynamic and fatigue behaviors of dental implant using finite element method. Adv Eng Softw 2006;37(10):649–58. [CrossRef]

Original research

Optimizing the primary stability of dental implants in type IV bone: in-vitro comparison of machine-driven and ratcheting insertion protocols

Purpose
The objective of this study was to assess the effects of various implant insertion techniques on the primary stability of dental implants in both type II and type IV cadaveric bovine.

Materials and Methods
A total of 48 dental implants (BEGO Semados RSX, BEGO Implant Systems GmbH & Co. KG, Germany) with a diameter of 3.75 mm and a length of 12 mm were used in the experiments. Bovine bone ribs were adjusted to mimic type II and type IV bone characteristics. Following the preparation of recipient sites, implants were inserted using three different protocols: machine-driven insertion (Standard group, Std group), ratchet insertion (Ratcheted, R Group), and a combination of both (Std + R group). The Osstell® Beacon device was used to record the implant stability quotient (ISQ) of each implant immediately after insertion. Two-way analysis of variance and Bonferroni tests were used for statistical evaluation.

Results
Bone type significantly influenced the ISQ values ($p<0.05$). However, when comparing insertion protocols separately for type II and type IV bone, no significant differences were observed. In type IV bone, both the Std group and R group exhibited significantly lower ISQ values compared to the same groups in type II bone ($p<0.05$ for each). Nevertheless, there were no significant differences in the ISQ values when employing the Std+R technique between the two types of bone.

Conclusion
Combining machine-driven and ratchet insertion techniques may prove beneficial in optimizing ISQ values in bovine samples simulating type IV bone.

Keywords: Dental implants, oral surgical procedures, osseointegration, resonance frequency analysis

Nuri Mert Taysi¹ iD,
Aysegul Erten Taysi² iD,
Pınar Erçal³ iD,
Soner Sismanoglu⁴ iD

ORCID IDs of the authors: N.M.T. 0000-0002-5595-9302; A.E.T. 0000-0002-9156-9109; P.E. 0000-0002-0763-3930; S.Ş. 0000-0002-1272-5581

¹İstanbul University-Cerrahpasa, Faculty of Dentistry, Department of Oral and Maxillofacial Surgery, İstanbul, Türkiye

²Altinbas University, Faculty of Dentistry, Department of Oral and Maxillofacial Surgery, İstanbul, Türkiye

³Eastern Mediterranean University, Faculty of Dentistry, Famagusta, North Cyprus, Mersin-10-Turkey

⁴İstanbul University-Cerrahpasa, Faculty of Dentistry, Department of Restorative Dentistry, İstanbul, Türkiye

Corresponding Author: Nuri Mert Tayşi

E-mail: nurimert.taysi@iuc.edu.tr

Introduction

In recent decades, dental implant treatments have increasingly been regarded as a viable solution for providing functional rehabilitation to both partially and completely edentulous patients. This shift in perception is largely attributable to significant advancements in oral implantology (1). Therefore, it is of paramount importance that research efforts are directed toward fostering a consensus on achieving implant success through optimal treatment options (2). The success of dental implants hinges on both biological processes and mechanical factors, with the osseointegration process standing out as the predominant parameter in oral implantology (3, 4).

One crucial step in establishing optimal osseointegration based on long-term clinical experience is achieving primary stabilization (5, 6). Primary stabilization is a mechanical aspect that refers to the implant's

ability to withstand axial, lateral, and rotational loads within the bone at the time of implant placement (5-7). This initial mechanical stability arises from the difference in stiffness between the implant and the surrounding bone. The ultimate goal is to attain a level of primary stability sufficient to support biological processes during the subsequent healing phase (5, 6).

Various techniques can be employed to assess the initial mechanical stability, such as surgical insertion torque, removal torque, damping capacity analysis, and resonance frequency analysis (8). Resonance frequency analysis (RFA) stands out as one of the most widely used clinical techniques for measuring the implant stability quotient (ISQ) and, thus, evaluating the primary stability of an implant (9). RFA offers a non-invasive and objective approach, enabling clinicians to monitor implant stability over time and make necessary adjustments to treatment protocols, such as immediate loading in dental implants (10, 11).

Multiple factors, including implant design, bone quality, osseous morphology at the surgical site, bone vascularity, drilling techniques, insertion protocols, and clinicians' skill, have been shown to influence primary stability in various studies (3, 12). Maintaining optimal primary stability is especially critical in cases with poor bone density, as it can significantly impact the long-term success of implant procedures (9, 13). Consequently, this investigation has two primary objectives. First, by examining changes in primary stability under different insertion protocols for dental implants, we aim to determine the significance of the chosen protocol. Second, through a comparison of different bone types, we seek to offer guidance to clinicians regarding protocol preferences for cases with poor bone density. The null hypothesis for this study is that the utilization of different insertion protocols would not result in any differences in the primary stability achieved after implant placement.

Materials and Methods

All preparations of bone specimens and surgical procedures described below were carried out at room temperature by the same oral surgeon (N.M.T) to ensure standardization.

Selection and preparation of bone specimens

The macroscopic composition of cortical and medullary bone makes ribs a suitable choice for simulating edentulous human bone (14-17). For this study, fresh bovine ribs were purchased from a slaughterhouse. After removing all soft tissues and the periosteum from the bones using scalpels and periosteal elevators, 7 cm-long bone block pieces were cut under copious amount of saline irrigation in room temperature using a surgical saw. A total of 12 fresh bone blocks were checked macroscopically for irregularities. Subsequently, they were randomly assigned to three groups representing different insertion protocols: manual insertion group, handpiece insertion group, and combination group. In each group, the preparation of the bone blocks was conducted in accordance with established procedures from previous studies (18-21).

For half of the bone blocks, the cortical bone layer was thinned using 220-grit sandpaper until it reached a thickness of 2 mm, mimicking type II bone, which represents cor-

ticocancellous bone (18, 19, 21). For the other half, the distal epiphysis along the longitudinal axis of the bone blocks was selected to mimic type IV bone, representing cancellous bone (18-20). Each block received four implants (Figure 1).
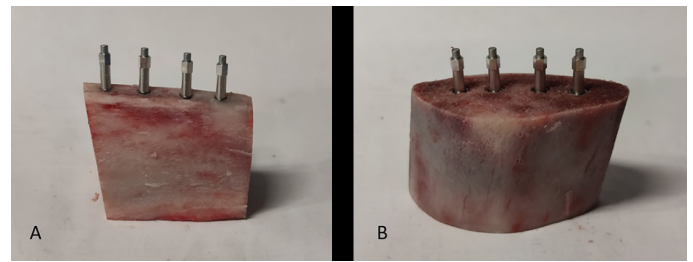
Figure 1. *Insertion of four dental implants for type II bone (A) and type IV bone (B).*

Experimental protocol and study groups

As part of the experimental protocol, bovine ribs were securely stabilized on a bench vise to prevent any micro-movements. The implant recipient site preparations for a total of 48 dental implants (BEGO Semados RSX, BEGO Implant Systems GmbH & Co. KG, Germany), each with a diameter of 3.75 mm and a length of 12 mm, were carried out in accordance with the BEGO Semados RS/RSX TrayPlus standard drilling protocol, following the manufacturer's recommendations. In the manual insertion group, 16 dental implants (8 implants for each bone type) were placed into the prepared sites using a ratchet connected to a torque wrench. The torque wrench was carefully adjusted to apply torque at a level of 35 Ncm, as per the manufacturer's guidelines. In the machine-driven group, the insertion of 16 dental implants (8 implants for each bone type) was executed using a 20:1 surgical contra-angle handpiece. The surgical motor was configured to operate at 25 rpm with a maximum torque of 35 Ncm, and no saline irrigation was used, as per the manufacturer's recommendations. In the combination group, the insertion of 16 dental implants was carried out in two steps. Initially, two-thirds of the dental implant's threads, approximately 8 mm in distance from the apex towards the neck of the implant, were inserted into the bone using a 20:1 surgical contra-angle handpiece. Subsequently, the dental implant was securely tightened to its final position using a ratchet connected to a torque wrench, with the torque wrench adjusted to apply torque at 35 Ncm, in accordance with the manufacturer's instructions.

Primary stability measurements

To assess primary stability measured in terms of ISQ values, we used the Osstell® Beacon device (W&H, Göteborg, Sweden) along with commercially available transducers (Smartpeg type 26, W&H, Göteborg, Sweden) attached to each implant. For each implant, two consecutive measurements were conducted, one from the frontal and another from the lateral direction, by positioning the probe laterally in relation to the transducer. The ISQ values acquired at the frontal site of each implant were recorded as buccolingual ISQ values, while those obtained at the lateral site were recorded as mesiodistal ISQ values. The second operator (S.S) was responsible for performing and recording all measurements. To validate ISQ values, the operator repeated both BL

and MD measurements at least three times, and the average value of these measurements was established as the reference for statistical analysis.

Statistical analysis

Statistical Package for Social Sciences (SPSS) software, version 22 (IBM SPSS Inc., Armonk, NY, USA) was used for statistical analysis. The Kolmogorov-Smirnov test and Shapiro-Wilk test were applied to verify normal data distributions. Two-way analysis of variance was used to assess the effects of insertion techniques and bone types on the ISQ measurements. Bonferroni post hoc analysis was performed for pairwise comparisons. The confidence level was set to 95% and p values less than 0.05 were considered significant.

Results

Two-way ANOVA analysis revealed that the bone type variable significantly affected the ISQ values ($p<0.05$), unlike the insertion protocols (Table 1).

For type II bone, primary stability recorded in the Std + R group was the highest at 75.4 ± 5.3 ISQ, followed in order by the value for the R group at 74.9 ± 7.0 ISQ and that of the Std group at 72.6 ± 2.7 ISQ (Table 2). No significant differences were observed when comparing the insertion protocols in type II bone.

In type IV bone, the primary stability of the samples in the Std group was the lowest at 62.7 ± 3.7 ISQ, while those of the other samples were 66.0 ± 6.8 and 69.8 ± 5.4 ISQ, respectively, for the R and Std + R groups. Comparing the three insertion protocols within type IV bone, no significant differences were found in primary stability values of the samples (Table 2).

When comparing the two bone types, the mean ISQ values of the Std and R groups in type II bone were significantly higher than those of their counterparts in type IV bone ($p<0.05$ for each). However, there were no significant differences in ISQ values when employing the Std+R technique between the two types of bone.

Discussion

Osseointegration, defined as the direct structural and functional connection between the implant surface and the patient's bone, plays a crucial role in the success of dental

implant procedures (22). Osseointegration, resulting from initial mechanical stability combined with biological stability, occurs at two stages: primary and secondary stabilization (23). Primary stabilization stands out as a key clinical objective during implant insertion (24). Achieving primary stability depends on numerous factors, including the implant's diameter, length, shape, thread design, as well as the surgical techniques employed by the operator and the type/density of the bone into which the implant is placed (25). Although advancements in oral implantology can assist in achieving predictable osseointegration even with low or non-primary stability, optimal primary stability can expedite and enhance the predictability of achieving strong secondary stability, especially when employing immediate loading protocols (26, 27). Furthermore, challenges in achieving optimal primary stability are common in clinical scenarios where medullary bone density is notably low, such as in the maxilla and posterior mandible, particularly among elderly patients (28). Multiple strategies exist to enhance primary stability in situations with poor bone density, including aspects of bone bed preparation like the osteotomy drilling process, drilling speed, irrigation during osteotomy to prevent overheating, and implant body insertion (3, 29, 30).

The aim of this study was to compare the effects of three different insertion protocols on the primary stability of dental implants placed in type II and IV bone. We hypothesized that advocating specific insertion protocols for a particular bone type could enhance primary stability and help clini-

Table 2. *Means and standard deviations of the ISQ measurements and post-hoc analysis for pairwise comparisons. p-values written in bold indicated significant differences for pairwise comparison related to bone types calculated by post hoc Bonferroni test. Parameters were described as mean ± SD. Different uppercase superscript letters present significant difference between insertion methods written in the same column.*

Bone Type	Insertion Methods		
	Std group	R group	Std + R group
Type II	72.6 (2.7) [A]	74.9 (7.0) [A]	75.4 (5.3) [A]
Type IV	62.7 (3.7) [A]	66.0 (6.8) [A]	69.8 (5.4) [A]
P-Value	**0.0185**	**0.0495**	0.8475

Std group: machine-driven insertion, R group: ratchet insertion, Std+R group: machine-driven and ratchet insertion

Table 1. *Effects of insertion method and bone type on the ISQ measurements according to the two-way analysis of variance.*

Source	Type III Sum of Squares	df	Mean Square	F	Sig.
Corrected Model	1035.042 [a]	5	207.008	6.291	.000
Intercept	236742.521	1	236742.521	7195.105	.000
Method	193.948	2	96.974	2.947	.063
Bone	800.333	1	800.333	24.324	.000
Method × Bone	40.760	2	20.380	.619	.543
Error	1381.937	42	32.903		
Total	239159.500	48			
Corrected Total	2416.979	47			

Note: [a] R Squared = .428 (Adjusted R Squared = .360)

cians select the appropriate protocol. To test this hypothesis, we specifically aimed to compare and evaluate ISQ values of dental implants inserted into type II and type IV bone using three insertion protocols: standard insertion (Std group), ratchet insertion (R group), and a combination of both (Std + R group) protocols. According to the main findings of this study, selecting the combination of insertion protocols may yield improved implant primary stability in conditions characterized by poor bone density.

ISQ values represent the predictability of the primary stability of a dental implant, at least on a macroscopic level, and provide the clinician with an idea of the prognosis they can expect for that specific implant or how soon it can be loaded (31). This study reaffirms that ISQ values were lower in low-density bone compared to high-density bone. This supports the findings of several studies (24, 32, 33) that have suggested that the accuracy of primary implant stability measurements obtained through resonance frequency analysis depends on bone density and can be influenced by different protocols. Orban *et al.* (34), in a prospective and randomized clinical study, evaluated the accuracy of implant placement by comparing the insertion torque for two types of insertion protocols: machine-driven and manual insertion. They concluded that there was no significant difference between the insertion protocols in terms of the accuracy of implant placement and mean insertion torque. In an in vivo study, Aliabadi *et al.* (35) focused on marginal bone loss around dental implants using two insertion methods, manual and mechanized. They observed that manually inserted implants showed less long-term marginal bone resorption. Similarly, Novsak *et al.* (36) aimed to evaluate differences between manual and mechanized techniques for orthodontic mini-implants in pig ribs and demonstrated higher stability and less bone resorption for manually inserted implants.

Furthermore, Misch *et al.* (37) stated that in compromised bone density situations, manual insertion of dental implants with the use of a handpiece is more suitable for providing the necessary force. Similarly, Cavallaro *et al.* (29) suggested that hand-ratcheting two to three threads was reasonable, but they emphasized not applying high hand-torque forces to seat the entire implant. However, in another article, Kim *et al.* (38) compared the success rates of manual and machine-driven methods for inserting mini screws. Regarding the insertion site, they claimed that the overall success rate of insertion with an engine driver was significantly higher than that with a hand driver for both the mandible and maxilla.

In our study, when comparing the effect of insertion protocols on primary stability within each bone type, no significant difference was observed in ISQ values. ISQ values measured following the utilization of standard insertion protocol or ratchet insertion protocol were significantly lower in type IV bone compared to type II bone. Importantly, the Std + R group did not exhibit a significant decrease in ISQ levels for type IV bone compared to type II bone. If proven clinically, this may suggest that the utilization of the combination protocol may be beneficial as it allows ISQ values to remain stable even in cases of lower bone density. Therefore, it may be a more promising and preferable insertion method for patients with poor bone density, as well as for immediate implant placement.

In a previous in vitro study, wood blocks were used as an alternative to low-density bone, simulating D4 and D3 bone. In this study, 32 implants were inserted using either a low-speed machine-driven handpiece or hand ratcheting, and a pull-out test was conducted (39). The results revealed that D3 bone exhibited statistically significantly higher pull-out strength than D4 samples. Additionally, implants inserted using the machine-driven handpiece seemed to exhibit enhanced stability compared to those placed manually. However, the authors acknowledged a limitation in using pullout force as a measure of stability, suggesting that Resonance Frequency Analysis (RFA) would have been a better choice for analyzing primary stability. RFA has become one of the most widely used techniques for assessing implant stability in both clinical trials and experimental studies (9, 25). This analysis ensures accurate control of implant stability, with repeatable and reproducible measurements over time, and facilitates precise communication among professionals (22).

Numerous experimental studies have been conducted using various bone models, including animal bones, human cadaver bones, and artificial bone, to simulate situations with different bone densities (40-42). The objective of these studies is to highlight the challenges posed by poor bone quality and investigate methods to enhance primary stability. Concerning animal bones, the macroscopic composition of cortical and medullary bone in bovine ribs serves as an acceptable model for reproducing edentulous human bone, as reported in numerous studies (14-17). While these studies endorse the use of this animal model in implant research to gain insights into edentulous human bone, it's important to note that there are various experimental designs addressing bone type variations. For example, Lanchmann *et al.* (14) characterized the distal aspect of the rib, with a smaller diameter, as type II bone according to the Lekholm/Zarb classification (43) or D2 to D3 according to Misch (44). In their study, the bone region with a greater diameter at the end of the ribs, containing less cortical components and a higher content of bone marrow and spongy trabeculae, represented type III bone according to the Leckholm & Zarb classification (43) or D3 to D4 according to the Misch classification (44). García-Vives *et al.* (15) referred to the distal end of the ribs as type IV bone according to the Leckholm & Zarb classification (45) or D4 according to the Misch classification (44).

In line with our experimental design, other relevant studies used the distal epiphysis on the longitudinal axis of bovine ribs, without any cortical bone, to mimic the morphological structure of type IV bone, resembling the human posterior maxilla (18). Toyoshima *et al.* (19) also used the distal epiphysis of the longitudinal axis of the bone block to represent the cancellous bone group. In their study, the authors adjusted the thickness of the cortical layer of bone blocks to 2 mm to reduce the effects of compressive forces, referring to them as the corticocancellous bone group. On the other hand, Moon *et al.* (20) and Anil and Aldosari (21) removed the entire cortical bone of bone rib blocks until trabecular bone was exposed to mimic type IV bone. In these two studies, the cortical bone was thinned to 1 mm to mimic type II bone.

Taking everything into consideration, we chose to use bovine ribs as an animal model for this study. This decision was based on well-established evidence in the literature demonstrating their effectiveness in evaluating the correlation be-

tween bone density and implant stability (14, 46, 47). Our experimental bone models were designed to resemble type II or type IV bone in line with the aforementioned literature. For the same reasons, we did not include type I or type III bone in the study, as each group represents a wider selection of bone density according to bone classifications.

The authors of this study acknowledge that the use of animal models may not perfectly represent human bones, which is a key limitation of the study. We recommend further studies in this area, including the assessment of bone type/density using advanced analysis methods such as micro-computed tomography or histomorphometric analysis. Therefore, the absence of any analysis defining the bone type may also be considered another limitation of the current study. Some other limitations of the present study include the fact that, we did not account for both the mechanical and biological aspects of in vivo conditions, such as access to the surgical site or the blood supply to the bone. Moreover, it should be noted that various types of implants with different geometrical designs may alter the ISQ values. Additionally, it should be considered that high ISQ values do not always correlate with successful osseointegration and the long-term survival of an implant. Further studies should also be conducted to estimate the long-term effects of insertion protocols, as the findings may influence clinicians' preferences for selecting the proper insertion protocols based on bone type.

Finally, ISQ values greater than 65 have been regarded as favorable for implant stability, whereas ISQ values below 45 indicate poor primary stability (48). In studies that investigated the predictive value of RFA analysis in the survival rates of dental implants, Baltayan *et al.* (49) showed that there was a significant difference in survival rate between early and traditional loading protocols for implants with ISQ values serving as cutoff points (ISQ of 45, 50, 55). It is emphasized that implants with ISQ values less than 60 are of questionable stability, while those with values greater than 70 are very stable, with the 60 to 70 range serving as the cutoff region (49, 50). Importantly, the values in our results for type IV bone fall within the cutoff region for each insertion protocol.

Conclusion

Considering the limitations of the present study, it can be concluded that utilizing a combination of machine and ratchet insertion techniques may prove beneficial in optimizing ISQ values in bovine samples simulating type IV bone.

Türkçe özet: *Tip IV kemikte dental implantların primer stabilizasyonunun optimize edilmesi amacıyla angldruva ve raşetle yerleştirme protokollerinin in-vitro karşılaştırılması. Amaç: Bu çalışmanın amacı farklı implant yerleştirme tekniklerinin implant stabilitesi üzerindeki etkilerinin Tip II ve Tip IV kemiği taklit eden sığır kadavrasında karşılaştırılmasıdır. Gereç ve Yöntem: 12 mm uzunluğunda, 3,75 mm çapında toplam 48 adet dental implant (BEGO Semados RSX, BEGO İmplant Sistemleri Lmt. Şti & Kom. Şti, Almanya) tip II ve tip IV kemiği taklit etmesi için hazırlanan sığır kaburga kemiklerinin içine yerleştirildi. İmplant yataklarının standart frezleme tekniği ile hazırlanmasından sonra dental implantlar kemik içerisine 3 farklı protokol ile yerleştirildi. Bu protokoller ile implant motoru yardımıyla yerleştirilen grup (Std grubu), raşet ile yerleştirilen grup (R grubu) ve iki yöntemin kombinasyonu şeklinde yerleştirilen grup (Std + R grubu) oluşturuldu. Her bir implantın primer stabilitesi, kemik içerisine yerleştirilmesinden hemen sonra, Osstell Beacon cihazı ile ölçülen implant stabilite katsayısı (ISQ) ile değerlendirildi. İstatistiksel analiz için iki yönlü varyans analizi ve Bonferroni testleri yapıldı. Bulgular: Kemik tipinin ISQ değerlerini anlamlı derecede etkilediği gözlendi (p<0.05). Ancak tip II ve tip IV kemik için yerleştirme protokolleri ayrı ayrı karşılaştırıldığında anlamlı bir fark gözlenmedi. Tip IV kemikte hem Std grubu hem de R grubu, tip II kemikte aynı gruplarla karşılaştırıldığında anlamlı derecede düşük ISQ değerleri gösterdi (her biri için p<0,05). Bununla birlikte, iki kemik türü arasında Std+R tekniği uygulandığında ISQ değerlerinde anlamlı bir fark bulunamadı. Sonuç: Tip IV kemiği taklit eden sığır numunelerinde, implant motoru ve raşet yerleştirme tekniklerinin birlikte kullanılmasının ISQ değerlerinin optimize edilmesinde faydalı olabileceği sonucuna varılmıştır. Anahtar kelimeler: dental implant, oral cerrahi işlemler, osseointegrasyon, rezonans frekans analizi*

REFERENCES

1. Rameh S, Menhall A, Younes R. Key factors influencing short implant success. Oral Maxillofac Surg 2020;24:263-75. [CrossRef]
2. Steigenga JT, al-Shammari KF, Nociti FH, Misch CE, Wang HL. Dental implant design and its relationship to long-term implant success. Implant Dent 2003;12:306-17. [CrossRef]
3. Kotsakis GA, Romanos GE. Biological mechanisms underlying complications related to implant site preparation. Periodontol 2000 2022;88:52-63. [CrossRef]
4. Papaspyridakos P, Chen CJ, Singh M, Weber HP, Gallucci GO. Success criteria in implant dentistry: a systematic review. J Dent Res 2012;91:242-8. [CrossRef]
5. Alghamdi H, Anand PS, Anil S. Undersized implant site preparation to enhance primary implant stability in poor bone density: a prospective clinical study. J Oral Maxillofac Surg 2011;69:506-12. [CrossRef]
6. Viceconti M, Brusi G, Pancanti A, Cristofolini L. Primary stability of an anatomical cementless hip stem: a statistical analysis. J Biomech 2006;39:1169-79. [CrossRef]
7. Staedt H, Kämmerer PW, Goetze E, Thiem DGE, Al-Nawas B, Heimes D. Implant primary stability depending on protocol and insertion mode - an ex vivo study. Int J Implant Dent 2020;6:49. [CrossRef]
8. Herrero-Climent M, Falcão A, López-Jarana P, Díaz-Castro CM, Ríos-Carrasco B, Ríos-Santos JV. In vitro comparative analysis of

two resonance frequency measurement devices: Osstell implant stability coefficient and Penguin resonance frequency analysis. Clin Implant Dent Relat Res 2019; 21:1124-31. [CrossRef]

9. Huang H, Wu G, Hunziker E. The clinical significance of implant stability quotient (ISQ) measurements: A literature review. J Oral Biol Craniofac Res 2020; 10, 629-38. [CrossRef]

10. Lozano-Carrascal N, Salomó-Coll O, Gilabert-Cerdà M, Farré-Pagés N, Gargallo-Albiol J, Hernández-Alfaro F. Effect of implant macro-design on primary stability: A prospective clinical study. Med Oral Patol Oral Cir Bucal 2016;21:214-21. [CrossRef]

11. Vanden Bogaerde L, Sennerby L. A Randomized Case-Series Study Comparing the Stability of Implant with Two Different Surfaces Placed in Fresh Extraction Sockets and Immediately Loaded. Int J Dent 2016;2016:8424931. [CrossRef]

12. Lemos BF, Lopez-Jarana P, Falcao C, Ríos-Carrasco B, Gil J, Ríos-Santos JV, Herrero-Climent M. Effects of Different Undersizing Site Preparations on Implant Stability. Int J Environ Res Public Health 2020;17:8965. [CrossRef]

13. Herekar M, Sethi M, Ahmad T, Fernandes AS, Patil V, Kulkarni H. A correlation between bone (B), insertion torque (IT), and implant stability (S): BITS score. J Prosthet Dent 2014; 112:805-10. [CrossRef]

14. Lachmann S, Jäger B, Axmann D, Gomez-Roman G, Groten M, Weber H. Resonance frequency analysis and damping capacity assessment. Part I: an in vitro study on measurement reliability and a method of comparison in the determination of primary dental implant stability. Clin Oral Implants Res 2006;17:75-9. [CrossRef]

15. García-Vives N, Andrés-García R, Rios-Santos V, Fernández-Palacín A, Bullón-Fernández P, Herrero-Climent M, Herrero-Climent F. In vitro evaluation of the type of implant bed preparation with osteotomes in bone type IV and its influence on the stability of two implant systems. Med Oral Patol Oral Cir Bucal 2009;14:455-60.

16. Baker JA, Vora S, Bairam L, Kim HI, Davis EL, Andreana S. Piezoelectric vs. conventional implant site preparation: ex vivo implant primary stability. Clin Oral Implants Res 2012;23:433-7. [CrossRef]

17. Santamaría-Arrieta G, Brizuela-Velasco A, Fernández-González FJ, Chávarri-Prado D, Chento-Valiente Y, Solaberrieta E, Diéguez-Pereira M, Vega JA, Yurrebaso-Asúa J. Biomechanical evaluation of oversized drilling technique on primary implant stability measured by insertion torque and resonance frequency analysis. J Clin Exp Dent 2016;8:307-11. [CrossRef]

18. Emmert M, Gülses A, Behrens E, Karayürek F, Acil Y, Wiltfang J, Spille JH. An experimental study on the effects of the cortical thickness and bone density on initial mechanical anchorage of different Straumann® implant designs. Int J Implant Dent 2021;7:83. [CrossRef]

19. Toyoshima T, Tanaka H, Ayukawa Y, Howashi M, Masuzaki T, Kiyosue T, Koyano K, Nakamura S. Primary Stability of a Hybrid Implant Compared with Tapered and Cylindrical Implants in an Ex Vivo Model. Clin Implant Dent Relat Res 2015;17:950-6. [CrossRef]

20. Moon SH, Um HS, Lee JK, Chang BS, Lee MK. The effect of implant shape and bone preparation on primary stability. J Periodontal Implant Sci 2010;40:239-43. [CrossRef]

21. Anil S, Aldosari AA. Impact of bone quality and implant type on the primary stability: an experimental study using bovine bone. J Oral Implantol 2015;41:144-8. [CrossRef]

22. Antequera-Diaz R, Quesada-García MP, Vallecillo C, Vallecillo-Rivas M, Muñoz-Soto E, Olmedo-Gaya MV. Intra- and inter-operator concordance of the resonance frequency analysis. A cross-sectional and prospective clinical study. Clin Oral Investig 2022; 26:6521-30. [CrossRef]

23. Javed F, Romanos GE. The role of primary stability for successful immediate loading of dental implants. A literature review. J Dent 2010;38:612-20. [CrossRef]

24. Bataineh AB, Al-Dakes AM. The influence of length of implant on

25. primary stability: An in vitro study using resonance frequency analysis. J Clin Exp Dent 2017;9:1-6. [CrossRef]

25. Romanos GE, Ciornei G, Jucan A, Malmstrom H, Gupta B. In vitro assessment of primary stability of Straumann® implant designs. Clin Implant Dent Relat Res 2014;16:89-95. [CrossRef]

26. Al-Sabbagh M, Eldomiaty W, Khabbaz Y. Can Osseointegration Be Achieved Without Primary Stability? Dent Clin North Am 2019;63:461-73. [CrossRef]

27. Norton MR. The Influence of Low Insertion Torque on Primary Stability, Implant Survival, and Maintenance of Marginal Bone Levels: A Closed-Cohort Prospective Study. Int J Oral Maxillofac Implants 2017;32:849-57. [CrossRef]

28. Cáceres F, Troncoso C, Silva R, Pinto N. Effects of osseodensification protocol on insertion, removal torques, and resonance frequency analysis of BioHorizons® conical implants. An ex vivo study. J Oral Biol Craniofac Res 2020;10:625-8. [CrossRef]

29. Cavallaro J Jr, Greenstein B, Greenstein G. Clinical methodologies for achieving primary dental implant stability: the effects of alveolar bone density. J Am Dent Assoc 2009;140:1366-72. [CrossRef]

30. Chen CH, Pei X, Tulu US, Aghvami M, Chen CT, Gaudillière D, Arioka M, Maghazeh Moghim M, Bahat O, Kolinski M, Crosby TR, Felderhoff A, Brunski JB, Helms JA. A Comparative Assessment of Implant Site Viability in Humans and Rats. J Dent Res 2018;97:451-9. [CrossRef]

31. Dottore AM, Kawakami PY, Bechara K, Rodrigues JA, Cassoni A, Figueiredo LC, Piattelli A, Shibli JA. Stability of implants placed in augmented posterior mandible after alveolar osteotomy using resorbable nonceramic hydroxyapatite or intraoral autogenous bone: 12-month follow-up. Clin Implant Dent Relat Res 2014;16:330-6. [CrossRef]

32. Farré-Pagés N, Augé-Castro ML, Alaejos-Algarra F, Mareque-Bueno J, Ferrés-Padró E, Hernández-Alfaro F. Relation between bone density and primary implant stability. Med Oral Patol Oral Cir Bucal 2011;16:62-7. [CrossRef]

33. Li T, Kong L, Wang Y, Hu K, Song L, Liu B, Li D, Shao J, Ding Y. Selection of optimal dental implant diameter and length in type IV bone: a three-dimensional finite element analysis. Int J Oral Maxillofac Surg 2009;38:1077-83. [CrossRef]

34. Orban K, Varga E Jr, Windisch P, Braunitzer G, Molnar B. Accuracy of half-guided implant placement with machine-driven or manual insertion: a prospective, randomized clinical study. Clin Oral Investig 2022;26:1035-43. [CrossRef]

35. Aliabadi E, Tavanafar S, Khaghaninejad MS. Marginal bone resorption of posterior mandible dental implants with different insertion methods. BMC Oral Health 2020;20:31. [CrossRef]

36. Novsak D, Trinajstic Zrinski M, Spalj S. Machine-driven versus manual insertion mode: influence on primary stability of orthodontic mini-implants. Implant Dent 2015;24:31-6. [CrossRef]

37. Misch CE, Qu Z, Bidez MW. Mechanical properties of trabecular bone in the human mandible: implications for dental implant treatment planning and surgical placement. J Oral Maxillofac Surg 1999;57:700-6. [CrossRef]

38. Kim JS, Choi SH, Cha SK, Kim JH, Lee HJ, Yeom SS, Hwang CJ. Comparison of success rates of orthodontic mini-screws by the insertion method. Korean J Orthod 2012;42:242-8. [CrossRef]

39. Bandela V, Munagapati B, Komala J, Basany RB, Patil SR, Kanaparthi S. Comparison of Primary Stability of Implants Installed by Two Different Methods in D3 and D4 Bone Types: An In Vitro Study. J Int Soc Prev Community Dent 2020;10:620-6. [CrossRef]

40. Chávarri-Prado D, Brizuela-Velasco A, Diéguez-Pereira M, Pérez-Pevida E, Jiménez-Garrudo A, Viteri-Agustín I, Estrada-Martínez A, Montalbán-Vadillo O. Influence of cortical bone and implant design in the primary stability of dental implants measured by two different devices of resonance frequency analysis: An in vitro study. J Clin Exp Dent 2020;12:242-8. [CrossRef]

41. Shetty V, Mishra D, Barui S, Basu B. Preclinical study probing primary stability of dental implants in synthetic and natural bones. Int J Appl Ceram 2023;20:842-55. [CrossRef]

42. Delgado-Ruiz R, Gold J, Somohano Marquez T, Romanos G. Under-Drilling versus Hybrid Osseodensification Technique: Differences in Implant Primary Stability and Bone Density of the Implant Bed Walls. Materials (Basel) 2020;13:390. [CrossRef]

43. Lekholm U, Zarb G. Patient selection and preparation. In: Brånemark P, Zarb G, Albrektsson T, editors. Tissue-Integrated Prostheses. Osseointegration in Dentistry.1st Ed., Chicago: Quintessence Publishing, 1985, p.199-209.

44. Misch CE. Divisions of available bone in implant dentistry. Int J Oral Implantol 1990;7:9-17.

45. Jemt T, Lekholm U. Implant treatment in edentulous maxillae: a 5-year follow-up report on patients with different degrees of jaw resorption. Int J Oral Maxillofac Implants 1995;10:303-11.

46. Rebaudi A, Trisi P, Cella R, Cecchini G. Preoperative evaluation of bone quality and bone density using a novel CT/microCT-based hard-normal-soft classification system. Int J Oral Maxillofac Implants 2010;25:75-85.

47. Iezzi G, Scarano A, Di Stefano DA, Arosio P, Doi K, Ricci L, Piattelli A, Perrotti V. Correlation between the bone density recorded by a computerized implant motor and by a histomorphometric analysis: a preliminary in vitro study on bovine ribs. Clin Implant Dent Relat Res 2015;17:35-44. [CrossRef]

48. Tettamanti L, Andrisani C, Bassi MA, Vinci R, Silvestre-Rangil J, Tagliabue A. Immediate loading implants: review of the critical aspects. Oral Implantol (Rome) 2017;10:129-39. [CrossRef]

49. Baltayan S, Pi-Anfruns J, Aghaloo T, Moy PK. The predictive value of resonance frequency analysis measurements in the surgical placement and loading of endosseous implants. J. Oral Maxillofac. Surg 2016;74:1145-52. [CrossRef]

50. Rodrigo D, Aracil L, Martin C, Sanz M. Diagnosis of implant stability and its impact on implant survival: a prospective case series study. Clin Oral Implants Res 2020;21:255-61. [CrossRef]

Original research

Comparison of calcium silicate-based materials in pulpotomies of primary molars: a randomized clinical trial

Purpose
The primary objective of this investigation is to evaluate the clinical and radiographic findings of mineral trioxide aggregate (MTA) and Biodentine (BD) as pulpotomy agents in primary molars.

Materials and Methods
Two hundred primary molars (N=200) were treated with pulpotomy. Clinical and radiographic outcomes, including both successes and failures, were documented throughout a 36-month follow-up period. Statistical analyses were performed using the Fisher Exact, McNemar, and Chi-Square tests.

Results
No statistically significant differences in success rates were found between the 1-, 3-, 6-, 24-, and 36-month assessments for each material when evaluated independently. However, at the twelfth month, the clinical and radiographic success rates for MTA (98% and 92%, respectively) were significantly higher than those for BD (90% and 80%, respectively) with a p-value of less than 0.05.

Conclusion
In this study, MTA demonstrated greater success than BD at 36 months. Nevertheless, higher quality randomized controlled trials with longer follow-up periods are necessary to obtain more reliable results.

Keywords: *Tricalcium silicate, mineral trioxide aggregate, pulpotomy, primary teethv*

Mine Koruyucu[1] (iD),
Sabiha Ceren İlisulu[2] (iD),
Sıla Yardımcı[3] (iD),
Figen Seymen[2] (iD)

Introduction

Pulpotomy stands as the preferred method of treatment for asymptomatic primary molars where caries has approximated the pulp (1). Pulpotomy involves the surgical removal of the coronal pulp followed by the application of a pulp-dressing agent to preserve the vitality of the remaining radicular pulp tissue (2). Pulpotomy can be classified based on the following treatment objectives: preservation, devitalization, and regeneration (3). An ideal pulpotomy medicament should effectively eliminate bacteria while being compatible with the biological environment to promote healing and minimize any negative effects on the patient's oral health. Additionally, it should facilitate root pulp healing while aligning with the natural physiological process of root resorption (4).

Formocresol (FC) is suggested as the ideal dressing agent in pulpotomy procedures by the American Academy of Pediatric Dentistry, despite concerns regarding its potential mutagenic and toxic effects (2,3). FC continues to be widely recognized and upheld as the gold standard against which all new materials, including calcium hydroxide, ferric sulfate, and glutaraldehyde, are compared (2).

The search for newer pulpotomy materials is ongoing. The objective of preserving pulp tissue has been replaced by the pursuit of regeneration

due to improvements in biocompatibility and bioinductivity of the materials. MTA and BD have been developed for these purposes (3). MTA has the ability to seal and stimulate hard tissue formation. Its biocompatibility enables its widespread use in pediatric dentistry. BD also has high biocompatibility combined with bioactivity, thanks to calcium silicate's improved properties, including rapid setting time and high strength (2).

The primary objective of this investigation is to evaluate, both clinically and radiographically, the success of two pulpotomy medicaments: Pro-Root White MTA and BD in primary molars. The null hypothesis is that there are no significant differences between MTA and BD in radiographic and clinical outcomes.

Material and Methods

Ethical statement

This randomized clinical trial was conducted from 2013 to 2016, with the study protocol receiving approval from the Ethics Committee of Istanbul University, Medical Faculty (file number: 2012/1742-1302). The research strictly adhered to the Declaration of Helsinki. The study was registered at ClinicalTrials.gov (NCT03395496), and meticulous adherence to the 2010 Consolidated Standards of Reporting Trials Statement was observed in the study design. Additionally, the study design followed the guidelines outlined in the CONSORT 2010 Statement for reporting parallel group randomized trials (5).

Study design

The patients who participated in this study were attending the Pediatric Dentistry clinic. The possible discomforts, risks, and benefits of the procedures were explained to the participants and their families. Before participating in the study, the parents gave their informed consent. Eligible participants were between 6 and 12 years of age (mean age 10 ±1.62). All patients were healthy and had one or two primary molars in need of pulpotomy treatment. Clinical and radiographic examinations were systematically performed to ensure compliance with the specified inclusion criteria.

Inclusion criterion

The inclusion criteria for teeth selection included the following parameters: teeth had to demonstrate extensive caries, teeth must radiographically demonstrate the existence of 2/3 of the root length, and there must be adequate tooth structure to be restored. Additionally, there should be no radiographic or clinical evidence of pulp pathology (such as spontaneous pain, tenderness to percussion or palpation, swelling, sinus tract, pathologic mobility, etc.). This study excluded teeth without permanent successors.

Sample size estimation

The sample size was calculated to have 80% power at a 5% level of statistical significance with a 10% level of difference between the groups, necessitating 71 teeth in each group. A total of 213 primary molars (108 molars in Group I

and 105 molars in Group II) were included from 106 children. Thirteen teeth were excluded from the study due to uncontrolled pulp bleeding (Figure 1).
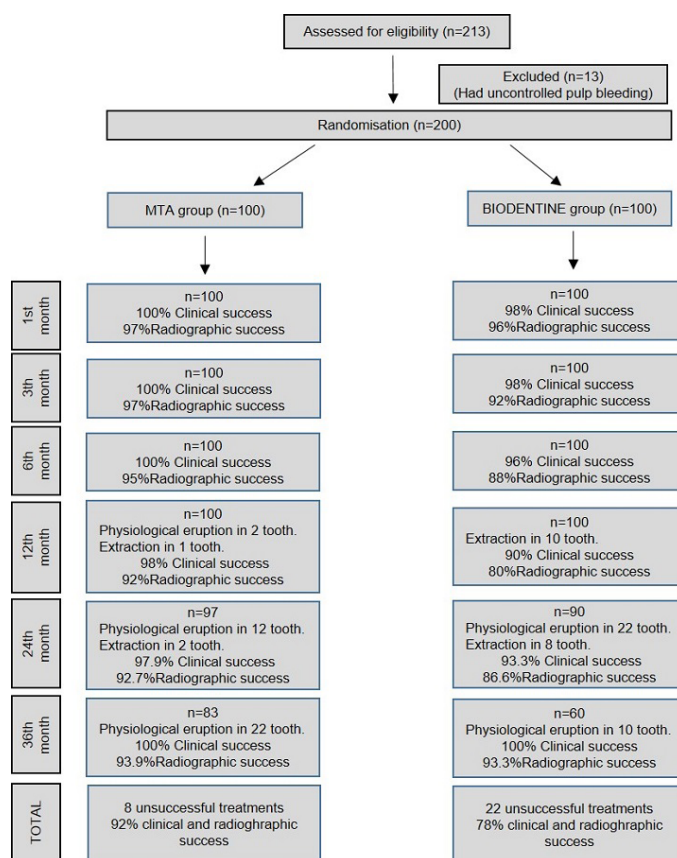
Figure 1. Flow chart of the clinical and radiographic success of the materials.

Pulpotomy protocols

Pulpotomy procedures were conducted following the application of local anesthesia and rubber dam isolation to ensure patient comfort and procedural precision. Caries removal and coronal access were performed using a high-speed bur with water spray to expose the pulp chamber. Patients were excluded from the study if hemostasis was not achieved within 3 minutes after placing a sterile cotton pellet gently against the amputated pulp, indicating a potential infection of the pulp tissue within the canal.

Two different pulpotomy medicaments were applied according to the manufacturer's instructions for 200 primary molars. Group I: Pro-Root MTA (Dentsply Tulsa Dental Specialties, Johnson City, U.S.) was formulated by combining three parts of powder with one part of water to achieve a putty-like texture. The prepared mixture was then inserted into the pulp chamber and gently condensed using a dampened cotton pellet. Following this, a glass ionomer base material was applied over the MTA. Group II: BD (Septodont, Saint Maur des Fosses, France) powder in the capsule was mixed with five drops of liquid in a triturator (4200 rpm) for 30 seconds. The resulting mixture was placed in the pulp chamber and left to set entirely, which took roughly 12 minutes. Permanent restoration was carried out during the same session.

After the pulpotomies, all molars were restored using amalgam materials. Clinical and radiographic assessments

were conducted during follow-up visits at 1, 3, 6, 12, and 36 months. In cases where a patient missed or cancelled a session, a new follow-up examination was rescheduled. Experienced pediatric dentists, unaware of the patients' assigned treatment groups, conducted the clinical examinations.

Treatment follow-up

A pulpotomized tooth was deemed clinically successful if there were no signs of swelling, pain, fistula, gingival inflammation, or pathologic mobility. A paralleling technique with a film holder (Rinn XCP; Dentsply, Elgin, U.S.) was used to capture the preoperative and control periapical radiographs. An automatic processor (Velopex® Intra-X Medivance Instruments, London, U.K.) was used to process the radiographs, which were then inspected and evaluated under optimal illumination. Radiographic examinations were performed by two experienced pediatric dentists. Each control was evaluated independently. Physiological eruption was considered a success. For intra-examiner reproducibility of radiographic assessment, 10% of the radiographs were re-evaluated after 2 weeks. The intra-examiner kappa value was determined to be 0.90.

Statistical analysis

Statistical analysis was conducted using the Statistical Package for the Social Sciences (SPSS, IBM Corporation, Version 21.0; Armonk, NY, USA) software. Group differences were assessed using Fisher's Exact Test, Student t-test, Shapiro-Wilk Test, McNemar Test, and Chi-square statistical tests. The significance level was set at $p<0.05$.

Results

As there were statistical differences between the two materials, null hypothesis was rejected. A total of 200 pulpotomized primary molars were evaluated in this study. Figure 1 shows a flow chart of the included pulpotomized teeth. The mean ages (± SD) were 9.82 ± 1.43 years for the MTA group and 10.18 ± 1.77 years for the Biodentine (BD) group, with no statistically significant difference between them (p=0.116).

Clinical findings for the two materials were significantly different at the 12-month follow-up (p=0.037). In the Biodentine group, statistically significant differences were observed between the 1st and 12th months (p=0.008), 3rd and 12th months (p=0.008), 3rd and 24th months (p=0.031), 6th and 12th months (p=0.031), and 24th and 36th months (p=0.031). No significant differences were noted between these timepoints in the MTA group (Table 1).

A significant difference in radiographic findings was also noted between the materials at the 12-month follow-up (p=0.025). In the Biodentine group, significant differences were found between the 1st and 6th months (p=0.08), 1st and 12th months (p=0.01), 1st and 24th months (p=0.02), 3rd and 12th months (p=0.01), 3rd and 24th months (p=0.02), 6th and 12th months (p=0.08), and 6th and 24th months (p=0.08). There was no statistically significant difference between these timepoints in the MTA group (Table 2).

Clinical evaluation at 6 months showed success rates of 100% for the MTA group and 98-96% for the Bioden-

Table 1. *Statistical analysis of the clinical success of the materials.*

Duration	Group I (MTA)	Group II (BD)	[1]p
	n (%)	n (%)	
1st month	100 (100%)	98 (98%)	[1]0.497
3th month	100 (100%)	98 (98%)	[1]0.497
6th month	100 (100%)	96 (96%)	[1]0.121
12th month	98 (98%)	90 (90%)	[2]0.037*
24th month	95 (97.9%)	84 (93.3%)	[1]0.157
36th month	83 (100%)	60 (100%)	-
1-3 months [3]p	1.000	1.000	
1-6 months [3]p	1.000	0.500	
1-12 months [3]p	0.500	0.008*	
1-24 months [3]p	0.500	0.289	
1-36 months [3]p	1.000	1.000	
3-6 months [3]p	1.000	0.500	
3-12 months [3]p	0.500	0.008*	
3-24 months [3]p	0.500	0.031*	
3-36 months [3]p	1.000	1.000	
6-12 months [3]p	0.500	0.031*	
6-24 months [3]p	0.500	0.289	
6-36 months [3]p	1.000	1.000	
12-24 months [3]p	1.000	1.000	
12-36 months [3]p	0.500	1.000	
24-36 months [3]p	0.500	0.031*	

[1]*Fisher Exact's test,* [2]*Continuity (Yates),* [3]*McNemar test, *p<0.05*

Table 2. *Statistical analysis of the radiographic success of the materials.*

Duration	Group I (MTA)	Group II (BD)	[1]p
	n (%)	n (%)	
1st month	97 (97%)	96 (96%)	[1]1.000
3th month	97 (97%)	92 (92%)	[2]0.215
6th month	95 (95%)	88 (88%)	[2]0.128
12th month	92 (92%)	80 (80%)	[2]0.025*
24th month	90 (92.8%)	78 (86.7%)	[2]0.254
36th month	78 (94%)	56 (93.3%)	[1]1.000
1-3 months [3]p	1.000	0.125	
1-6 months [3]p	0.500	0.008*	
1-12 months [3]p	0.063	0.001*	
1-24 months [3]p	0.063	0.002*	
1-36 months [3]p	0.250	0.125	
3-6 months [3]p	0.500	0.125	
3-12 months [3]p	0.063	0.001*	
3-24 months [3]p	0.063	0.002*	
3-36 months [3]p	0.250	0.125	
6-12 months [3]p	0.250	0.008*	
6-24 months [3]p	0.250	0.008*	
6-36 months [3]p	1.000	0.500	
12-24 months [3]p	1.000	0.500	
12-36 months [3]p	1.000	1.000	
24-36 months [3]p	1.000	1.000	

[1]*Fisher Exact's test,* [2]*Continuity (Yates),* [3]*McNemar test, *p<0.05*

tine group (Table 1). Radiographic evaluation at 6 months showed success rates of 97-95% for the MTA group and 96-88% for the Biodentine group (Table 2). After the eruption and extraction of the teeth, the success rates started to decrease. When the total success rates of the groups were compared after 36 months, a statistically significant difference was found (p=0.010) (Table 3).

Table 3. *Statistical analysis of the total success of the materials.*

Total Success	Group I (MTA)	Group II (BD)	[1]p
	n (%)	n (%)	
Successul	92 (92%)	78 (78%)	0.010*
Unsuccessful	8 (8%)	22 (22%)	

*Continuity (Yates), *p<0.05*

Discussion

This preliminary randomized clinical trial assessed the clinical and radiographic performance rates of pulpotomies using either MTA or BD in primary molars. Both groups demonstrated clinical and radiographic success, with a significant difference in success rates found at the 36-month follow-up.

Clinical research has centered on comparing various pulpotomy agents. Many studies examining pulpotomy materials have employed FC and Ferric sulfate (FS) as control medicaments, consistently concluding that these materials yield comparable results (1-3, 6-10).

After a Cochrane review, it was concluded that no pulpotomy medicament or technique produces better results than another. Studies comparing FC and MTA in pulpotomy treatment in primary teeth showed that MTA is a better pulpotomy agent than FC (11). Fuks (2008) reviewed multiple randomized clinical trials comparing MTA and FC and recommended MTA as an alternative to FC because it showed better results in all cases (12). A recent meta-analysis examining the clinical effects of MTA and FC in primary molar pulpotomies included thirty clinical trials across seven databases. It concluded that MTA is a more promising agent, with a success rate of 95% compared to FC's success rate of 87% (2,13).

Following these findings, MTA was chosen as the control material. In previous studies, the success rates of MTA as a pulpotomy material have varied between 66-100% (1,3,4,7-10,12-23). Similar radiographic and clinical success rates of MTA pulpotomy were observed in our study (92-100%).

El-Meligy *et al.* (2016) compared the clinical and radiographic success rates of BD and FC as pulpotomy agents in primary teeth. The success rate for BD was reported as 100%, while that of FC was 94% at the 6-month follow-up (6). Carıkçıoglu *et al.* (2017) defined the clinical and radiographic success rates of BD and FS. The success rates were 97.1% for BD and 64.6% for FS-ZOE between 6 to 12 months (24).

Juneja and Kulkarni (2017) compared FC, MTA, and BD in their randomized controlled clinical trial. After follow-ups at 12 and 18 months, they noticed significant differences in clinical outcomes between FC, MTA, and BD. Radiographic outcomes were also significantly different between FC and MTA at 6, 12, and 18 months. They showed that MTA has a superior success rate (100%) to BD (86.7%) and that BD has

a superior success rate to FC (73.3%) at the 18-month follow-up (3). Güven *et al.* (2017) conducted a clinical and radiographic comparison of calcium silicate-based materials (Pro-Root MTA, MTA-P, BD) and FS in primary molar pulpotomies. After 24 months, the total success rates for the PR-MTA, MTA-P, BD, and FS groups were reported as 93.1%, 86.2%, 82.75%, and 75.86%, respectively (4).

In another study, Kusum *et al.* (2015) evaluated MTA, BD, and propolis in primary dentition pulpotomies. MTA and BD were found to be more successful than propolis, both clinically and radiographically, at the 9-month follow-up (20). Niranjani *et al.* (2015) compared the success of pulpotomy outcomes using MTA, lasers, and BD. The results showed that MTA offers the best outcome as a pulpotomy agent, though the comparison of MTA, BD, and Laser was not statistically significant at the 6-month follow-up (21).

Cuadros-Fernandez *et al.* (2016) also evaluated the MTA and BD materials. The clinical success rate for MTA was 95.3%, and 97.5% for BD at 6 months. The clinical success rates at 12 months were 97.4% for MTA and 100% for BD. The radiographic success rate was 100% in both groups at 6 months and 97.4% in the MTA group and 94.9% in the BD group at 12 months (2). Bani et al. (2017) compared BD and MTA. The clinical success rate was 100% in both the MTA and BD groups at 6 months, 96.9% in both groups at 12 months, 96.9% in both groups at 18 months, and 96.8% in both groups at 24 months. The radiographic success rate was 100% in both groups at 6 months, 96.9% in both groups at 12 months, 90.6% in MTA and 93.8% in BD at 18 months, and 87.1% in MTA and 93.6% in BD at 24 months (19).

Comparing these two studies with our research, Bani *et al.*'s (2017) clinical findings are similar to ours in that MTA was clinically more successful than BD at the 6-, 12-, and 24-month follow-ups. Interestingly, their radiographic success rate was higher for BD at 24 months. In contrast, Cuadros-Fernandez *et al.* (2016) showed better clinical outcomes with BD at the 6- and 12-month follow-ups; however, at the 12-month follow-up, MTA was more successful radiographically. Clinically and radiographically, MTA was found to be more successful than BD in all months (2). Many studies have shown that radiographic success rates are lower than clinical success rates, aligning with the findings of the current study (2,3,19,20,24,25). Thus, it is important and necessary to perform radiographic follow-ups after pulpotomies.

This study constitutes a long-term clinical investigation with a substantial sample size and an extended follow-up period. It is essential to interpret the study findings in the context of certain limitations inherent in the study design. A significant constraint is the utilization of amalgam for coronal restoration. Financial constraints precluded the availability of stainless steel crowns, compelling the authors to employ amalgam restorations in all pulpotomies. To mitigate potential inconsistencies arising from disparate restorations, teeth exhibiting extensive structural loss that requires extensive restorations were deliberately excluded from the study.

Conclusion

Within the limitations of this clinical study, it can be concluded that MTA exhibits a higher overall success rate compared to BD at the 36-month follow-up for pulpotomies in

primary molars. However, to substantiate these findings, further high-quality randomized controlled trials with extended follow-up periods are necessary.

Türkçe özet: *Süt azı dişi pulpotomilerinde kalsiyum silikat esaslı malzemelerin karşılaştırılması: randomize bir klinik çalışma. Amaç: Bu çalışmanın amacı, süt azı dişleri için pulpotomi ajanları olarak mineral trioksit agregat (MTA) ve Biodentine (BD) materyallerini klinik ve radyografik olarak karşılaştırmaktır. Hastalar ve Yöntem: Toplam 200 süt azı dişine pulpotomi tedavisi uygulandı. 36 aylık takiplerde klinik ve radyografik başarı ve başarısızlıklar kaydedildi. Gruplar arasındaki farklar Fisher Exact, McNemar ve Chi-Square testleri kullanılarak istatistiksel olarak analiz edildi. Bulgular: Materyaller kendi içinde değerlendirildiği birinci, üçüncü, altıncı, yirmi dördüncü ve otuz altıncı aylar arasında başarı oranlarında istatistiksel olarak anlamlı bir fark yoktu. On ikinci ayda MTA materyalinin klinik ve radyografik başarı oranları (sırasıyla %98 ve %92), BD materyalinden (sırasıyla %90 ve %80) istatistiksel olarak anlamlı bulundu (p<0,05).Sonuç: 36 ayın sonunda MTA materyali BD'den daha başarılı bulundu. Bununla birlikte, güvenilir sonuçlar için daha uzun takip süreli yüksek kaliteli randomize kontrollü çalışmalara ihtiyaç duyulmaktadır. Anahtar Kelimeler: trikalsiyum silikat; mineral trioxide aggregat; pulpotomi; süt dişleri*

References

1. Fuks AB et al. Ferric sulfate versus dilute formocresol in pulpotomized primary molars: long-term follow-up. Pediatr Dent 1997;19:327-30.
2. Cuadros-Fernández C el al. Short-term treatment outcome of pulpotomies in primary molars using mineral trioxide aggregate and Biodentine: a randomized clinical trial. Clin Oral Invest 2016;20:1639–45. [CrossRef]
3. Juneja P, Kulkarni S. Clinical and radiographic comparison of biodentine, mineral trioxide aggregate and formocresol as pulpotomy agents in primary molars. Eur Arch Paediatr Dent 2017;18:271-8. [CrossRef]
4. Guven Y et al. Success Rates of Pulpotomies in Primary Molars Using Calcium Silicate-Based Materials: A Randomized Control Trial. Biomed Res Int 2017;2017:4059703. [CrossRef]
5. Schulz KF, Altman DG, Moher D. CONSORT Statement: updated guidelines for reporting parallel group randomised trials. BMC Med 2010;24:8-18 [CrossRef]
6. El Meligy OA, Allazzam S, Alamoudi NM. Comparison between biodentine and formocresol for pulpotomy of primary teeth: A randomized clinical trial. Quintessence Int 2016;47:571-80.
7. Yıldız E, Tosun G. Evaluation of formocresol, calcium hydroxide, ferric sulfate, and MTA primary molar pulpotomies. Eur J Dent 2014;8:234-40. [CrossRef]
8. Erdem AP et al. Success rates of mineral trioxide aggregate, ferric sulfate, and formocresol pulpotomies: a 24-month study. Pediatr Dent 2011;33:165-70.
9. Sonmez D, Sari S, Cetinbas T. A Comparison of four pulpotomy techniques in primary molars: a long-term follow-up. J Endod 2008;34:950-5. [CrossRef]
10. Cuadros-Fernandez C et al. Clinical and radiographic outcomes of the use of four dressing materials in pulpotomized primary molars: a randomized clinical trial with 2-year follow-up. Int J Paediatr Dent 2013;23:400-7. [CrossRef]
11. Smail-Faugeron V et al. Pulp treatment for extensive decay in primary teeth. Cochrane Database Syst Rev 2014;2014;6:CDOO322O. [CrossRef]
12. Fuks AB. Vital pulp therapy with new materials for primary teeth: new directions and treatment perspectives. J Endod 2008;34:S18–S24. [CrossRef]
13. Stringhini Junior E, Vitcel ME, Oliveira LB. Evidence of pulpotomy in primary teeth comparing MTA, calcium hydroxide, ferric sulphate, and electrosurgery with formocresol. Eur Arch Paediatr Dent 2015;16:303–12. [CrossRef]
14. Moretti AB et al. The effectiveness of mineral trioxide aggregate, calcium hydroxide and formocresol for pulpotomies in primary teeth. Int Endod J 2008;41:547-55. [CrossRef]
15. Yildirim C et al. Clinical and Radiographic Evaluation of the Effectiveness of Formocresol, Mineral Trioxide Aggregate, Portland Cement, and Enamel Matrix Derivative in Primary Teeth Pulpotomies: A Two Year FollowUp. J Clin Pediatr Dent 2016;40:14-20. [CrossRef]
16. Farsi N et al. Success of mineral trioxide aggregate in pulpotomized primary molars. J Clin Pediatr Dent 2005;29:307-11. [CrossRef]
17. Noorollahian H. Comparison of mineral trioxide aggregate and formocresol as pulp medicaments for pulpotomies in primary molars. Br Dent J 2008;204: E20. [CrossRef]
18. Sushynski JM et al. Comparison of gray mineral trioxide aggregate and diluted formocresol in pulpotomized primary molars: a 6- to 24-month observation. Pediatr Dent 2012;34:120-8.
19. Bani M et al. The Clinical and Radiographic Success of Primary Molar Pulpotomy Using Biodentine™ and Mineral Trioxide Aggregate: A 24-Month Randomized Clinical Trial. Pediatr Dent 2017;39:284-8.
20. Kusum B, Rakesh K, Richa K. Clinical and radiographical evaluation of mineral trioxide aggregate, biodentine and propolis as pulpotomy medicaments in primary teeth. Restor Dent Endod 2015;40:276-85. [CrossRef]
21. Niranjani K et al. Clinical evaluation of success of primary teeth pulpotomy using mineral trioxide aggregate, laser and biodentin an in vivo study. J Clin Diagn Res 2015;9:ZC35-ZC37. [CrossRef]
22. Hugar SM et al. In vivo comparative evaluation of mineral trioxide aggregate and formocresol pulpotomy in primary molars: A 60-month follow-up study. Contemp Clin Dent 2017;8:122-7. [CrossRef]
23. Olatosi OO, Sote EO, Orenuga OO. Effect of mineral trioxide aggregate and formocresol pulpotomy on vital primary teeth: A clinical and radiographic study. Niger J Clin Pract 2015;18:292-6. [CrossRef]
24. Çarıkçıoğlu B, Derelioğlu SŞ, Yılmaz Y. Clinical Assessment of Pulp Therapy for Primary Molars Performed Under General Anesthesia, Using Two Pulpotomy Agents-A Retrospective Cohort Study. Int J Dent Sci and Res 2017;5:110-5. [CrossRef]
25. Rajasekharan S et al. Efficacy of three different pulpotomy agents in primary molars: a randomized control trial. Int Endod J 2017;50:215-28. [CrossRef]

Invited Review

The evolving role of MRI in dentomaxillofacial diagnostics: a comprehensive review

Melisa Öçbe[1] iD

Magnetic Resonance Imaging (MRI) has emerged as a pivotal diagnostic tool in dentomaxillofacial radiology, surpassing conventional imaging techniques by offering superior contrast resolution for soft tissue lesions without the use of ionizing radiation. This comprehensive review explores the expanding applications of MRI in dentistry, highlighting its integration into routine diagnostic protocols and its significance in the evaluation of oral and maxillofacial structures. The article delves into the physics of MRI, detailing the various sequences such as Spin Echo (SE), Gradient Echo (GRE), and Short-Tau Inversion Recovery (STIR), each tailored for specific diagnostic needs. Advanced techniques like Dynamic Contrast-Enhanced MRI and Diffusion-Weighted Imaging (DWI) are discussed for their roles in assessing tissue perfusion and differentiating between benign and malignant lesions. The review emphasizes the necessity of appropriate coil selection and parameter optimization to enhance image quality, particularly in dental applications where artifacts from restorative and prosthetic materials can pose challenges. Furthermore, the article addresses the utility of MRI in visualizing dental hard tissues, the temporomandibular joint, and neurovascular structures, providing a comprehensive overview of its diagnostic capabilities. The integration of MRI into global health systems and the role of Personal Electronic Health Records in reducing redundant imaging are also examined. Conclusively, the review underscores the transformative impact of MRI on dentomaxillofacial diagnostics, advocating for its broader adoption in clinical practice to facilitate accurate diagnosis and effective treatment planning.

Keywords: Dental imaging, magnetic resonance imaging, radiology, dentomaxillofacial diagnostics

Introduction

Magnetic resonance imaging (MRI) has evolved into a well-established diagnostic tool in the oral and maxillofacial radiology as a gold standard with its superior contrast resolution in imaging of soft tissue lesions (1, 2-4). Avoidance of ionizing radiation distinguishes MRI from other advanced imaging methods and constitutes its non-invasive characteristics (5, 6). MRI utilizes powerful magnetic fields and radiofrequency pulses to generate detailed images of tissues. This process provides a comprehensive view of oral and maxillofacial structures with high resolution images. As this technology continues to evolve, considerations about its integration into dental practice requires further attention in the emerging dentomaxillofacial diagnostic methodologies (3, 7-13).

Basic concepts of MRI in dental applications

Understanding the basic principles of MRI is vital for optimizing image quality and clinical data extraction. Dental clinicians need concise knowledge of imaging sequences to make informed decisions (14). MRI relies

on magnetic properties of atomic nuclei, particularly hydrogen protons, interacting with magnetic fields and radiofrequency pulses (15). Manipulating radiofrequency signals in pulse sequences controls hydrogen atom movement, crucial for image formation (16). Protons emit signals when aligned and disturbed, resulting in relaxation processes influencing image contrast (17). Regarding to these relaxation processes, T1 refers to the time constant for longitudinal relaxation, representing how quickly protons realign with the magnetic field, while T2 refers to the time constant for transverse relaxation, indicating how quickly protons lose phase coherence in the transverse plane (3, 14, 16, 17). MRI sequences are critical for identification of anatomical structures and pathological conditions. Each sequence of MRI offers unique advantages with various imaging parameters.

T1 and T2-weighted images

T1-weighted (T1W) and T2-weighted (T2W) images relies on the Time of Repetition (TR) and Time of Echo (TE) characteristics of the image. TR and TE can be manipulated to emphasize different properties in MRI. While short TR and TE emphasizing T1w images, long TR and TE emphasizes T2w images (3, 14, 16). Alterations in T1 and T2 properties are main parameters in generation of those sequences (2, 15, 18, 19).

Spin Echo (SE) sequence

SE is a commonly used MRI sequence particularly used in reducing artifacts and provides high-contrast images for the diagnostic process (14, 17). T1W SE sequences offer anatomical detail, while T2W SE sequences highlight water content differences which is critical in identification of pathological conditions (5, 20, 21).

Gradient echo (GRE) sequence

Gradient echo sequence is an MRI technique that uses variable flip angles and gradient fields which provides faster imaging with enhanced contrast (16, 17). It is specifically used for dynamic imaging of blood flow and functional MRI (fMRI), and commonly used for high-resolution anatomical imaging and detecting hemorrhages (17, 19).

Short-tau inversion recovery (STIR) sequence

STIR sequence is an MRI technique that suppresses fat signal by using an inversion recovery pulse. This technique is commonly used for detection of pathologies such as edema, inflammation, and tumors, as it provides high contrast between fat and water-containing tissues (18, 19) (Figure 1).

3D fast low-angle shot (3D FLASH)

The 3D FLASH sequence provides excellent contrast between tissues, particularly useful for visualizing anatomical structures and dynamic processes. It is commonly used in contrast-enhanced studies to assess vascular structures and abnormalities. (22).

Figure 1. *Coronal sections in T2W MRI showing Spin Echo (a) and STIR (b) sequences. Hyperintense appearance observed in maxillary sinus mucosal thickening and nasal cavity in the STIR image due to fat signal suppression.*

Magnetic resonance angiography (MRA) and MR perfusion

MRA sequences provide detailed images of blood vessels without the need for contrast agents by highlighting the flow of blood. In dentomaxillofacial imaging, MRA can be valuable for assessing vascular anatomy, arteriovenous malformations, and to evaluate the blood supply to tumors or other pathologies (23, 24).

Time-resolved angiography with interleaved stochastic trajectories (TWIST) or time-resolved imaging of contrast kinetics (TRICS) MR angiography is a method that delivers high temporal resolution images across arterial, capillary, and venous phases. This technique is effective for evaluating the feeding arteries, nidus, and draining veins of arteriovenous malformations in the dentomaxillofacial region (14, 25).

Dynamic contrast-enhanced (DCE) MRI

DCE MRI is an advanced technique for the analysis of microvascular parameters of tissue perfusion. It involves placing a region of interest within the tumor to calculate time-intensity curves and semiquantitative parameters (5, 16, 25).

3D fluid attenuated inversion recovery (3D-FLAIR)

3D-FLAIR suppresses the signal from cerebrospinal fluid to increase the visibility of lesions. It is commonly used for detecting abnormalities such as multiple sclerosis plaques, subarachnoid hemorrhages, and other pathologies (5, 8, 25).

3D double-echo steady-state (3D DESS)

3D DESS sequence captures both T2W and GRE images by simultaneously acquiring two echo signals with different weighting during each repetition of the sequences. In the dentomaxillofacial region, it is commonly used to visualize and assess the temporomandibular joint anatomy and disorders (14, 16, 25).

Ultrashort echo time (UTE)

UTE is a specialized method designed to capture images with extremely short echo times, typically less than 1 millisecond. This allows UTE MRI to visualize tissues with very

short T2 relaxation times, such as cortical bone and ligaments. UTE MRI is particularly useful in orthopedic and musculoskeletal imaging for assessing bone structure, cartilage, and tendon integrity, as well as in imaging dental structures such as enamel and dentin (14, 25, 26).

Diffusion-weighted imaging (DWI) and diffusion tensor imaging (DTI)

DWI measures the random motion of water molecules within tissues, providing information about tissue cellularity and integrity. It is commonly used in the dentomaxillofacial region to evaluate lesions, such as tumors or abscesses, based on their cellular density and the restriction of water diffusion. DTI is an extension of DWI that assesses the directionality and coherence of water diffusion in tissues, allowing for the visualization of white matter tracts and nerve fibers. In the maxillofacial region, DTI can be used to map the course of cranial nerves or assess the integrity of neural pathways, aiding in the diagnosis and surgical planning for conditions like trigeminal neuralgia or facial nerve disorders (8, 25, 27, 28) (Table 1).

Integration of spesific sequences

MRI offers sequence options for specific tissues or pathologies, facilitating precise diagnostic imaging. Proficiency in sequence selection is crutial for optimizing MRI examinations. Arteriovascular malformations or malignant lesions necessitate different sequence choices. Furthermore, variations in tissue characteristics may necessitate additional parameter adjustments in MRI protocols. Consideration of scanning duration may be a criterion for optimizing image acquisition. These factors collectively underscore the significance of sequence selection in MRI.

SE and GRE sequences offer contrast advantages, while STIR and DESS protocols improve lesion detection (13). To reduce image acquisition, quick overview scans could be achieved. For instance, by employing rapid T1W 3D FLASH sequences, allowing comprehensive evaluation of the jaw with isotropic spatial resolution within minutes at slightly reduced spatial resolution. This provides adequate anatomical detail for identifying specific areas. Integrating rapid overview imaging with subsequent high-definition local imaging of identified areas could lead to a significant decrease in the overall scan time, potentially reaching the 15-minute range (5, 22).

DCE MRI utilizes pharmacokinetic modeling to derive quantitative parameters like Ktrans, which has shown promise as a marker for tumor hypoxia and treatment response in squamous cell carcinoma. Tumor characteristics such as vascularity and perfusion can be evaluated such as angiogenesis, which lead to the differentiation of squamous cell carcinoma from benign lesions or other malignancies. However, the technique remains subjective and lacking full standardization due to variations in analysis, choice of regions of interest, scanner models, pharmacokinetic models, and treatment time points (25).

MRI of hard tissues as bone, enamel and dentin, presents a challenge due to their limited water content and solid structure. Conventional MRI sequences struggle with these tissues due to their ultrashort T2 relaxation times. However, addressing this specific challenge requires sequences that are sensitive to ultrashort T2 relaxation and can provide a detailed analysis of these tissues with high spatial resolution and signal-to-noise ratio. Ultrashort Time Echo (UTE) MRI is a sequence that fulfills these requirements, allowing for effective imaging of dental hard tissues by capturing signals from rapidly decaying echoes and overcoming the limitations associated with their short relaxation times (26).

Recently, there has been a surge in popularity of Diffusion Tensor Imaging (DTI) and Diffusion-Weighted Imaging (DWI) sequences in oral and maxillofacial imaging (8, 25, 27, 28). The degree of anisotropy and directional information obtained through DTI contribute to a more comprehensive understanding of the organization and integrity of tissue structures. Overall, DTI, by unraveling the complexities of water diffusion at a microscopic level, proves to be a pivotal tool in tissue microstructure and pathology (27, 29, 30). DWI and DTI can assist in characterizing lesions and evaluating treatment responses in dentomaxillofacial imaging. Specifically, the apparent diffusion coefficient (ADC) ratios derived from DWI and DTI can facilitate the differentiation between benign and malignant lesions (29-35). Koontz *et al.* (29) stated that DTI serves as a valuable predictor of malignancy in head and neck lesions, with the ADC values of malignant lesions

Table 1: *Commonly used sequences for strategic MRI ordering*

Commonly used sequences	Justification
Spin Echo (SE)	Provides T1- and T2-weighted images with versatile soft tissue contrast
Griadient Echo (GRE)	Enables dynamic imaging and susceptibility-weighted imaging
Short-tau Inversion Recovery (STIR)	Suppresses fat signal for enhanced visualization of pathology
3D Fluid Attenuated Inversion Recovery (3D-FLAIR)	Supresseses fluid signal and produces high-resolution 3D images
3D Double-Echo Steady-State (3D DESS)	Provides multiple contrasts in a single acquisition
3D Fast Low-Angle Shot (3D FLASH)	Offers high-resolution images with short acquisition times
Ultrashort Echo Time (UTE)	Able to view the dental hard tissue
Dynamic contrast-enhanced (DCE)	Assesses blood flow and tissue perfusion
Magnetic Resonance Angiography (MRA)	Visualizes blood vessels without the use of contrast agents
Diffusion Tensor Imaging (DTI)	Quantifies the direction and magnitude of water diffusion in tissues
Diffusion-Weighted Imaging (DWI)	Provides information about the microstructure and cellularity of tissues

being significantly lower than benign lesions. In addition, Li *et al.* (31) found that not only the malignant lesions ADC values are lower, ADC values of benign solid lesions were significantly lower than cystic lesions. In the studies of Baba *et al.* (33, 34) it was found that ADC values were significantly higher in osteomyelitis when its compared with nasopharyngeal cancer.

Evaluation of MRI databases in global health systems

In the context of escalating healthcare costs, healthcare providers bear the responsibility of seeking advanced imaging modalities. Dental clinicians are prompted to consider whether the prevailing clinical issue has been recently addressed through existing imaging resources. Oral and Maxillofacial Radiology consultations can provide insights into the appropriateness of the requested diagnostic workup (36). From a global perspective, Personal Electronic Health Records Systems (PEHRSs) are avaible in various countries network systems which allows to view the previous MRI records. PEHRSs have been widely utilized on a global scale. utilized by 82% of the Turkish population (e-Nabız), with similar implementations in Denmark (e-Record), Estonia (e-Health Record), and Germany (Elektronische Patientenakte – ePA) (37, 38). The appropriate utilization of PEHRSs and familiarity with the aforementioned systems are importantant in avoiding unnecessary or redundant MR imaging, thereby addressing healthcare cost concerns. An extensive study involving 196,314 patients revealed a 7.7% repetition rate within 90 days when prior imaging data was inaccessible. Additionally, it was stated that 18% of the patients had at least one image in this cohort study. Findings indicated that accessing PEHRSs within 90 days subsequent to an initial imaging procedure significantly reduced the repetition of imaging. This underscores the significant increase in imaging redundancy in the absence of PEHRS access. To avoid repetitive and unnecessary imaging, it is crutial to consult PEHRSs prior to ordering new imaging studies (36).

In evaluation of the MRI data existing in the PEHRSs, another important consideration is sequence assesment with respect to targeted pathological condition. A majority of MR imaging is conducted for medical purposes which may be problematic in analyzing data for dentomaxillofacial diagnostic purposes. MR images acquired for other medical purposes may occasionally lack the adequacy needed for evaluating oral and maxillofacial conditions. For instance, SE or GRE MR images can be employed to assess the position and anatomical variations of the inferior alveolar nerve before surgeries involving the posterior mandibular region (39). Yet, if the objective is to discriminate between benign and malignant pathologies, pulse sequence MR imaging may prove insufficient, necessitating the application of different MR imaging techniques depending on the characteristics of the lesion (29, 31).

Factors influencing image quality in MRI

Coil selection

In MRI, a coil refers to a radiofrequency (RF) coil, an essential component of the MRI system and play a crucial role in capturing detailed images, used to transmit radiofrequency pulses and receive signals during the imaging process (40). Different coils are tailored for specific body parts or imaging goals. The application of a specific coil enables a nuanced and differential diagnosis of suspicious lesions within the head and neck region (41). The choice of coil depends on the imaging requirements and the anatomical structures being examined (42, 43). While gradient coils and surface coils are the most commonly used coil in MR imaging (44), using specific coils for dentomaxillofacial imaging improves the image quality (45). Although not common, intraoral coil design is implemented using an appliance placed inside the mouth. The current literature indicates that MR images obtained with this type of coil provide detailed dentomaxillofacial imaging (42, 43).

Al-Haj Husain *et al.* (9) reported a case of irritation fibroma. Imaging of the lesion prior to the excision was perfomed with a 15-channel mandibular coil. The STIR and DESS sequences was in that case report, while the authors stated that these sequences are best suited to overcome the limitations of hard tissue imaging in dentomaxillofacial imaging. According to the study of Grandoch *et al.* (45), MR imaging with an intraoral coil can be a non-invasive alternative of cone-beam computed tomography in dental treatment planning such as third molar extraction or implant procedures concerning mandibular posterior region.

In addition to coils, various imaging parameters such as Signal-to-Noise Ratio (SNR), Contrast-to-Noise Ratio (CNR), FOV, matrix size, slice thickness, bandwidth play significant roles in influencing image quality in MRI (14, 44, 46, 47).

Signal-to-noise ratio (SNR)

The primary objective of RF receiver coils is to maximize the SNR, which is influenced by the coil's loop size and electrical properties (44). SNR compares the level of the target signal to the level of background noise in an MRI image (14). An increase in SNR can lead to higher spatial resolution or faster scanning speeds, resulting in clearer, more detailed images and improved diagnostic accuracy (5, 44, 46).

Contrast-to-noise ratio (CNR)

CNR measures the difference in signal strength between two adjacent tissues compared to the background noise level. High CNR is vital for distinguishing between different tissues or structures in an image and is particularly useful for detecting lesions with low contrast. Improved image quality is associated with higher SNR and CNR values (47).

Field of view (FOV)

FOV refers to the extent of the area being imaged, typically measured in millimeters (14). Increasing the FOV may reduce spatial resolution, as the MRI scanner distributes the available imaging resources over a larger area, resulting in less detailed images (46).

Slice thickness

Slice thickness refers to the thickness of the anatomical

slices captured during imaging, measured in millimeters. Thinner slices provide better spatial resolution and reduce partial volume effects, but may increase scan time and noise (44, 46, 47).

Bandwidth

Bandwidth in MRI refers to the range of frequencies used to encode the signal. Higher bandwidth can reduce image distortion and chemical shift artifacts but may decrease SNR, while lower bandwidth improves SNR but can increase artifacts and distortions (46) (Table 2).

Dental materials and MRI

As stated in the 2020 guideline of the American College of Radiology, whether an implant or a foreign body, a ferromagnetic material can cause image distortion and signal loss artifacts (48). Materials employed in dental applications for restorative, endodontic, prosthodontic and orthodontic treatments may contribute to the occurrence of imaging artifacts (14, 49, 50). The severity and extent of artifacts were influenced by factors such as material location, size, and thickness, with orthodontic appliances covering a large area of the oral cavity being of particular concern.

Restorative and endodontic materials

In restorative dentistry, certain materials like glass-ionomer cements and composite resins exhibit minimal distortion on MR imaging. Amalgam contains various metals including non-ferromagnetic silver, which does not significantly affect MR image quality (14). In addition, resin-based sealer and gutta-percha seem not to produce detectable distortions on MRI as well (14, 46).

Prosthetic materials

In prosthetic dentistry, gold crowns exhibit minimal ferromagnetic effects. Ceramic and zirconia crowns typically do not produce artifacts (50-52), although Reda *et al.* (14) stated that there are conflicting statements regarding the effect of zirconia, with some comparing it to metal effects. Metal-ceramic restorations, often made with nickel alloys, tend to generate artifacts (14). (Figure 2).

Dental implants

Dental implants contributed to localized artifacts in the oral cavity, affecting the assessment of adjacent structures, and susceptibility artifacts were observed in brain imaging as well. Current conventional techniques, like employing lower field strength or utilizing a SE sequence, are available to mitigate artifacts. Research indicates that 3 Tesla MRI tends to produce larger artifacts compared to 1.5 Tesla MRI, and using a SE sequence has been shown to decrease artifacts when contrasted with a GRE sequence (14, 49).

Orthodontic materials

While artifacts from titanium and ceramic materials were mostly confined to the oral cavity, stainless steel alloy caused more widespread distortion of the magnetic field due to its ferromagnetic properties. Removal of orthodontic appliances before MRI may be necessary to mitigate artifact severity. The decision to remove the orthodontic wire prior to MRI acquisition should be considered based on the chosen sequence, irrespective of whether the brackets are retained.
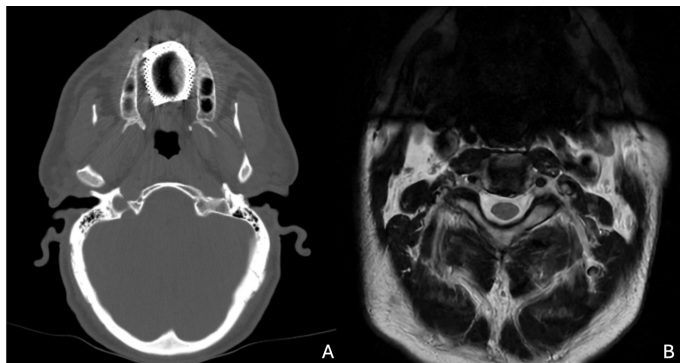

Figure 2. *Computed tomography (a) and MRI (b) axial sections showing significant signal loss in the anterior region due to the removable prosthetics in the maxilla.*

Table 2. *Imaging parameters in MRI*			
Parameter	**Definition**	**Effect on Image Quality**	**Impact**
Signal-to-Noise Ratio (SNR)	A measure of the strength of the signal compared to noise	Higher SNR improves image quality, providing clearer details	Increased SNR results in higher image quality, essential for better visualization of structures and pathology.
Contrast-to-Noise Ratio (CNR)	Represents the difference in signal intensity between two regions relative to the noise.	Higher CNR enhances the visibility of differences between tissues.	Improved CNR aids in better differentiation of structures.
Field of View (FOV)	The size of the imaging area	Larger FOV captures a larger anatomical area	Larger FOV is suitable for imaging larger anatomical regions but may reduce spatial resolution for smaller structures.
Slice Thickness	The thickness of each imaging slice	Thinner slices provide better detail but may extend scan time	Thinner slices improve spatial resolution and are preferred for detailed imaging, although this may increase the overall scan time.
Bandwidth	The range of frequencies acquired during signal collection	Narrower bandwidth can improve image quality	Narrower bandwidth refines frequency resolution, potentially reducing chemical shift artifacts and improving overall image quality.

Retainers crafted from gold or titanium generate insignificant artifacts, preserving diagnostic quality in dental and head/neck MRI. Conversely, ferromagnetic steel retainers induce notable artifacts, persistently compromising image quality, particularly with proximity to orthodontic retainers like rectangular steel and twistflex-steel, which can also impact remote anatomical structures (14, 49, 50).

MRI of dentomaxillofacial structures

MRI in detecting the normal anatomy of dentomaxillofacial structures is crucial for the accurate detection of pathologies. Advancements in MRI technology have also enhanced its importance in evaluating bone structures for a comprehensive dentomaxillofacial assessments (46, 54-57).

Dental anatomy

The appearance of enamel and dentin in MRI is typically dark due to the absence of unbound protons. Surrounding structures are clearly visible, with cortical bone delineated as a black zone outlined by a moderate signal from external soft tissues (46) (Figure 3).
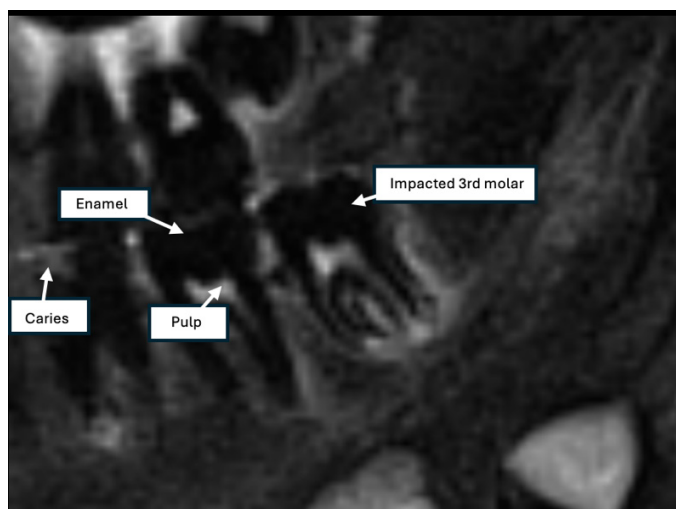

Figure 3. *T2W SE MRI sagittal section showing dental structures. Mote that peripheral area of the impacted 3rd molar is hyperintense compared to the normal bone and the impacted tooth is in close relation with inferior alveolar nerve.*

It is recognized that a minimum of 30% mineral loss is necessary to identify a bony lesion through radiation-based imaging technique (53). In contrast, MRI can detect signal changes before significant mineral loss occurs, as it is sensitive to alterations in the number of water molecules within a lesion (54, 55). Bracher *et al.* (54) found that UTE-MRI may offer advantages in certain aspects of caries detection by visualizing hard tissues with limited water content. It was stated that UTE MR imaging can be applied for the identification of caries lesions wtih the ability to differentiate between dentine, enamel, and cementum. Despite the high sensitivity provided by this technique, the increased acquisition time (approximately 45 minutes) and the higher costs still represent a concrete obstacle for widespread clinical application of UTE-MRI (3, 55).

In the in vivo study of Assaf *et al.* (56), with 3 Tesla MR scanner, four sequences were tested: non-contrast-enhanced

T1w, non-contrast-enhanced fat-saturated T1w, fat-saturated T2w, and constructive interference steady state. The findings revealed that the pulp chamber, periodontal space, and periapical lesions were observable without the need for contrast media. However, as anticipated, the differentiation between the enamel-dentin junction and the cementum-dentin junction of the teeth was limited. Dental MRI's characteristics enable the distinction between vital and nonvital teeth. When contrast media is employed, the vital pulp exhibits increased brightness, while older teeth display lower signal intensity due to reduced perfusion of the pulp. In contrast, nonvital or endodontically treated teeth do not exhibit any brightness (46, 56, 57).

Floor of the mouth

The mylohyoid muscle divides the sublingual space from the submandibular space, serving as a crucial landmark in imaging the oral cavity and upper neck. Surgical strategies are determined by a lesion's proximity to the mylohyoid muscle. Additionally, sublingual lesions often extend into the submandibular space at the muscle's posterior edge. Consequently, pre-surgical MRI of the floor of the mouth is important for assessing the submental area (58, 59).
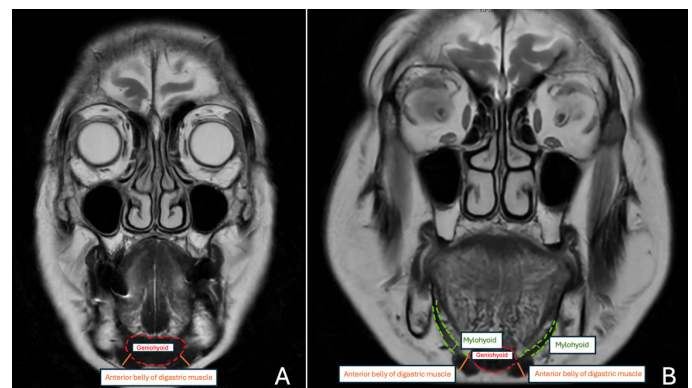

Figure 4. *Coronal SE T2W images of submental muscle group. Note the geniohyoid muscle, mylohyoid muscle and anterior bellies of digastric muscle.*

Neurovascular structures of dentomaxillofacial region

Inferior alveolar nerve and lingual Nerve

Inferior alveolar nerve and lingual nerve are branches of trigeminal nerve's mandibular division. The visualization of the inferior alveolar nerve and lingual nerve with various MRI sequences and field strengths were stated in the literature previosly (10, 60-62). Borges and Casselman (63) stated that best sequences for neurovascular imaging are the non-contrast-enhanced fat-saturated T1W and T2W images. In T1W images, the outer cortical plate exhibits a dark appearance, diverging from the typical radiopacity observed in radiographs attributable to increased bone density. This manifestation in MRI results from the significant low signal, attributed to the absence of water or lipid protons. Conversely, the more organic cancellous bone presents a distinctly bright appearance in T1W images. Therefore, as

Malaro and Kolokythas (64) stated, the course of the inferior alveolar nerve and the mandibular trigeminal division can be followed with high-resolution T1W sequences (64).

Nasopalatine nerve

The nasopalatine nerve is a branch of the maxillary division of the trigeminal nerve which innervates the mucosa of the anterior hard palate, the lingual gingiva adjacent to the maxillary central and lateral incisors, and the lower part of the nasal septum. A study of Grandoch *et al.* (65), highlights the potential of employing a dedicated dental coil, revealing that MR imaging provides superior detail in both axial and coronal planes compared to CBCT for imaging the nasopalatine and inferior alveolar nerves. Nevertheless, Müller *et al.* (66) stated that SE sequences also offer precise diagnostic capabilities and imaging quality concerning the components of the trigeminal nerve. Imaging of the inferior alveolar canal and nasopalatine canal with conventional methods typically visualize the surrounding bone cortex rather than the contained nerve or vascular structures. Conversely, MRI enables the visualization of not only the bone cortex but also the neurovascular structures within it. Consequently, MRI holds potential for evaluation in cases where monitoring the relationship between lesions or teeth and neurovascular structures in the dentomaxillofacial region is necessary.

Exploring temporomandibular joint (TMJ) through MRI

MRI offers superior visualization of the TMJ and masticatory muscles, with high spatial and contrast resolution without the use of ionizing radiation and enables detailed assessment of the TMJ anatomy, including the disc, articular surfaces, ligaments, and surrounding muscles. Additionally, MRI allows for the detection of pathologies such as disc displacement, degenerative joint disease, and inflammatory conditions (67) (Figure 5).

For the detection of disc displacement, MRI provides detailed images of the disc, comprised mainly of collagen, allowing differentiation from synovial fluid and vessel-rich retrodiscal tissue on proton density (PD) and T2W imaging. While MRI allows examination of bone marrow integrity and osseous component morphology, it is also useful for detecting joint effusion and evaluating soft tissue neoplasia or neoplastic-like lesions. Commonly used protocols involve

Figure 5. *Axial T2W SE images showing masticatory muscles in axial plane. *: Mandibular foramen.*

T1W (or PD) and T2W imaging in closed and open mouth positions, with cross-sectional views including axially corrected sagittal oblique and coronal oblique sections along the long axes of the condyles. The closed mouth position helps assess disc position and soft tissue conditions, especially for detecting disc displacement, while the open mouth position aids in determining if a displaced disc was recaptured by the condyle upon opening (59-61) (Figure 6).
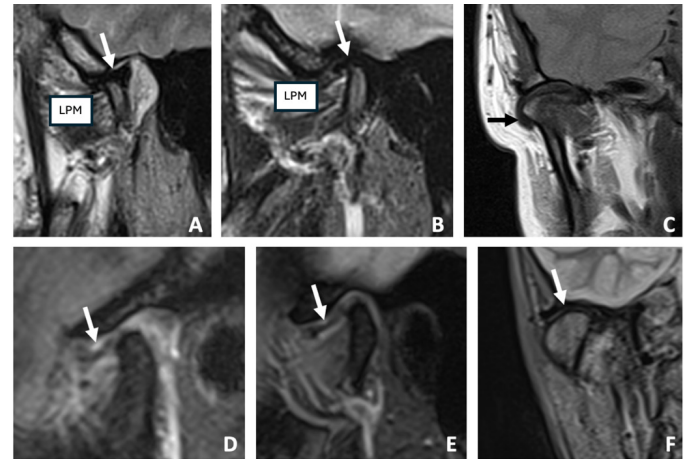
Figure 6. *A and B: T2-weighted images in open (A) and closed (B) mouth positions, depicting normal disc position and lateral pterygoid muscle (LPM) C: Proton Density Turbo Spin Echo (PD TSE) image showing lateral disc displacement. D and E: T2-weighted images in open (D) and closed (E) mouth positions displaying anterior disc displacement. F: T2-weighted Spin Echo (SE) with Short Tau Inversion Recovery (STIR) sequence demonstrating the normal position of the disk in the coronal plane.*

Traditional MRI methods typically provide only static morphological and qualitative assessments of TMJ disorders, lacking the ability to capture the dynamic movement of the TMJ disc and mandibular condyle. In addition, while CBCT can depict osseous pathologies of the TMJ, such as arthropathies and osteoarthritis, MRI is still insufficient regarding bone pathologies of TMJ. A review of Xiong *et al.* *(67)* examines recent advancements in dynamic and quantitative MRI techniques, including DWI, T2 mapping, and UTE MRI, which show promise in TMJ imaging. Future directions in TMJ imaging involve the use of 7 Tesla MRI scanners with specialized sequences and improved SNR. While quantitative analysis of biochemical structures and MRI parameters has room for improvement, it remains achievable, particularly with ADC values (67, 68). In a retrospective MRI study by Jin Jeon *et al.* (68), 3 Tesla MR images of patients with TMJ disorders were analyzed using a specific sequence known as 'chemical shift-encoded magnetic resonance imaging', aiming to evaluate muscle parameters. Quantification of MR images through fat fraction analysis suggested its potential as a biomarker for TMJ disorders.

Conclusion

In conclusion, the integration of MRI into dentomaxillofacial imaging represents a significant advancement, offering a non-invasive imaging method with high-resolution imaging capabilities. MRI provides valuable insights that contribute to more accurate diagnoses.
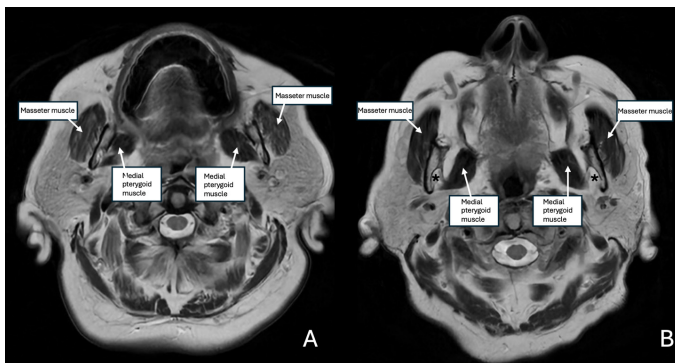
Türkçe öz: *Dentomaksillofasiyal Tanıda MRG'nin Gelişen Rolünün Değerlendirilmesi. Manyetik Rezonans Görüntüleme (MRG), yumuşak doku lezyonları için üstün kontrast çözünürlüğü sunan ve iyonize radyasyon kullanmayan, dentomaksillofasiyal radyolojide geleneksel görüntüleme tekniklerine önemli bir tanı aracı alternatifi olarak ortaya çıkmıştır. Bu inceleme, MRG'nin diş hekimliğinde genişleyen uygulamalarını inceleyerek, rutin tanısal protokollere entegrasyonunu ve oral ve maksillofasiyal yapıların değerlendirilmesindeki önemini vurgulamaktadır. Spin Echo (SE), Gradient Echo (GRE) ve Short-Tau Inversion Recovery (STIR) gibi çeşitli sekansların her birinin belirli tanı ihtiyaçlarına göre özelleştirildiği MRG fiziğini ayrıntılı olarak ele almaktadır. Dinamik Kontrastlı MRG ve Difüzyon Ağırlıklı Görüntüleme (DWI) gibi ileri tekniklerin doku perfüzyonunu değerlendirme ve iyi huylu ile kötü huylu lezyonları ayırt etmedeki rolleri tartışılmaktadır. Özellikle restoratif ve protez malzemelerinden kaynaklanan artefaktların zorluklar oluşturabileceği diş hekimliği uygulamalarında görüntü kalitesini artırmak için uygun bobin seçimi ve parametre optimizasyonunun gerekliliği vurgulanmaktadır. Ayrıca, MRG'nin diş sert dokularını, temporomandibular eklemi ve nörovasküler yapıları görselleştirmedeki kullanımını ele alarak, tanısal yeteneklerinin kapsamlı bir özetini sunulmaktadır. MRG'nin küresel sağlık sistemlerine entegrasyonu ve kişisel elektronik sağlık kayıtlarının tekrarlayan görüntülemeyi azaltmadaki rolü de incelenmiştir. Sonuç olarak, MRG'nin dentomaksillofasiyal tanı sürecinde dikkate değer derecede olumlu etkisi olduğu, klinik uygulamalarda daha geniş çapta kullanılmasının doğru teşhis ve etkili tedavi planlamasına sanılandan daha fazla katkısı olabileceği öne sürülmektedir. Anahtar kelimeler: dental görüntüleme, manyetik rezonans görüntüleme, radyoloji, dentomaksillofasiyal tanı*

References

1. Lurie AG. Doses, Benefits, Safety, and Risks in Oral and Maxillofacial Diagnostic Imaging. Health Phys 2019;116:163-9. doi: 10.1097/HP.0000000000001030. [CrossRef]

2. Ekprachayakoon I, Miyamoto JJ, Inoue-Arai MS, Honda EI, Takada JI, Kurabayashi T, Moriyama K. New application of dynamic magnetic resonance imaging for the assessment of deglutitive tongue movement. Prog Orthod 2018;19:45. doi: 10.1186/s40510-018-0245-x. [CrossRef]

3. Mendes S, Rinne CA, Schmidt JC, Dagassan-Berndt D, Walter C. Evaluation of magnetic resonance imaging for diagnostic purposes in operative dentistry-a systematic review. Clin Oral Investig 2020;24:547-57. doi: 10.1007/s00784-019-03103-8. [CrossRef]

4. Xu J, Wang D, Yang C, Wang F, Wang M. Reconstructed magnetic resonance image-based effusion volume assessment for temporomandibular joint arthralgia. J Oral Rehabil 2023;50:1202-10. doi: 10.1111/joor.13551. [CrossRef]

5. Pykett IL, Newhouse JH, Buonanno FS, Brady TJ, Goldman MR, Kistler JP, Pohost GM. Principles of nuclear magnetic resonance imaging. Radiology 1982;143:157-68. doi: 10.1148/radiology.143.1.7038763. [CrossRef]

6. Lam EW, Hannam AG, Wood WW, Fache JS, Watanabe M. Imaging orofacial tissues by magnetic resonance. Oral Surg Oral Med Oral Pathol 1989;68:2-8. doi: 10.1016/0030-4220(89)90106-0. [CrossRef]

7. Hisatomi M, Asaumi J, Konouchi H, Shigehara H, Yanagi Y, Kishi K. MR imaging of epithelial cysts of the oral and maxillofacial region. Eur J Radiol 2003;48:178-82. doi: 10.1016/S0720-048X(02)00218-8. [CrossRef]

8. Terra GT, Oliveira JX, Hernandez A, Lourenço SV, Arita ES, Cortes AR. Diffusion-weighted MRI for differentiation between sialadenitis and pleomorphic adenoma. Dentomaxillofac Radiol 2017;46:20160257. doi: 10.1259/dmfr.20160257. [CrossRef]

9. Al-Haj Husain A, Schönegg D, Valdec S, Stadlinger B, Piccirelli M, Winklhofer S. Appearance of nasopalatine duct cysts on dental magnetic resonance imaging using a mandibular coil: Two case reports with a literature review. Imaging Sci Dent 2023;53:161-8. doi: 10.5624/isd.20220215. [CrossRef]

10. Burian E, Probst FA, Weidlich D, Cornelius CP, Maier L, Robl T, Zimmer C, Karampinos DC, Ritschl LM, Probst M. MRI of the inferior alveolar nerve and lingual nerve-anatomical variation and morphometric benchmark values of nerve diameters in healthy subjects. Clin Oral Investig 2020;24:2625-34. doi: 10.1007/s00784-019-03120-7. [CrossRef]

11. Li M, Yuan Z, Tang Z. The accuracy of magnetic resonance imaging to measure the depth of invasion in oral tongue cancer: a systematic review and meta-analysis. Int J Oral Maxillofac Surg 2022;51:431-40. doi: 10.1016/j.ijom.2021.07.010. [CrossRef]

12. Kennerley AJ, Mitchell DA, Sebald A, Watson I. Real-time magnetic resonance imaging: mechanics of oral and facial function. Br J Oral Maxillofac Surg 2022;60:596-603. doi: 10.1016/j.bjoms.2021.10.008. [CrossRef]

13. Al-Haj Husain A, Stadlinger B, Özcan M, Schönegg D, Winklhofer S, Al-Haj Husain N, Piccirelli M, Valdec S. Buccal bone thickness assessment for immediate anterior dental implant planning: A pilot study comparing cone-beam computed tomography and 3D double-echo steady-state MRI. Clin Implant Dent Relat Res 2023;25:35-45. doi: 10.1111/cid.13160. [CrossRef]

14. Reda R, Zanza A, Mazzoni A, Cicconetti A, Testarelli L, Di Nardo D. An Update of the Possible Applications of Magnetic Resonance Imaging (MRI) in Dentistry: A Literature Review. J Imaging 2021; 7:75. doi: 10.3390/jimaging7050075. [CrossRef]

15. Calle D, Navarro T. Basic Pulse Sequences in Magnetic Resonance Imaging. Methods Mol Biol 2018;1718:21-37. doi: 10.1007/978-1-4939-7531-0_2. [CrossRef]

16. Pooley RA. Fundamental physics of MR imaging. RadioGraphics 2005;25,1087-99. doi:10.1148/rg.254055027 [CrossRef]

17. Jackson EF, Ginsberg LE, Schomer DF, Leeds NE. A review of MRI pulse sequences and techniques in neuroimaging. Surg Neurol 1997;47:185-99. doi: 10.1016/s0090-3019(96)00375-8. [CrossRef]

18. Berger A. Magnetic resonance imaging. BMJ 2002;5:324-35. doi: 10.1136/bmj.324.7328.35. [CrossRef]

19. Tourais J, Coletti C, Weingärtner S. Chapter 1 - Brief Introduction to MRI Physics. In: Akçakaya M, Doneva M, Prieto C, editors. Advances in Magnetic Resonance Technology and Applications. Academic Press 2022;3-36. https://doi.org/10.1016/B978-0-12-822726-8.00010-5. [CrossRef]

20. Minami M, Kaneda T, Ozawa K, Yamamoto H, Itai Y, Ozawa M, Yoshikawa K, Sasaki Y. Cystic lesions of the maxillomandibular region: MR imaging distinction of odontogenic keratocysts

and ameloblastomas from other cysts. AJR Am J Roentgenol 1996;(4),943-9. https://doi.org/10.2214/ajr.166.4.8610578 [CrossRef]

21. Probst FA, Probst M, Pautke Ch, Kaltsi E, Otto S, Schiel S, Troeltzsch M, Ehrenfeld M, Cornelius CP, Müller-Lisse UG. Magnetic resonance imaging: a useful tool to distinguish between keratocystic odontogenic tumours and odontogenic cysts. Br J Oral Maxillofac Surg 2015;53:217-22. doi: 10.1016/j.bjoms.2014.10.014 [CrossRef]

22. Geibel MA, Schreiber ES, Bracher AK, Hell E, Ulrici J, Sailer LK, Ozpeynirci Y, Rasche V. Assessment of apical periodontitis by MRI: A feasibility study. Rofo 2015;187:269-75. doi: 10.1055/s-0034-1385808. [CrossRef]

23. Kramer M, Schwab SA, Nkenke E, Eller A, Kammerer F, May M, Baigger JF, Uder M, Lell M. Whole body magnetic resonance angiography and computed tomography angiography in the vascular mapping of head and neck: an intraindividual comparison. Head Face Med 2014;10:16. doi: 10.1186/1746-160X-10-16. [CrossRef]

24. Yang G, Wilson TD, Lehman MN, Cui D. Comparison of Magnetic Resonance Angiography and Computed Tomography Angiography Stereoscopic Cerebral Vascular Models. Adv Exp Med Biol 2019;1205:1-9. doi: 10.1007/978-3-030-31904-5_1. [CrossRef]

25. Widmann G, Henninger B, Kremser C, Jaschke W. MRI Sequences in Head & Neck Radiology - State of the Art. Rofo 2017;189:413-22. English. doi: 10.1055/s-0043-103280. [CrossRef]

26. Timme M, Borkert J, Nagelmann N, Schmeling A. Evaluation of secondary dentin formation for forensic age assessment by means of semi-automatic segmented ultrahigh field 9.4 T UTE MRI datasets. Int J Legal Med 2020;134:2283-8. doi: 10.1007/s00414-020-02425-7. [CrossRef]

27. Grover VP, Tognarelli JM, Crossey MM, Cox IJ, Taylor-Robinson SD, McPhail MJ. Magnetic Resonance Imaging: Principles and Techniques: Lessons for Clinicians. J Clin Exp Hepatol 2015;5:246-55. doi: 10.1016/j.jceh.2015.08.001. [CrossRef]

28. Norris CD, Quick SE, Parker JG, Koontz NA. Diffusion MR Imaging in the Head and Neck: Principles and Applications. Neuroimaging Clin N Am 2020;30:261-82. doi: 10.1016/j.nic.2020.04.001. [CrossRef]

29. Koontz NA, Wiggins RH 3rd. Differentiation of Benign and Malignant Head and Neck Lesions With Diffusion Tensor Imaging and DWI. AJR Am J Roentgenol 2017;208:1110-15. doi: 10.2214/AJR.16.16486. [CrossRef]

30. Bao D, Zhao Y, Wu W, Zhong H, Yuan M, Li L, Lin M, Zhao X, Luo D. Added value of histogram analysis of ADC in predicting radiation-induced temporal lobe injury of patients with nasopharyngeal carcinoma treated by intensity-modulated radiotherapy. Insights Imaging 2022;13:197. doi: 10.1186/s13244-022-01338-w. [CrossRef]

31. Li S, Cheng J, Zhang Y, Zhang Z. Differentiation of benign and malignant lesions of the tongue by using diffusion-weighted MRI at 3.0T. Dentomaxillofac Radiol 2015;44:20140325. doi: 10.1259/dmfr.20140325. [CrossRef]

32. Vidiri A, Minosse S, Piludu F, Curione D, Pichi B, Spriano G, Marzi S. Feasibility study of reduced field of view diffusion-weighted magnetic resonance imaging in head and neck tumors. Acta Radiol 2017;58:292-300. doi: 10.1177/0284185116652014. [CrossRef]

33. Baba A, Kurokawa R, Kurokawa M, Ota Y, Srinivasan A. Dynamic Contrast-Enhanced MRI Parameters and Normalized ADC Values Could Aid Differentiation of Skull Base Osteomyelitis from Nasopharyngeal Cancer. AJNR Am J Neuroradiol 2023;44:74-8. doi: 10.3174/ajnr.A7740. [CrossRef]

34. Baba A, Kurokawa R, Kurokawa M, Srinivasan A. Dynamic contrast-enhanced MRI parameters and apparent diffusion coefficient as treatment response markers of skull base osteomyelitis: a preliminary study. Pol J Radiol 2023;88:319-24. doi: 10.5114/pjr.2023.130383. [CrossRef]

35. Panyaping T, Tepkidakarn N, Kiatthanabumrung S, Wattanatranon D, Tritanon O. Usefulness of apparent diffusion coefficient values for distinguishing between squamous cell carcinoma and malignant salivary gland tumor of the head and neck. Neuroradiol J 2023;36:548-54. doi: 10.1177/19714009231163561. [CrossRef]

36. Vest JR, Kaushal R, Silver MD, Hentel K, Kern LM. Health information exchange and the frequency of repeat medical imaging. Am J Manag Care 2014;20:16-24

37. Nøhr C, Parv L, Kink P, Cummings E, Almond H, Nørgaard JR, Turner P. Nationwide citizen access to their health data: analysing and comparing experiences in Denmark, Estonia and Australia. BMC Health Serv Res 2017;17:534. doi: 10.1186/s12913-017-2482-y. [CrossRef]

38. Birinci Ş. A Digital Opportunity for Patients to Manage Their Health: Turkey National Personal Health Record System (The e-Nabız). Balkan Med J 2023;40:215-21. doi: 10.4274/balkanmedj.galenos.2023.2023-2-77. Epub 2023 Apr 28. Erratum in: Balkan Med J 2023;40:307. [CrossRef]

39. Kreutner J, Hopfgartner A, Weber D, Boldt J, Rottner K, Richter E, Jakob PM, Haddad D. High isotropic resolution magnetic resonance imaging of the mandibular canal at 1.5 T: a comparison of gradient and spin echo sequences. Dentomaxillofac Radiol 2017;46:20160268. doi: 10.1259/dmfr.20160268. [CrossRef]

40. Kozlov M, Kalloch B, Horner M, Bazin PL, Weiskopf N, Möller HE. Patient-Specific RF Safety Assessment in MRI: Progress in Creating Surface-Based Human Head and Shoulder Models. 2019;28. In: Makarov S, Horner M, Noetscher G, editors. Brain and Human Body Modeling: Computational Human Modeling at EMBC 2018 [Internet]. Cham (CH): Springer 2019. Chapter 13. [CrossRef]

41. Al-Haj Husain A, Sekerci E, Schönegg D, Bosshard FA, Stadlinger B, Winklhofer S, Piccirelli M, Valdec S. Dental MRI of Oral Soft-Tissue Tumors-Optimized Use of Black Bone MRI Sequences and a 15-Channel Mandibular Coil. J Imaging 2022;8:146. doi: 10.3390/jimaging8050146. [CrossRef]

42. Özen AC, Ilbey S, Jia F, Idiyatullin D, Garwood M, Nixdorf DR, Bock M. An improved intraoral transverse loop coil design for high-resolution dental MRI. Magn Reson Med 2023;90:1728-37. doi: 10.1002/mrm.29744. [CrossRef]

43. Tymofiyeva O, Rottner K, Jakob PM et al. Three-dimensional localization of impacted teeth using magnetic resonance imaging. Clin Oral Investig 2010;14:169-176. [CrossRef]

44. Gruber B, Froeling M, Leiner T, Klomp DWJ. RF coils: A practical guide for nonphysicists. J Magn Reson Imaging 2018;48:590–604. doi: 10.1002/jmri.26187. [CrossRef]

45. Grandoch A, Peterke N, Hokamp NG, Zöller JE, Lichenstein T, Neugebauer J. 1.5 T MRI with a Dedicated Dental Signal-Amplification Coil as Noninvasive, Radiation-Free Alternative to CBCT in Presurgical Implant Planning Procedures. Int J Oral Maxillofac Implants 2021;36:1211-8. doi: 10.11607/jomi.8103. [CrossRef]

46. Di Nardo D, Gambarini G, Capuani S, Testarelli L. Nuclear Magnetic Resonance Imaging in Endodontics: A Review. J Endod 2018;44:536-42. doi: 10.1016/j.joen.2018.01.001. [CrossRef]

47. Demirturk Kocasarac H, Kursun-Cakmak ES, Ustaoglu G, Bayrak S, Orhan K, Noujeim M. Assessment of signal-to-noise ratio and contrast-to-noise ratio in 3 T magnetic resonance imaging in the presence of zirconium, titanium, and titanium-zirconium alloy implants. Oral Surg Oral Med Oral Pathol Oral Radiol 2020;129:80-6. doi: 10.1016/j.oooo.2019.08.020. Epub 2019 Sep 16. PMID: 31628073. [CrossRef]

48. American Collage of Radiology 2020. https://www.acr.org/Clinical-Resources/Radiology-Safety/MR-Safety

49. Bohner L, Hanisch M, Sesma N, Blanck-Lubarsch M, Kleinheinz J. Artifacts in magnetic resonance imaging caused by dental materials: a systematic review. Dentomaxillofac Radiol 2022;51:20210450. doi: 10.1259/dmfr.20210450. [CrossRef]

50. Juerchott A, Roser CJ, Saleem MA, Nittka M, Lux CJ, Heiland S, Bendszus M, Hilgenfeld T. Diagnostic compatibility of various fixed orthodontic retainers for head/neck MRI and dental MRI. Clin Oral Investig 2023;27:2375-84. doi: 10.1007/s00784-023-04861-2. [CrossRef]

51. Hilgenfeld T, Prager M, Heil A, Schwindling FS, Nittka M, Grodzki D, Rammelsberg P, Bendszus M, Heiland S. PETRA, MSVAT-SPACE

and SEMAC sequences for metal artefact reduction in dental MR imaging. Eur Radiol 2017;27:5104-12. doi: 10.1007/s00330-017-4901-1. [CrossRef]

52. Duttenhoefer F, Mertens ME, Vizkelety J, Gremse F, Stadelmann VA, Sauerbier S. Magnetic resonance imaging in zirconia-based dental implantology. Clin Oral Implants Res 2015;26:1195-202. doi: 10.1111/clr.12430. [CrossRef]

53. Bender IB, Seltzer S. Roentgenographic and direct observation of experimental lesions in bone: I. 1961. J Endod 2003;29:702-6; discussion 701. doi: 10.1097/00004770-200311000-00005. [CrossRef]

54. Bracher AK, Hofmann C, Bornstedt A, Boujraf S, Hell E, Ulrici J, Spahr A, Haller B, Rasche V. Feasibility of ultra-short echo time (UTE) magnetic resonance imaging for identification of carious lesions. Magn Reson Med 201;66:538-45. doi: 10.1002/mrm.22828. [CrossRef]

55. Bracher AK, Hofmann C, Bornstedt A, Boujraf S, Hell E, Ulrici J, Spahr A, Haller B, Rasche V. Feasibility of ultra-short echo time (UTE) magnetic resonance imaging for identification of carious lesions. Magn Reson Med 2011;66:538-45. doi: 10.1002/mrm.22828. [CrossRef]

56. Assaf AT, Zrnc TA, Remus CC, Khokale A, Habermann CR, Schulze D, Fiehler J, Heiland M, Sedlacik J, Friedrich RE. Early detection of pulp necrosis and dental vitality after traumatic dental injuries in children and adolescents by 3-Tesla magnetic resonance imaging. J Craniomaxillofac Surg 2015;43:1088-93. doi: 10.1016/j.jcms.2015.06.010. [CrossRef]

57. Kress B, Buhl Y, Hähnel S, Eggers G, Sartor K, Schmitter M. Age- and tooth-related pulp cavity signal intensity changes in healthy teeth: a comparative magnetic resonance imaging analysis. Oral Surg Oral Med Oral Pathol Oral Radiol Endod 2007;103:134-7. doi: 10.1016/j.tripleo.2006.04.007. [CrossRef]

58. Macrae PR, Jones RD, Myall DJ, Melzer TR, Huckabee ML. Cross-sectional area of the anterior belly of the digastric muscle: comparison of MRI and ultrasound measures. Dysphagia 2013;28:375-80. doi: 10.1007/s00455-012-9443-8. Epub 2013 Jan 20. Erratum in: Dysphagia 2013;28:381. [CrossRef]

59. Otonari-Yamamoto M, Nakajima K, Tsuji Y, Otonari T, Curtin HD, Okano T, Sano T. Imaging of the mylohyoid muscle: separation of submandibular and sublingual spaces. AJR Am J Roentgenol 2010;194:431-8. doi: 10.2214/AJR.09.3516. [CrossRef]

60. Fujii H, Fujita A, Yang A, Kanazawa H, Buch K, Sakai O, Sugimoto H. Visualization of the Peripheral Branches of the Mandibular Division of the Trigeminal Nerve on 3D Double-Echo Steady-State with Water Excitation Sequence. AJNR Am J Neuroradiol 2015;36:1333-7. doi: 10.3174/ajnr.A4288. [CrossRef]

61. Mazza D, Di Girolamo M, Cecchetti F, Baggi L. Appearance of normal MRI anatomy of the lingual nerve using steady-state free precession sequences at 3-T. J Biol Regul Homeost Agents 2020;34:19-26. DENTAL SUPPLEMENT.

62. Al-Haj Husain A, Solomons M, Stadlinger B, Pejicic R, Winklhofer S, Piccirelli M, Valdec S. Visualization of the Inferior Alveolar Nerve and Lingual Nerve Using MRI in Oral and Maxillofacial Surgery: A Systematic Review. Diagnostics (Basel) 2021;11:1657. doi: 10.3390/diagnostics11091657. [CrossRef]

63. Borges A, Casselman J. Imaging the trigeminal nerve. Eur J Radiol 2010;74:323-40. doi: 10.1016/j.ejrad.2010.02.006. [CrossRef]

64. Miloro M, Kolokythas A. Inferior alveolar and lingual nerve imaging. Atlas Oral Maxillofac Surg Clin North Am 2011;19:35-46. doi: 10.1016/j.cxom.2010.11.003. [CrossRef]

65. Grandoch A, Oeser J, Zöller JE, Grosse Hokamp N, Lichtenstein T, Neugebauer J. Morphological Studies to Identify the Nasopalatine and Inferior Alveolar Nerve Using a Special Head and Neck MRI Coil. J Craniofac Surg 2023;34:1351-6. doi: 10.1097/SCS.0000000000009219. [CrossRef]

66. Müller S, Khadhraoui E, Khanafer A, Psychogios M, Rohde V, Tanrikulu L. Differentiation of arterial and venous neurovascular conflicts estimates the clinical outcome after microvascular decompression in trigeminal neuralgia. BMC Neurol 2020;20:279. doi: 10.1186/s12883-020-01860-8. [CrossRef]

67. Xiong X, Ye Z, Tang H, Wei Y, Nie L, Wei X, Liu Y, Song B. MRI of Temporomandibular Joint Disorders: Recent Advances and Future Directions. J Magn Reson Imaging 2021;54:1039-52. doi: 10.1002/jmri.27338. [CrossRef]

68. Jeon KJ, Choi YJ, Lee C, Kim HS, Han SS. Evaluation of masticatory muscles in temporomandibular joint disorder patients using quantitative MRI fat fraction analysis-Could it be a biomarker? PLoS One 2024;19:0296769. doi: 10.1371/journal.pone.0296769. [CrossRef]